2017

Finite Element Analysis Of A High-Speed Suspension Boat Fuselage

Lean Fang
Lehigh University

FINITE ELEMENT ANALYSIS OF A HIGH-SPEED SUSPENSION BOAT FUSELAGE

by

Lean Fang

A Thesis

Presented to the Graduate and Research Committee

of Lehigh University

in Candidacy for the Degree of

Master of Science

in

Machanical Engineering

Lehigh University

August 2017

This thesis is accepted and approved in partial fulfillment of the requirements for the Master of Science.

_____

Date

_____

Thesis Advisor

_____

Chairperson of Department

ACKNOWLEDGMENTS

I would like to thank Prof. Grenestedt for his support and guidance that always enabled me on my journey through this project. I also really appreciate his efforts in cultivating the engineering and scientific mindset in his students.

I would like to say thank you to all of my lab mates, it has always been so refreshing talking to you guys after I spend a whole day staring at computers in the CAD labs.

I am also forever grateful to my parents. I would not have been able to study at Lehigh without their support.

TABLE OF CONTENTS

LIST OF TABLES

LIST OF FIGURES

LIST OF ABBREVIATIONS

FEA	Finite Element Analysis
CFRP	Carbon Fiber Reinforced Plastics/Polymer
UD	Unidirectional
UIM	The Union Internationale Motonautique
CAD	Computer-aided design
PVC	Polyvinyl chloride
APDL	Ansys Parametric Design Language

ABSTRACT

The ongoing suspension boat project at Lehigh University Composites Lab presents new challenges for design since a suspension boat will encounter entirely different loads than a conventional boat. High strength yet low weight are as always of major importance.

The suspension boat presently under consideration consists of four sponsons connected to a center hull, or fuselage. An FEA study of the composite fuselage was conducted. Crash loads were applied as evenly distributed pressures over parts of the top of the cockpit. Suspension loads were applied at discrete points on the fuselage, where the suspension components will be mounted, and inertia relief calculations were performed. Masses representing occupants, engine etc were included in the model. The fuselage is built of carbon fiber reinforced epoxy skins on foam core sandwich. Different carbon fiber ply layups and foam core thicknesses were studied. A satisfactory layup scheme was achieved for the fuselage.

1. INTRODUCTION

Background

Lehigh University Composites Lab has been developing a suspension boat capable of running stably and smoothly on off-shore water at high speed [1-4]. The unconventional suspension systems introduced some unique challenges into the design process of this speed boat. Unlike a traditional boat that takes the loads from water at its bottom through slamming, the suspension boat would take large loads through the suspension systems which are mounted to the fuselage. The fuselage of the suspension boat must be strong enough to withstand the suspension loads, it should maintain structural integrity in a crash in order to protect the pilots, and last but not the least, the total mass of the fuselage should be as low as possible.

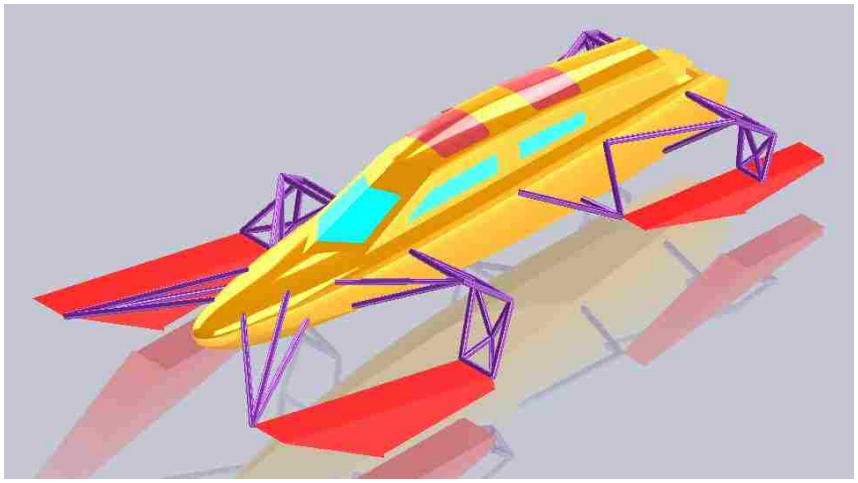

Figure 1.1-1: A CAD illustration of the fuselage equipped with suspension systems (the fuselage has the correct shape whereas the four sponsons are only place holders)

The fuselage is made of sandwich composites with Carbon Fiber Reinforced Plastics (CFRP) skins and a closed-cell PVC foam core, and the window panels would be made of Polycarbonate (PC) because of its optic properties, its impact resistance and its relatively low density.

Prior to this study, the external composite structure of the fuselage was already built with a layup that showed excellent strength in the four-point bending test used as a cockpit safety benchmark by UIM. The sizes and locations of the internal bulkheads and frames were also determined by functional and utility requirements, but the layups of the bulkheads and frames as well as the window panel thicknesses needed to be determined. Thus the main goal of this study was to:

- develop feasible layups of the internal bulkheads and frames
- perform a study on the thicknesses of the window panels
- estimate deformations and stresses in the fuselage when subjected to various loads

Figure 1.1-2: Fuselage structure built prior to this study

Overview of the FEA-based Analyses

The Finite Element Analysis (FEA) approach suits this design problem well because it allows for thorough examinations of the structural behaviors of the suspension boat fuselage under various loads without the risk of damaging a prototype or the need to modify it. The FEA approach also puts significant challenges onto the shoulders of the practitioners: the finite element model and boundary conditions must be accurate enough to capture the physics, yet they must also be of relatively low computational cost in order to allow for rapid changes in the design.

For the above reason the fuselage was modeled with layered linear shear-deformable shell elements (Ansys SHELL181) and meshed from a simplified CAD geometry. Linear elastic static analyses with Inertia Relief were performed to mimic the loads the fuselage would encounter during high speed operation, as well as in a crash. In Inertia Relief calculations, rigid body translational and rotational accelerations are calculated to balance externally applied forces. Forces balancing these accelerations are calculated for all elements and added to the external forces. A static analysis is then performed. The static analysis requires boundary conditions that eliminate rigid body translations and rotations. There will be no reactions at the nodes where these boundary conditions are applied. It should be noted that these boundary conditions are used only to obtain a unique solution and have nothing to do with the actual motion of the structure. See Ansys manual [5,6].

The first step of the FEA-based analyses was to come up with a group of incrementally reinforced layup or thickness options for each of the bulkheads, frames, and window panels. The PC window panels would have the thicknesses 12.7 mm or 15.9 mm (1/2" and 5/8", respectively). The core material of the internal bulkheads and frames would be Divinycell H80 and the thickness would be either 10mm or 15mm. The transverse bulkheads and cockpit frames would have $(45, -45, 0, 90)_m$ skin layups, and the longitudinal bulkheads would have skin layups of $(45, -45)_n$ because their main task was to provide torsional stiffness and strength; *m* and *n* are integers.

If a bulkhead, frame or window panel met the strength requirements for most of its elements but had very large strains on relatively small areas, then the layup or thickness would still be considered satisfactory. Local stresses will be dealt with by adding local reinforcements when the boat is built.

A very simple optimization was performed to gain a viable layup and thickness design with low weight by using a Python script. This script scanned through a number of (laminate and core) thicknesses of each bulkhead, frame, and window panel.

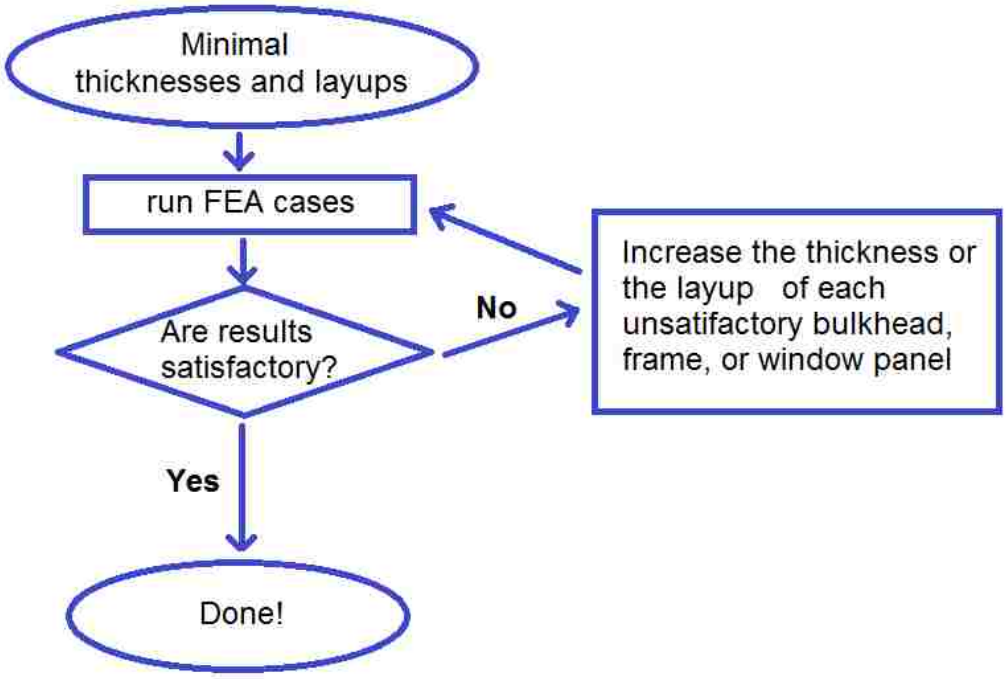

Figure 1.2-1: A process flow diagram of the Python script to find a viable design with low weight

2. METHODOLOGY

Materials and Their Properties

In Finite Element Analyses the CFRP laminates were modeled as layups of unidirectional (UD) plies of an orthotropic CFRP material. The material properties of a single UD CFRP ply are given in Table 2.1-1. They were obtained from Table 10.2.4.1 of Composite Materials Handbook Volume 3. (MIL-HDBK-17-3F) [7].

Unidirectional Carbon Fiber Reinforced Polymer (UD CFRP)	
Material Property	Value
E_1	113.6 GPa
E_2	9.65 GPa
E_3	9.65 GPa
ν_{12}	0.334
ν_{13}	0.328
ν_{23}	0.540
G_{12}	6.0 GPa
G_{13}	6.0 GPa
G_{23}	3.1 GPa
ρ	1530 kg/m³

Table 2.1-1: Material properties of UD CFRP

Closed-cell PVC foams from Diab were chosen as the core materials for the sandwich. The heavier-duty Diab HM130 would be used for the construction of the external structure and the lighter-duty Diab H80 was chosen for the internal bulkheads and frames. The cores were modeled as linear elastic isotropic materials and their properties are shown in Table 2.1-2 and Table 2.1-3. The density, shear modulus and shear strength are taken from Diab's datasheets [8]. A Poisson's ratio of 0.32 was used for both cores and Young's modulus was calculated from shear modulus and Poisson ration assuming isotropy ($E=2(1+\nu)G$). Real foams are not perfectly isotropic so these values differ slightly from those given by Diab; however, the most important properties (shear modulus and shear strength) are the same and the influence of the other properties are expected to be of less importance. The critical shear strain was calculated as τ^{cr}/G. This is significantly less that the failure strains of real foams, which exhibit considerable non-linear deformation similar to yielding before final failure.

Diab HM130 Foam	
Material Property	Value
E_1	132 MPa
ν_{12}	0.32
ρ	130 kg/m^3
G	50 MPa
τ^{cr}	2.2 MPa (Nominal) 1.9 MPa (Minimum)
γ^{cr}	4.4% (Nominal) 3.8% (Minimum)

Table 2.1-2: Material properties of Diab HM130 foam

Diab H80 Foam	
Material Property	Value
E_1	71.28 MPa
ν_{12}	0.32
ρ	80 kg/m^3
G	27 MPa
τ^{cr}	1.15 MPa (Nominal) 0.95 MPa (Minimum)
γ^{cr}	4.3% (Nominal) 3.5% (Minimum)

Table 2.1-3: Material properties of Diab H80 foam

Polycarbonate (PC) was the material of choice for the window. PC is viscoelastic in nature, but since we are only interested in its pre-failure behaviors under relatively high strain rates it was assumed that a linear elastic time-independent material model would give satisfactory results. See [9] for properties of PC. The following properties were used:

Polycarbonate (PC)	
Material Property	Value
E_1	2.35 GPa
ν_{12}	0.38
ρ	1200 kg/m^3
ε_i^{cr}	8%
ε_{iii}^{cr}	-8%

Table 2.1-4: Material properties of polycarbonate

Post-Process and Failure Criteria

In this study the failure of the sandwich was assumed to be caused by excessive tensile or compressive strain in the thin CFRP skins or excessive out-of-plane shear strain in the foam cores. The failure of the PC was also assumed to be caused by excessive tensile or compressive strain. The customized post-process to evaluate these failure criteria was made by a Python script.

I. Failure criteria for CFRP skins

For each of the UD CFRP plies, the maximum principal strain and the minimum principal strain were evaluated. If the maximum principal strain was higher than 1.2% or the minimum principal strain lower than -0.7%, then the CFRP was assumed to fail.

Since each UD CFRP ply was very thin compared to the core, the change of strain through the thickness of a ply could be neglected, so for each of the UD CFRP plies only the strains at the ply mid-plane were evaluated. For every element, the maximum value of maximum principal strains and the minimum value of minimum principal strains through all UD CFRP plies were then calculated and used in the contour plots.

II. Failure criteria for foam cores

For both H80 and HM130, it was assumed that the maximum out-of-plane shear strain that they could take is 4%. This value was based on the minimum and nominal critical shear strains calculated as τ^{cr}/G (see Table 2.1-2 and Table 2.1-3) and assuming linear elastic behavior up to failure.

If γ_{13} and γ_{23} are the out-of-plane shear strains at a point in the sandwich core, it is easy to show that the maximum out-of-plane shear strain is $\sqrt{\gamma_{13}^2+\gamma_{23}^2}$.

Because the foam cores were much thicker than a UD CFRP ply, the change of strain through the thickness of a foam core could not be neglected. At the top-plane, the mid-plane and the bottom-plane, the maximum out-of-plane shear strains were first calculated as $\sqrt{\gamma_{13}^2+\gamma_{23}^2}$ from γ_{13} and γ_{23}, then for every element the maximum value of the (absolute value of the) three maximum out-of-plane shear strains was calculated and used for the contour plotting.

III. Failure criteria for PC

PC was assumed to allow 8% maximum principal strain and -8% minimum principal strain before failure, see Table 2.1-4.

The strain changes through the thickness of the window panels and therefore for every element the maximum and minimum principal strains at the top-plane, the mid-plane and the bottom-planes were evaluated. From these three locations the most severe principal strains were extracted and used in the contour plots that follow.

[redacted] Comparison with a Four-Point Bend Experiment

Lehigh University Composites Lab had conducted four-point bend tests on specimens with the layup of the cockpit of the actual Suspension Boat being built. These tests are required by UIM, an international governing body of powerboat racing. The specimens

must meet stiffness and strength requirements under four-point bending [10]. Results of this experiment were presently used to check whether the layered linear shear-deformable FE shell elements and the selected material properties were capable of predicting the experimental deflection and strength.

The cockpit specimen measured 800 mm in length and 100 mm in width, it had an asymmetrical sandwich composite layup with a thicker CFRP skin on the outside and a thinner CFRP skin on the inside. The layup is shown in the table below. The reference direction, which the 0° fibers align to, is the x-axis (in red) shown in Figure 2.3-1.

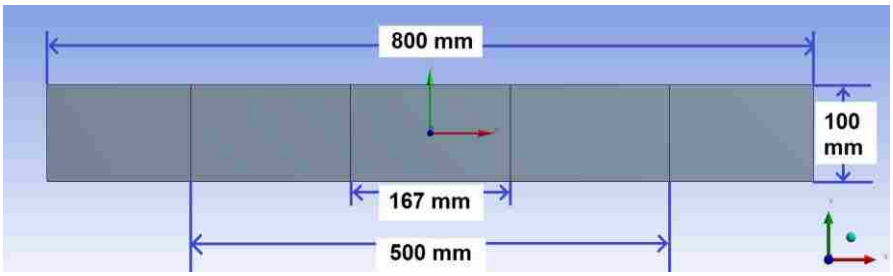

Figure 2.3-1: A sketch of the cockpit specimen and the four-point bending setup

Outside		
Material	Angle	Thickness
UD CFRP	45°	0.1515 mm
UD CFRP	-45°	0.1515 mm
UD CFRP	0°	0.189 mm
UD CFRP	90°	0.189 mm
UD CFRP	45°	0.1515 mm
UD CFRP	-45°	0.1515 mm
UD CFRP	0°	0.292 mm
HM130	isotropic	15 mm
UD CFRP	0°	0.292 mm
UD CFRP	-45°	0.1515 mm
UD CFRP	45°	0.1515 mm
UD CFRP	90°	0.189 mm
UD CFRP	0°	0.189 mm
Inside		

Table 2.3-1: Layup of the cockpit panel test specimen

The UIM four-point bending procedure set 500 mm between the outer roller supports, and 167mm between the inner roller supports, where the loads were applied and the deflections were measured. According to the UIM rule books, the specimens should not fail and should deflect no more than 25 mm under a 3000 N load [10].

In the tests at Lehigh Composites Lab, three specimens were tested with the thicker outside skin in compression, and two specimens were tested with the thinner inside skin in compression. The specimens deflected 9.46mm under a 3000 N load and started to exhibit non-linear deformation at roughly 6000N before ultimate failure at roughly 7000N. The results were:

- No specimen deflected more than 10 mm with 3000 N applied.
- The three specimens with the outer skin in compression failed at:
  - Specimen 1: max load 7047 N at 29 mm deflection (specimen taken from edge of panel),
  - Specimen 2: max load 7089 N at 29 mm deflection,
  - Specimen 3: max load 7211 N at 31 mm deflection,
- while the two specimens with the inner skin in compression failed at:
  - Specimen 4: max load 7067 N at 27 mm deflection,
  - Specimen 5: max load 6521 N at 23 mm deflection (specimen taken from edge of panel).
- All specimens exhibited substantial non-linear deformation, similar to yielding, before final failure.

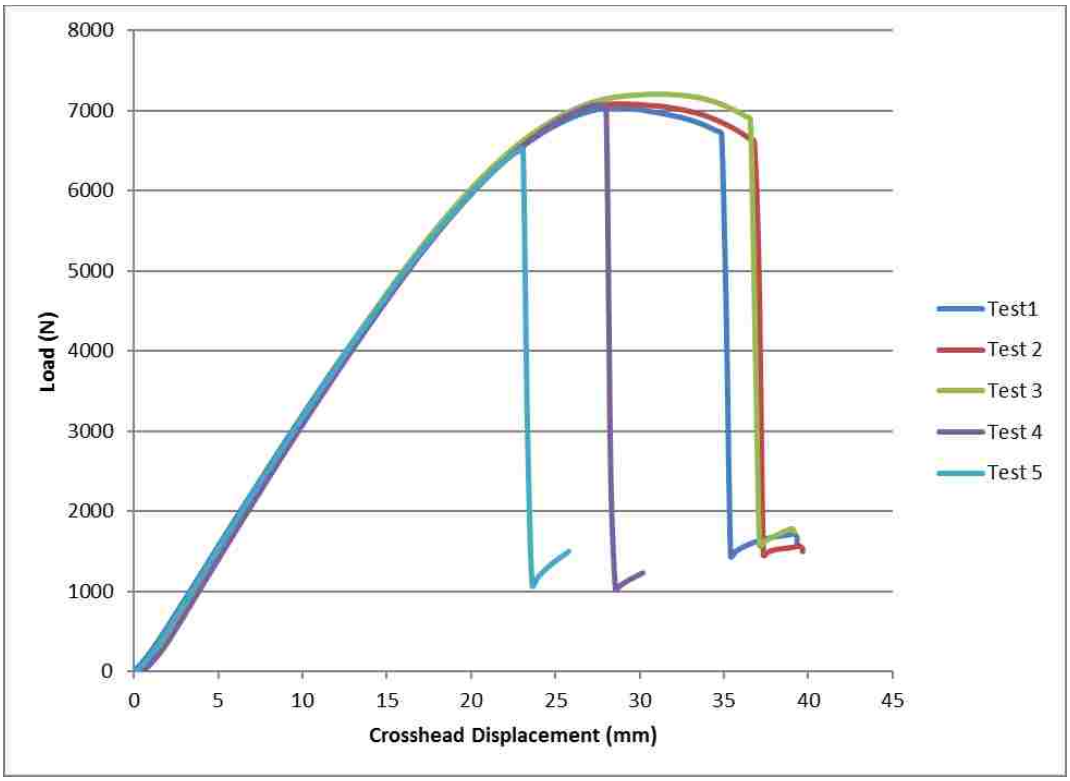

Figure 2.3-2: Deflections of the cockpit specimens tested with UIM procedure (Courtesy of Prof. Grenestedt at Lehigh Composites Lab)

In the validation FEA case, the outer supports were modeled with constrained displacements, and the inner supports were modeled with evenly distributed line pressure over the two lines of the inner supports, as outlined in Table 2.3-1. The mesh was uniform and mesh dependence studies with the element size of 20 mm, 10 mm and 5 mm were conducted. Below are a sketch and table showing the boundary conditions for the FEA.

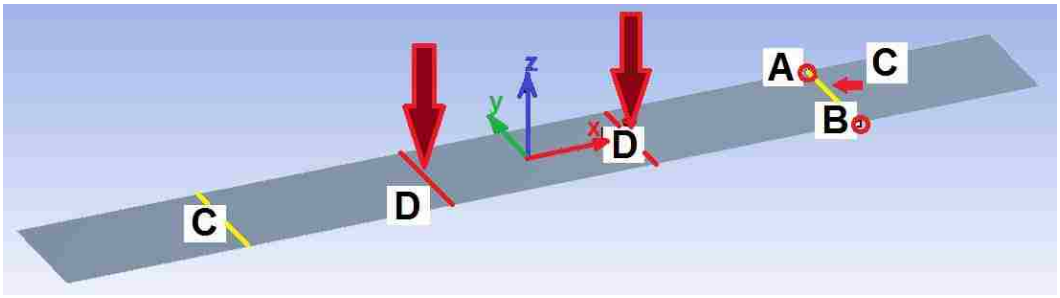

Figure 2.3-3: A sketch of the boundary conditions of the four-point bending case

Description of the geometry	**Description of the boundary conditions**
Point A	$U_x = 0$ $U_y = 0$
Point B	$U_x = 0$
Two yellow lines marked with C	$U_z = 0$
Two red lines marked with D	Evenly distributed line pressure along the negative z-axis, with the total force 3000 N or 6000 N, and the thicker outside skin under compression
Note: This table uses Figure 2.3-3 as the reference for the geometry and coordinate system.	

Table 2.3-2: Description of the boundary conditions of the four-point bending case

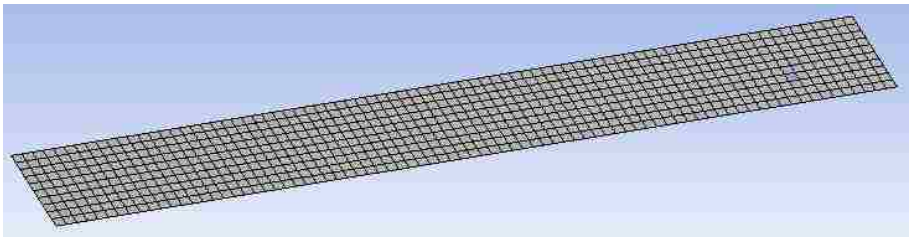

Figure 2.3-4: A sketch of the uniform mesh, element size = 10 mm

I. Comparison of the deflections under a 3000N load

From the table below, we can see that the deflection under a 3000 N load was captured very well by FEA for all three mesh resolutions when we compare the FEA results to the experimental data. There was a small difference between the max deflection and min deflection probed at the inner supports in the FEA case, this was expected due to the out-of-plane warp caused by anticlastic bending, and even the coarsest mesh which had only 5 rows of elements y-axis wise was able to capture this behavior with good accuracy.

	Min Deflection	Max Deflection
FEA, element size = 20 mm	9.45 mm	9.55 mm
FEA, element size = 10 mm	9.46 mm	9.56 mm
FEA, element size = 5 mm	9.46 mm	9.56 mm
Experiment	9.46 mm	

Table 2.3-3: Comparison of deflections of a cockpit panel specimen under a 3000 N load and different element sizes

II. Core failure under a 6000 N load

The specimens all started to exhibit substantial non-linear deformation at roughly 6000 N, presumably due to (shear) yielding of the foam core.

With the total load P = 6000 N, the core thickness d = 15 mm and the width of the specimen w = 100 mm, the shear stress in the core is approximately 2 MPa which is near the published shear strength of H130.

As indicated in Figure 2.3-5, the FEA also predicted the maximum out-of-plane shear strain of core that caused the core failure in experiments at 6000 N quite well.

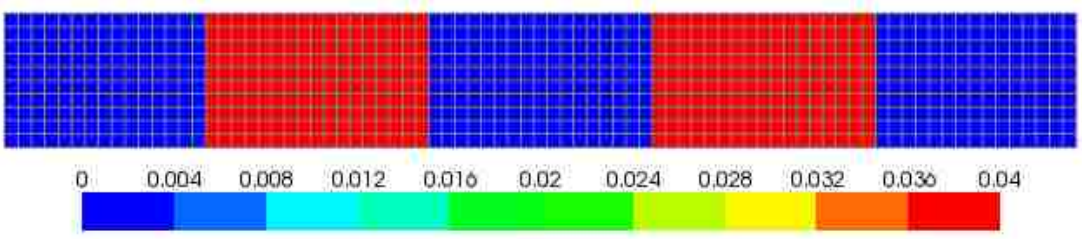

Figure 2.3-5: Maximum out-of-plane shear strain of core at 6000 N

Geometry and Finite Element Mesh of the Suspension Boat Fuselage

The CAD model of the suspension boat fuselage measures 6.53 m in length, 1.48 m in height, and 1.07 m in width. It is composed of surfaces that represent the external structure of the hull, cockpit, hatches and windows, the internal bulkheads and frames. Many minor features such as fillets and sharp corners were removed or simplified before the mesh was generated in Ansys Mechanical. The coordinate system shown in the sketches below aligns with the principal axes of the boat: the x-axis is parallel with the boat lateral axis, the y-axis is parallel with the boat vertical axis, and the z-axis is parallel with the boat longitudinal axis. Throughout the thesis this coordinate system was used.

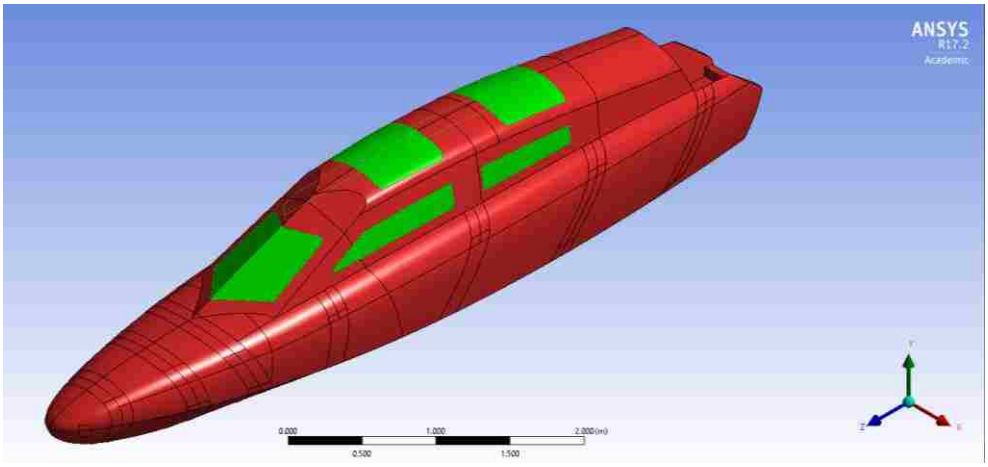

Figure 2.4-1: Simplified CAD model with the window panels (front & sides) and the cockpit hatches (top) highlighted in green

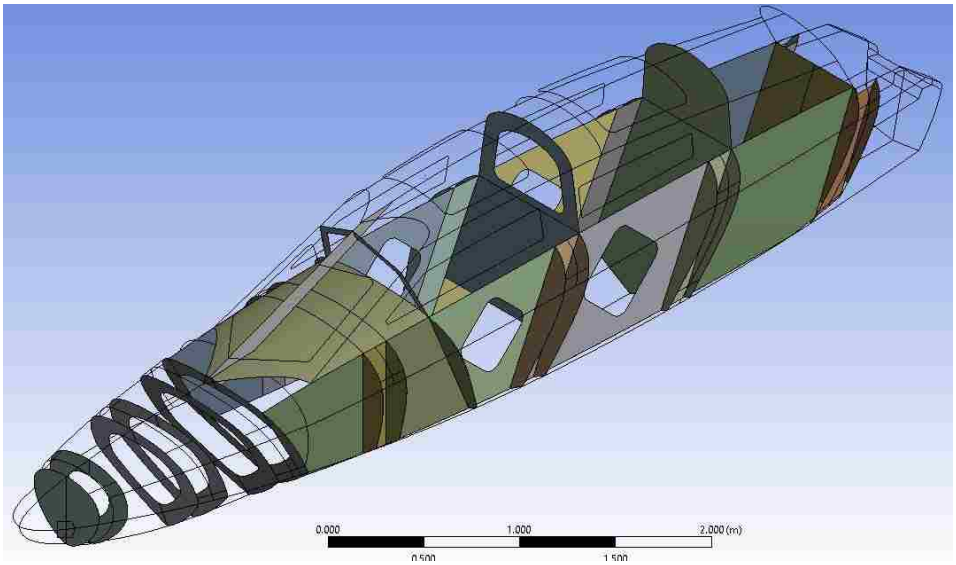

Figure 2.4-2: Internal structure of the simplified CAD model

The Finite Element mesh of the fuselage is mostly composed of quadrilateral elements with a few triangular elements as fillers. The total element count is 41562 and the element quality is excellent everywhere. All narrow areas such as the cockpit frames, lower ring-shaped and stripe-shaped bulkhead panels have a mesh resolution of about 5 rows of elements.

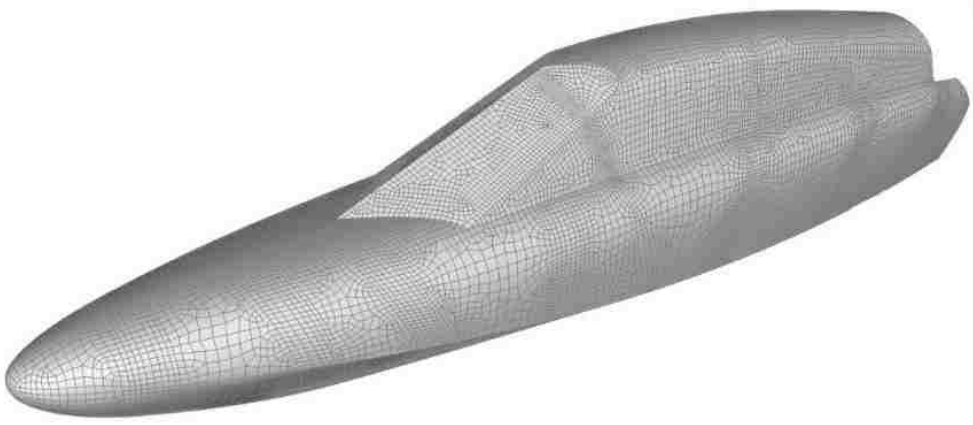

Figure 2.4-3: Mesh of the external structure of the fuselage

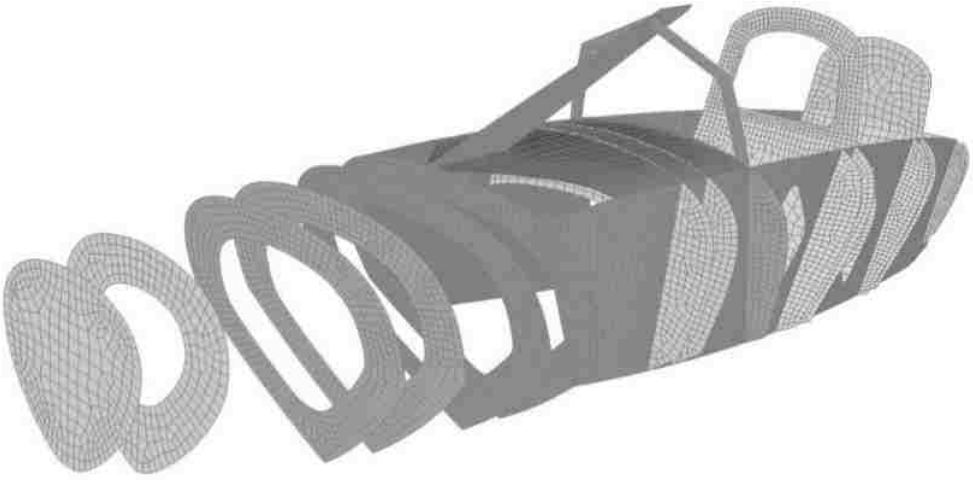

Figure 2.4-4: Mesh of the internal structure of the fuselage

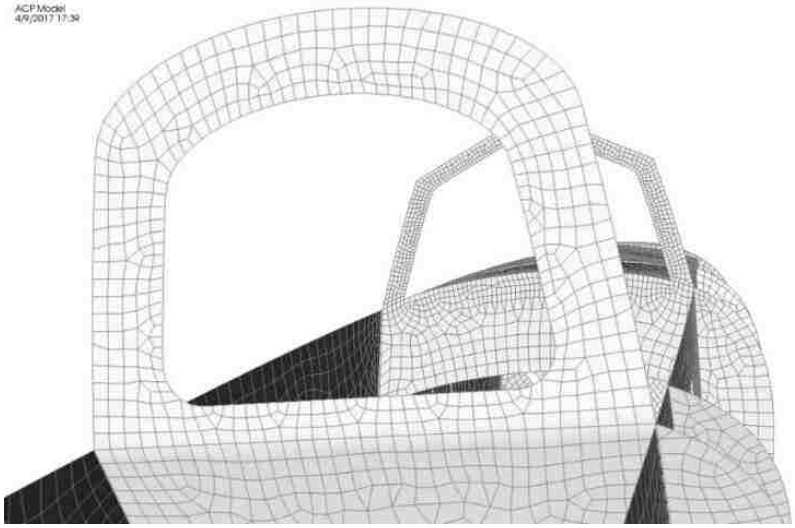

Figure 2.4-5: Close-up look of the mesh

Sandwich Composite Layups and Window Panel Thicknesses

I. Window panel thicknesses

The window panels need to have adequate strength to protect the pilots in a crash. The proposed thickness options were 12.7mm (1/2”) and 15.9mm (5/8”). As shown in the results in section 3.1, the window panels do not need to be any thicker.

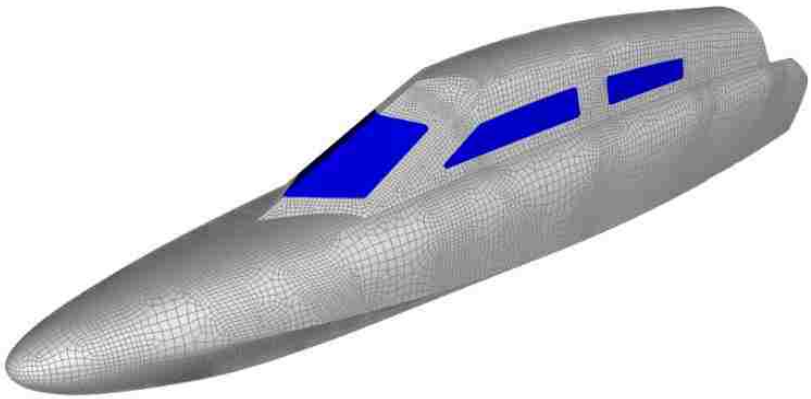

Figure 2.5-1: Window panels highlighted in blue

II. Layups of the external composites structure

Prior to this FEA study the external composite structure of the fuselage had been built. The bottom of the hull has a 19mm thick HM130 core while the rest of the external composite structure including the hatches has a 15mm thick HM130 core. The bottom of the boat will be subjected to slamming loads hence a thicker core is needed. To mimic the effect that the two hatches are not bonded to the main body of fuselage, the hatches were surrounded by fairly thin (5 mm) flanges that have low bending stiffness. Below is a table showing the layups of the external composite structure of the fuselage. The reference direction, which is the direction of a zero degree fiber, is defined as the projection of the z-axis (boat longitudinal axis) onto the elements.

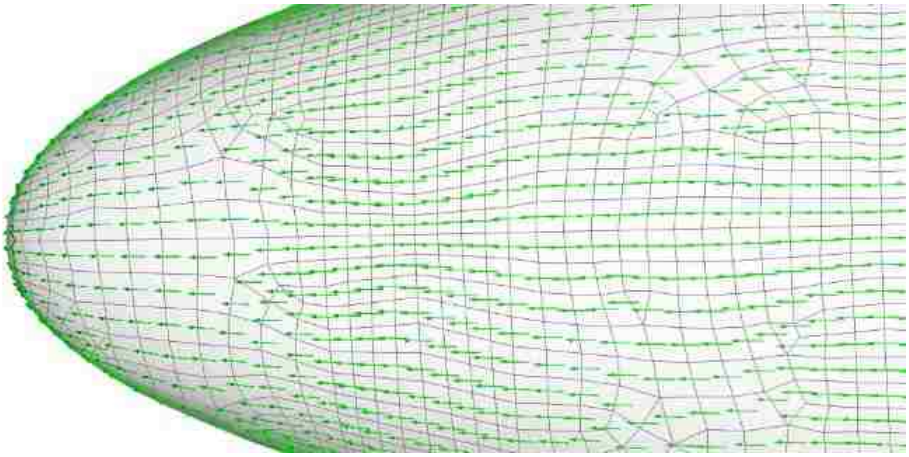

Figure 2.5-2: Close-up look of the element reference directions at the front end of the fuselage

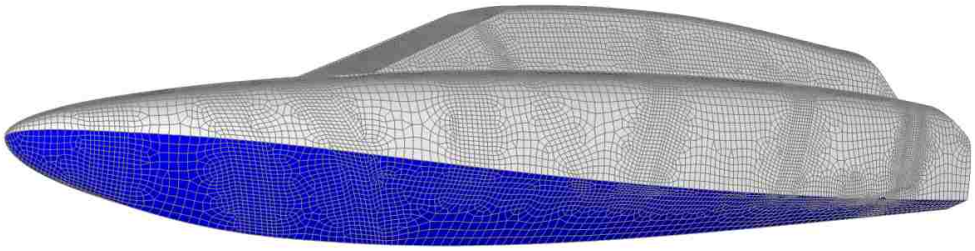

Figure 2.5-3: The bottom of fuselage where the core thickness is 19mm, highlighted in blue

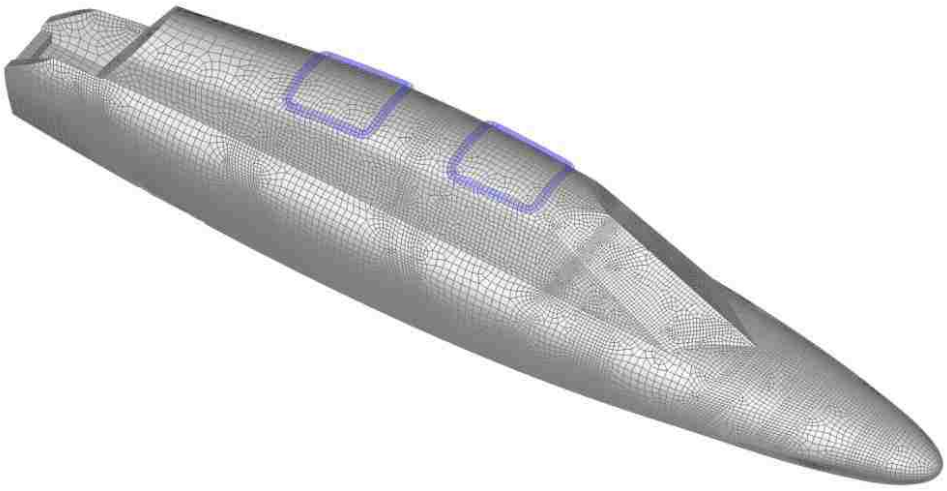

Figure 2.5-4: The hatch edges where the core thickness is 5 mm (same layup of skins as the rest of the external composites structure)

Outside		
Material	Angle	Thickness
UD CFRP	45°	0.1515 mm
UD CFRP	-45°	0.1515 mm
UD CFRP	0°	0.189 mm
UD CFRP	90°	0.189 mm
UD CFRP	45°	0.1515 mm
UD CFRP	-45°	0.1515 mm
UD CFRP	0°	0.292 mm
HM130	isotropic	If bottom: 19 mm If edges of the hatches: 5mm Otherwise: 15 mm
UD CFRP	0°	0.292 mm
UD CFRP	-45°	0.1515 mm
UD CFRP	45°	0.1515 mm
UD CFRP	90°	0.189 mm
UD CFRP	0°	0.189 mm
Inside		

Table 2.5-1: Layup of the external sandwich composite structure of the fuselage

III. Layups of the cockpit frames and transverse bulkheads

For defining the skin layups of the transverse bulkheads and frames, the projections of the y-axis (boat vertical axis) was used as the reference direction. The proposed skin layup options were in the form of $(45, -45, 0, 90)_m$, where *m* is a positive. The thickness of a 45° or -45° ply is 0.1515 mm, and the thickness of a 0° or 90° ply is 0.189mm.

For thinner skin laminates, such as (45, -45, 0, 90) and $(45, -45, 0, 90)_2$, the proposed thickness of the H80 core was 10mm. For thicker skin laminates, $(45, -45, 0, 90)_3$ and $(45, -45, 0, 90)_4$, the proposed thickness of the H80 core was 15mm. This was due to the consideration that a bulkhead or frame requiring thicker and stronger skins could also benefit from more bending stiffness and to resist buckling. As we can see later in section

3.1, a pair of $(45, -45, 0, 90)_4$ skins and a 15mm H80 core was the strongest layup needed in the fuselage.

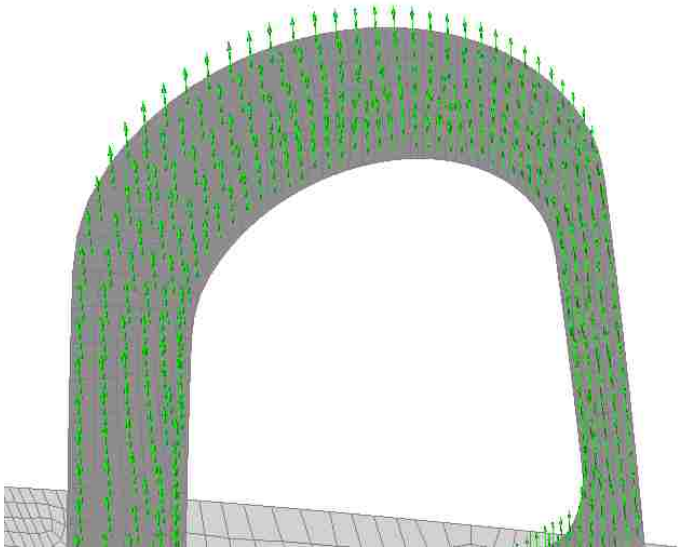

Figure 2.5-5: Close-up look of the element reference directions at a frame

Layups of the longitudinal bulkheads

The projections of the z-axis (boat longitudinal axis) was used as the reference direction for defining the skin layups of the longitudinal bulkheads. The proposed skin layup was in the form $(45, -45)_n$, where n is a positive integer. The thickness of a 45° or -45° ply is 0.1515 mm. The proposed H80 core thickness was 10mm. As seen in section 3.1, a pair of $(45, -45)_2$ skins and a 10mm H80 core was the strongest layup we would need for the longitudinal bulkheads.

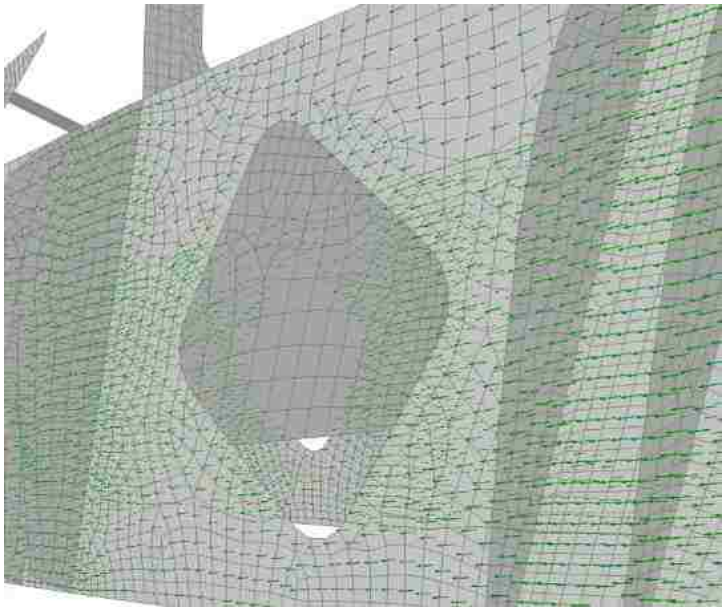

Figure 2.5-6: Close-up look of the element reference directions at a longitudinal bulkhead

Mass Distribution for the Inertia Relief FEA

The Inertia Relief approach required a mass distribution to capture the inertia behaviors of the boat, the pilots, the engine, etc. Besides the mass defined by the sandwich structure and window panels in **Section 2.6**, the following mass was added:

- 414 kg of evenly distributed mass (per area) to all the surfaces representing sandwich composites. This additional mass was to account for the painting, various hardware, equipment, etc.
- 150 kg of evenly distributed mass each to the two lower bulkheads where the two pilots sit, shown in the sketches below. This corresponds to the mass of the person, his or her safety gear, the seat and its mounting hardware.
- 280 kg of evenly distributed mass to the location where the engine is mounted, shown in the sketches below.

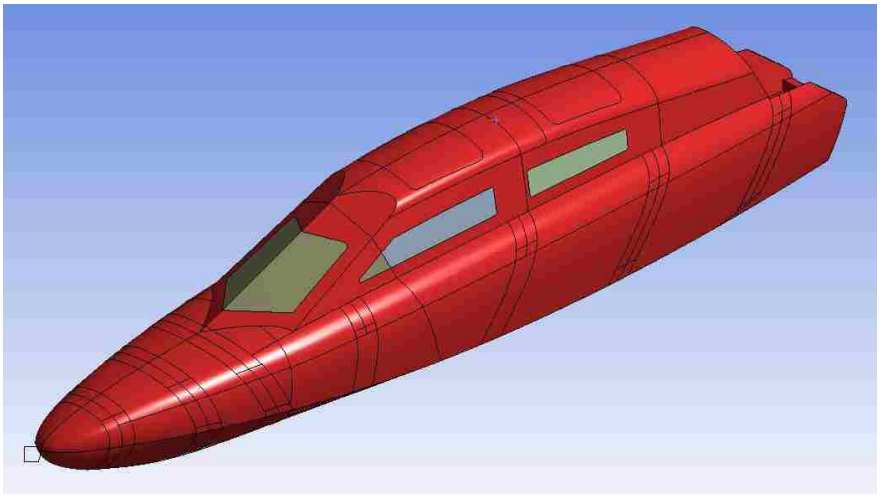

Figure 2.6-1: 414 kg of mass added to the all the sandwich surfaces colored in red. Surfaces representing window panels were left out

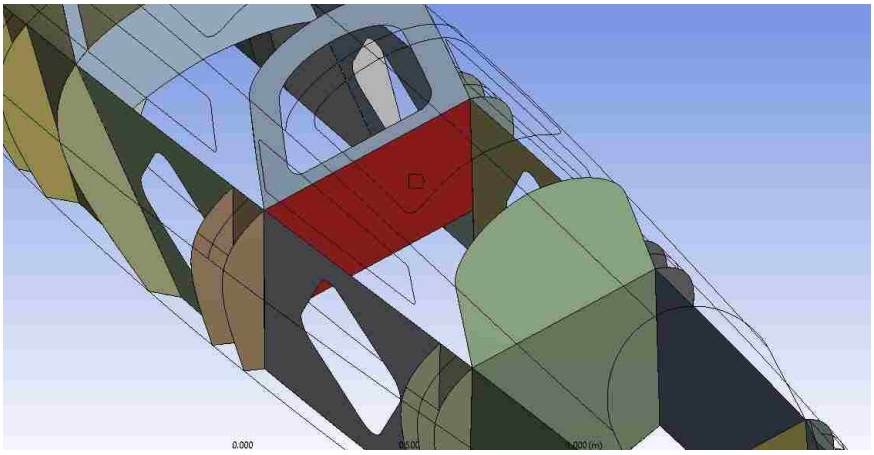

Figure 2.6-2: 150 kg of mass added to the bulkhead where the front pilot sits, highlighted in red

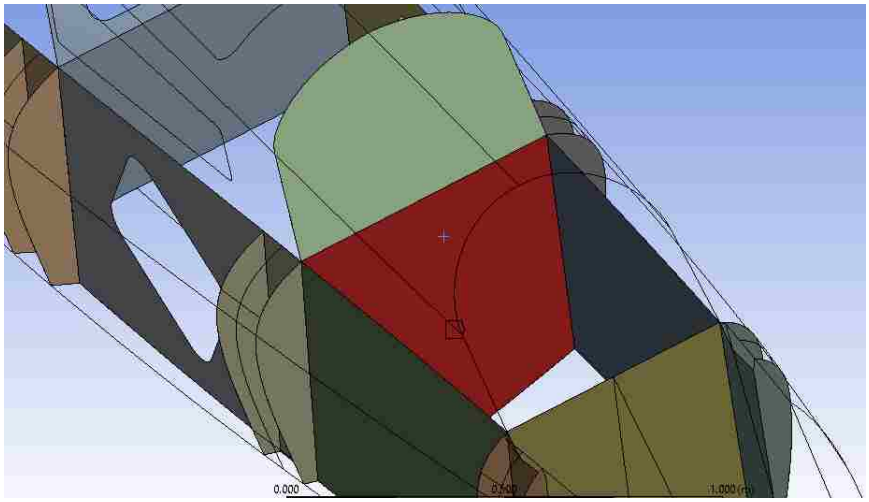

Figure 2.6-3: 150 kg of mass added to the bulkhead where the rear pilot sits, highlighted in red

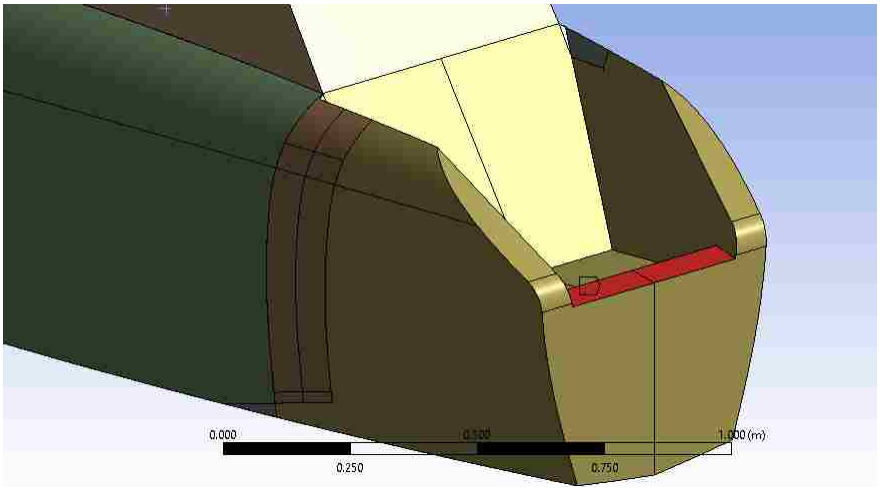

Figure 2.6-4: 280 kg of mass added to the surface where the engine is mounted, highlighted in red

Crash Scenario – Front under Hydrodynamic Load

The cockpit has to be sufficiently strong to maintain structural integrity and ensure the survival of the pilots in the case of a crash. The first crash scenario studied was when the front of the cockpit hits the water, sketched in the figure below.

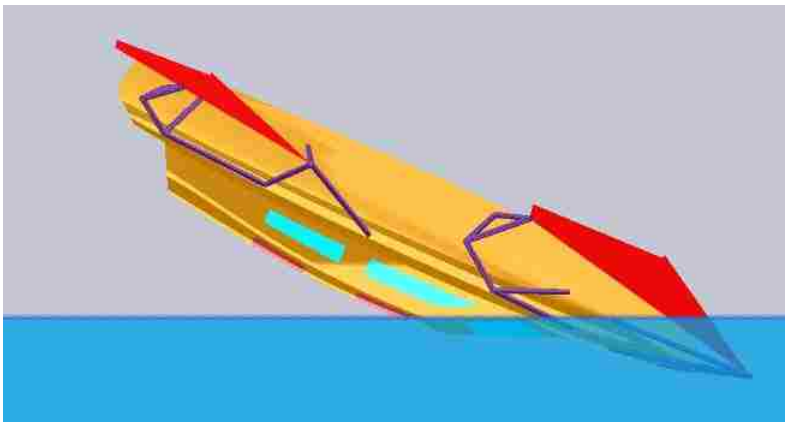

Figure 2.7-1: The front of the cockpit hitting the water

In the corresponding linear static FEA study, a uniform pressure of 1.25 MPa, which is the dynamic pressure at 50 m/s, was applied to the front of the cockpit. The Inertia Relief option was enabled with just enough fixed displacements applied preventing rigid body motion.

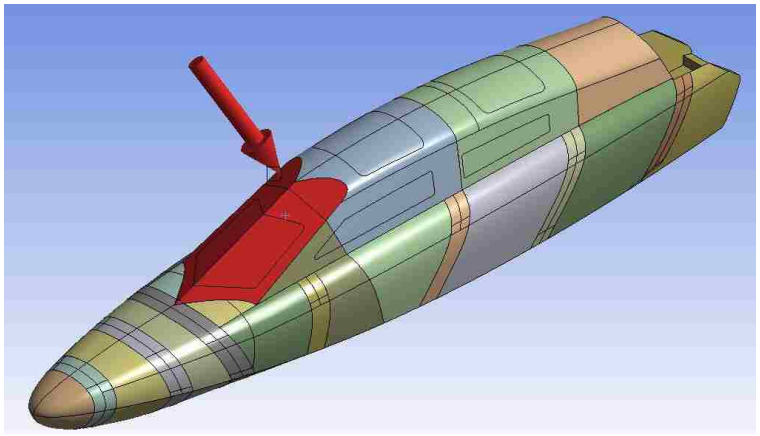

Figure 2.7-2: Hydrodynamic pressure applied normal to the surfaces of the front of the cockpit, highlighted in red

Crash Scenario – Top under Hydrodynamic Load

Another crash scenario is when the top of the cockpit lands on the water as outlined in Figure 2.8-1. In a linear static FEA, a uniform hydrodynamic pressure of 1.25 MPa was applied onto the top surfaces of the cockpit, as shown in the figures below. The Inertia Relief option was enabled with just enough fixed displacements applied preventing rigid body motion.

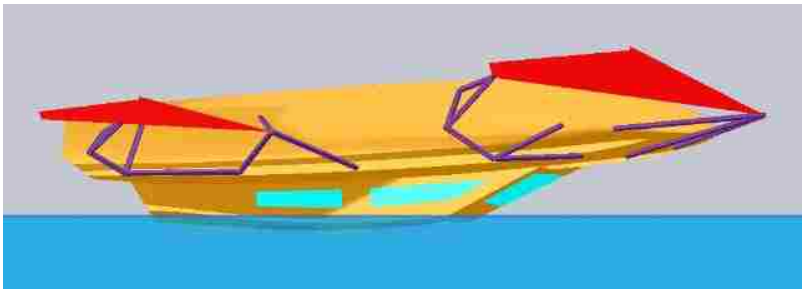

Figure 2.8-1: The top of the cockpit hitting the water

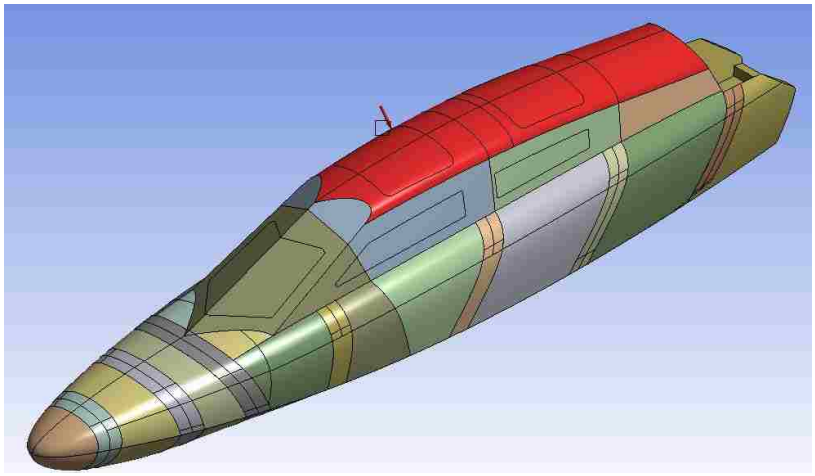

Figure 2.8-2: Hydrodynamic pressure normal to the surfaces applied to the top of the cockpit, highlighted in red

Side Window Panels under Hydrodynamic Loads

This section investigates if the side window panels could survive the hydrodynamic loads. As shown in Figure 2.9-2, in this FEA the window panels on the right side including the right half of the front window screen were loaded with the hydrodynamic load of 1.25 MPa. The Inertia Relief option was enabled with just enough fixed displacements applied preventing rigid body motion.

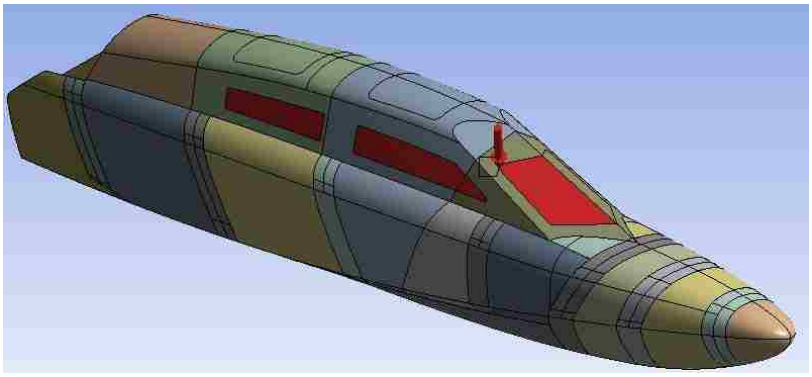

Figure 2.9-1: Hydrodynamic pressure applied normal to the right side window panels, highlighted in red

Operating at High Speed in High Waves – Loads from the Suspension System

I. Methodology of determining the loads on fuselage

Other major load cases for the suspension boat come from operating at high speed in high waves. While the loads from waves would primarily be applied to the bottom of a boat of conventional design, the suspension boat fuselage would mostly take the quite concentrated loads through the suspension system. An examination of the cases where the boat was operating at high speed in high waves was necessary.

The loads on the fuselage in this FEA study were loosely based on sea trials of the *Numerette*, a heavily instrumented 9 m long high-speed hybrid steel/composite boat designed and built at Lehigh University Composites Lab. In the *Numerette*, vertical accelerations of 10 g is common, 15 g is not uncommon, and 20+ g has occasionally

occurred [11,12]. The plan is to adjust the speed of the suspension boat to avoid surpassing 10 g vertical and 20 g transverse accelerations. Seven loading cases were devised. These are believed to reasonably well represent some of the highest loads that are expected during operation at high speeds. Four of these load cases assumed a total load equivalent to 10 g vertical acceleration, and three of them assumed a total load equivalent to 20 g horizontal transverse acceleration. The vertical cases assumed half of the load of the horizontal cases. This is because the suspension would reduce the vertical load significantly. However, depending on springs and compression dampings the forces could still be substantial.

For each of the seven load cases, a load calculator written in APDL (Ansys Parametric Design Language) was used to calculate the loads on the fuselage from assumed loads on the sponsons. In this APDL code, the suspension systems and sponsons were modeled as rigid links that allowed no deformation but free rotations and translations. The hardpoints where the suspensions are mounted to the fuselage were locked in all three transitional directions, the assumed loads on sponsons were applied at the connection points between the suspensions and sponsons, and then the reaction forces at the hardpoints were calculated.

Figure 2.10-1 shows the left front suspension and sponson modeled in APDL. Nodes *1*, *2, 3, 5, 6,* and *7* are the hardpoints. Nodes *4, 11,* and *12* are where the left front suspension components connect to the left front sponson. Figure 2.10-2 shows the left rear suspension and sponson modeled in APDL. Nodes *101, 102, 103, 105,* and *106* are hardpoints. Nodes *104, 110,* and *111* are where the left rear suspension connects to the left rear sponson. A Mathematica code showed that both of the systems are statically determinate with unique solutions.

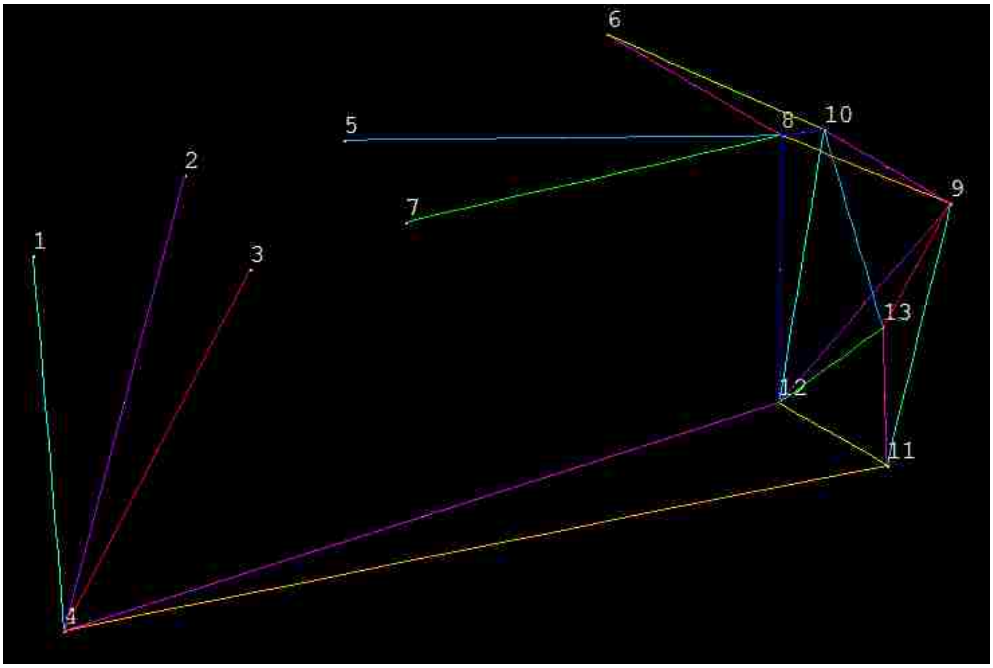

Figure 2.10-1: Left front suspension and sponson modeled as rigid links. The link between nodes 8 and 12 represents the shock absorber.

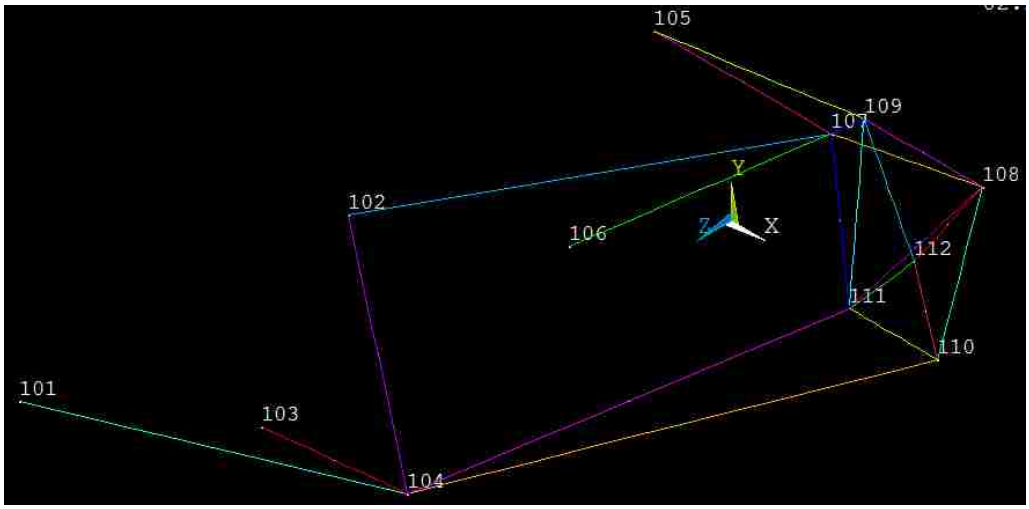

Figure 2.10-2: Left rear suspension and sponson modeled as rigid links. The link between nodes 107 and 111 represents the shock absorber.

The connection points between the suspensions and the sponsons were labeled in Figure 2.10-3. The hardpoints were labeled in Figure 2.10-4, 2.10-5, 2.10-6, and 2.10-7. The remaining of Section 2.10 uses the labels for defining the load cases.

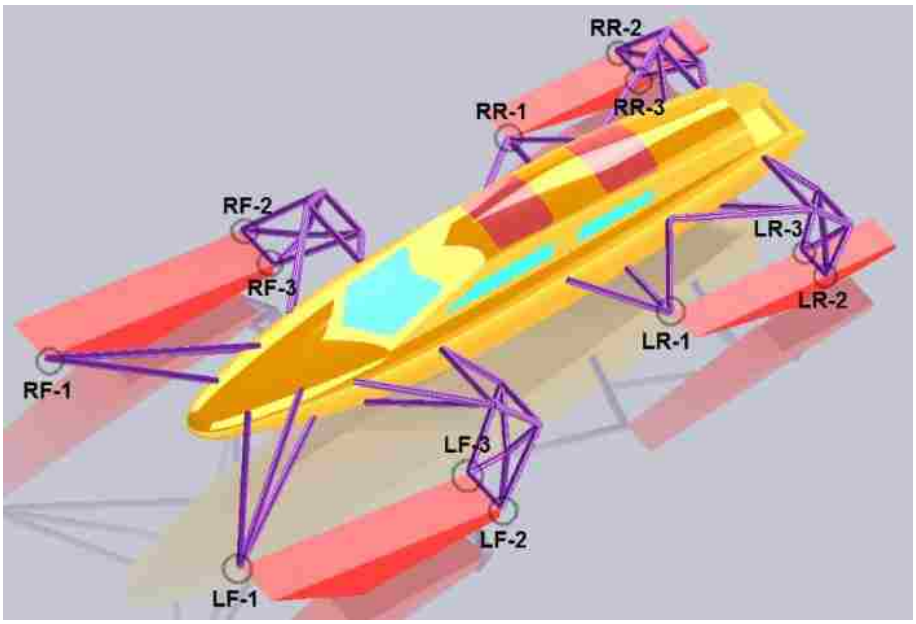

Figure 2.10-3: The points that connect the sponsons and the suspension systems, circled and labeled

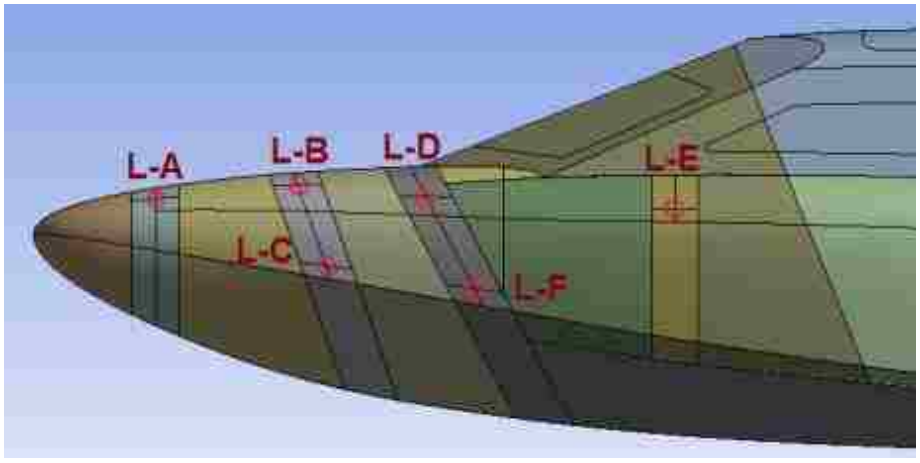

Figure 2.10-4: Left front hardpoints, circled and labeled

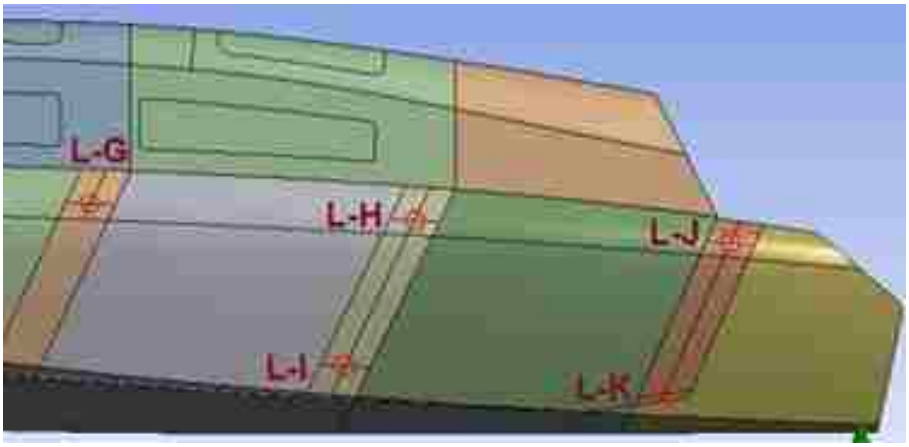

Figure 2.10-5: Left rear hardpoints, circled and labeled

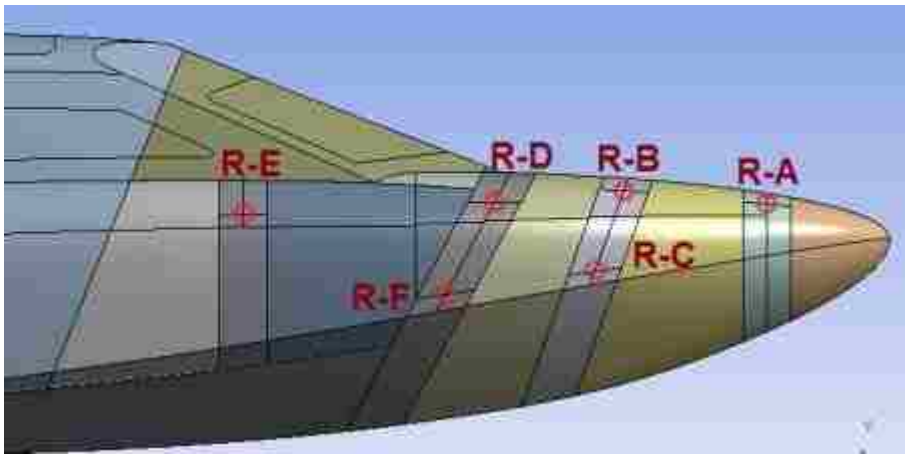

Figure 2.10-6: Right front hardpoints, circled and labeled

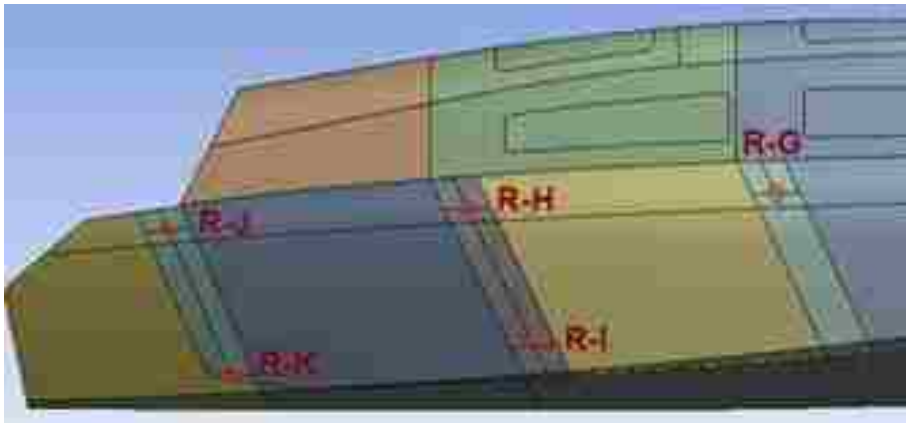

Figure 2.10-7: Right rear hardpoints, circled and labeled

II. Load Case 1: all four sponsons land on water, vertical loads only

This load case corresponds to the boat hitting a wave with all four sponsons at high speed. The total vertical load is 118000 N (10 g and total mass 1180 kg).

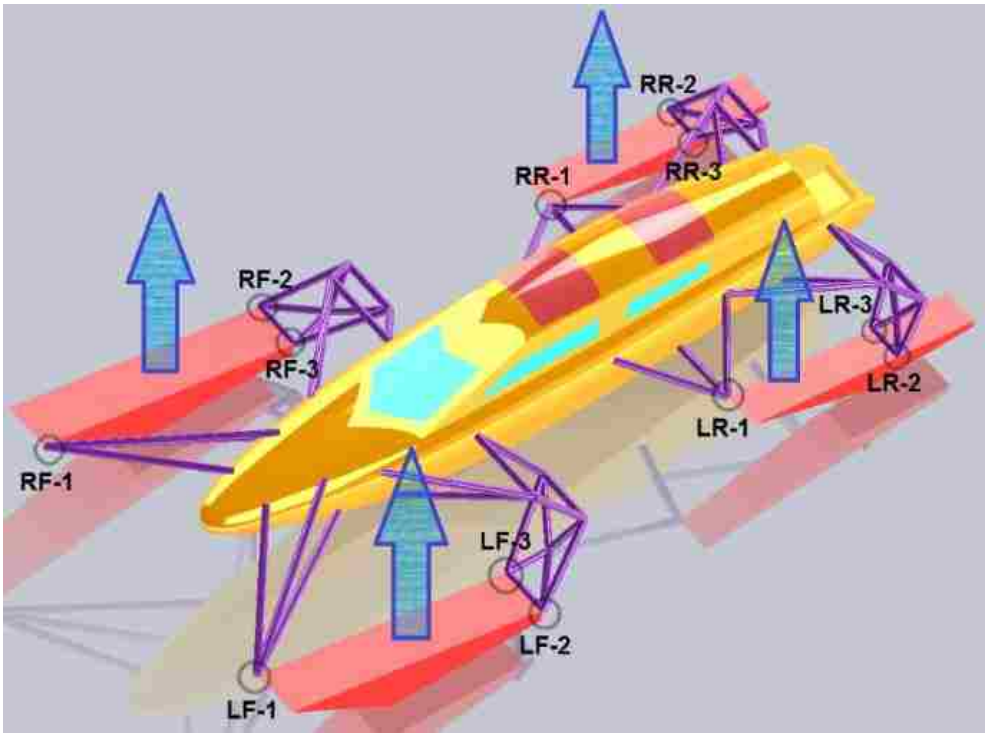

Figure 2.10-8: Illustration of Load Case 1 (the shock absorbers, which are assumed rigid for this load case, are not shown)

Load Case 1: vertical loads on all four sponsons			
	X-component of load	Y-component of load	Z-component of load
LF-1	0	9545 N	0
LF-2	0	10000 N	0
LF-3	0	10000 N	0
LR-1	0	9545 N	0
LR-2	0	10000 N	0
LR-3	0	10000 N	0
RF-1	0	9545 N	0
RF-2	0	10000 N	0
RF-3	0	10000 N	0
RR-1	0	9545 N	0
RR-2	0	10000 N	0
RR-3	0	10000 N	0

Table 2.10-1: Loads on sponsons for Load Case 1

Load Case 1: vertical loads on all four sponsons			
	X-component of load	Y-component of load	Z-component of load
L-A	23101 N	-5528.5 N	20473 N
L-B	-51567 N	15776 N	-75994 N
L-C	30623 N	-379.7 N	56955 N
L-D	-57932 N	3305.5 N	66759 N
L-E	-3119.1 N	-7000.1 N	-8918.8 N
L-F	58895 N	23372 N	-59276 N
L-G	-1419.8 N	1225.7 N	2324.4 N
L-H	-15726 N	6481.3 N	13379 N
L-I	12016 N	3049.5 N	2033 N
L-J	-23819 N	-5162.6 N	-7275.2 N
L-K	28948 N	23951 N	-10461 N
R-A	-23101 N	-5528.5 N	20473 N
R-B	51567 N	15776 N	-75994 N
R-C	-30623 N	-379.7 N	56955 N
R-D	57932 N	3305.5 N	66759 N
R-E	3119.1 N	-7000.1 N	-8918.8 N
R-F	-58895 N	23372 N	-59276 N
R-G	1419.8 N	1225.7 N	2324.4 N
R-H	15726 N	6481.3 N	13379 N
R-I	-12016 N	3049.5 N	2033 N
R-J	23819 N	-5162.6 N	-7275.2 N
R-K	-28948 N	23951 N	-10461 N

Table 2.10-2: Loads on fuselage for Load Case 1

III. Load Case 2: two front sponsons land on water, vertical loads only

This load case correspond to the boat hitting a wave with the two front sponsons at high speed. The total vertical load is 118000 N (10 g and total mass 1180 kg).

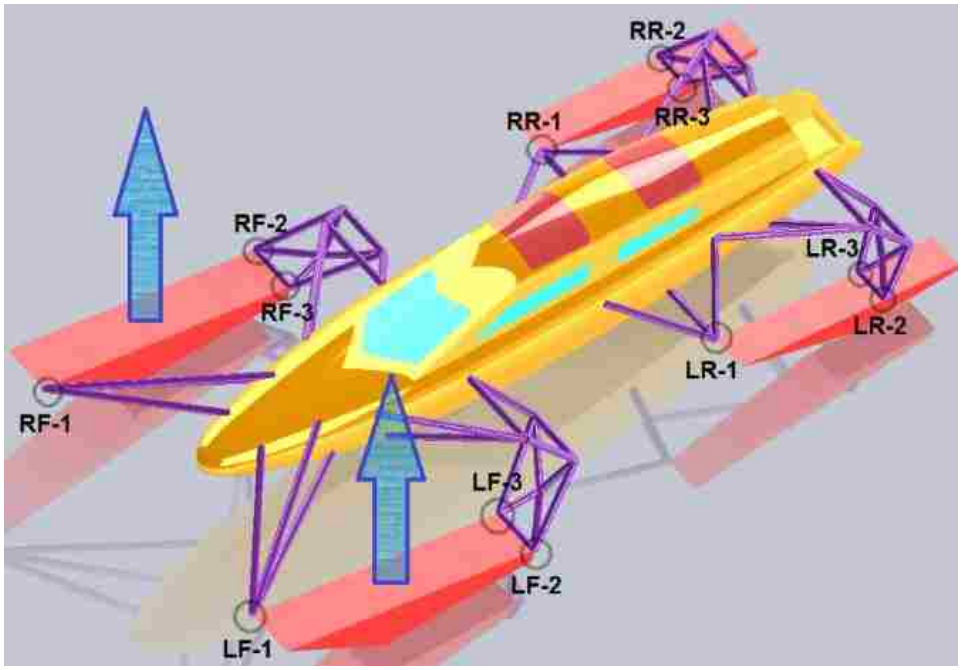

Figure 2.10-9: Illustration of Load Case 2 (the shock absorbers, which are assumed rigid for this load case, are not shown)

Load Case 2: vertical loads on the two front sponsons			
	X-component of load	Y-component of load	Z-component of load
LF-1	0	19090 N	0
LF-2	0	20000 N	0
LF-3	0	20000 N	0
LR-1	0	0	0
LR-2	0	0	0
LR-3	0	0	0
RF-1	0	19090 N	0
RF-2	0	20000 N	0
RF-3	0	20000 N	0
RR-1	0	0	0
RR-2	0	0	0
RR-3	0	0	0

Table 2.10-3: Loads on sponsons for Load Case 2

Load Case 2: vertical loads on the two front sponsons			
	X-component of load	Y-component of load	Z-component of load
L-A	46201 N	-11057 N	40947 N
L-B	-103130 N	31553 N	-151990 N
L-C	61246 N	-759.4 N	113910 N
L-D	-115860 N	6611 N	133520 N
L-E	-6238.2 N	-14000 N	-17838 N
L-F	117790 N	46743 N	-118550 N
L-G	0	0	0
L-H	0	0	0
L-I	0	0	0
L-J	0	0	0
L-K	0	0	0
R-A	-46201 N	-11057 N	40947 N
R-B	103130 N	31553 N	-151990 N
R-C	-61246 N	-759.4 N	113910 N
R-D	115860 N	6611 N	133520 N
R-E	6238.2 N	-14000 N	-17838 N
R-F	-117790 N	46743 N	-118550 N
R-G	0	0	0
R-H	0	0	0
R-I	0	0	0
R-J	0	0	0
R-K	0	0	0

Table 2.10-4: Loads on fuselage for Load Case 2

IV. Load Case 3: two rear sponsons land on water, vertical loads only

This load case corresponds to the boat hitting a wave with the two rear sponsons at high speed. The total vertical load is 118000 N (10 g and total mass 1180 kg).

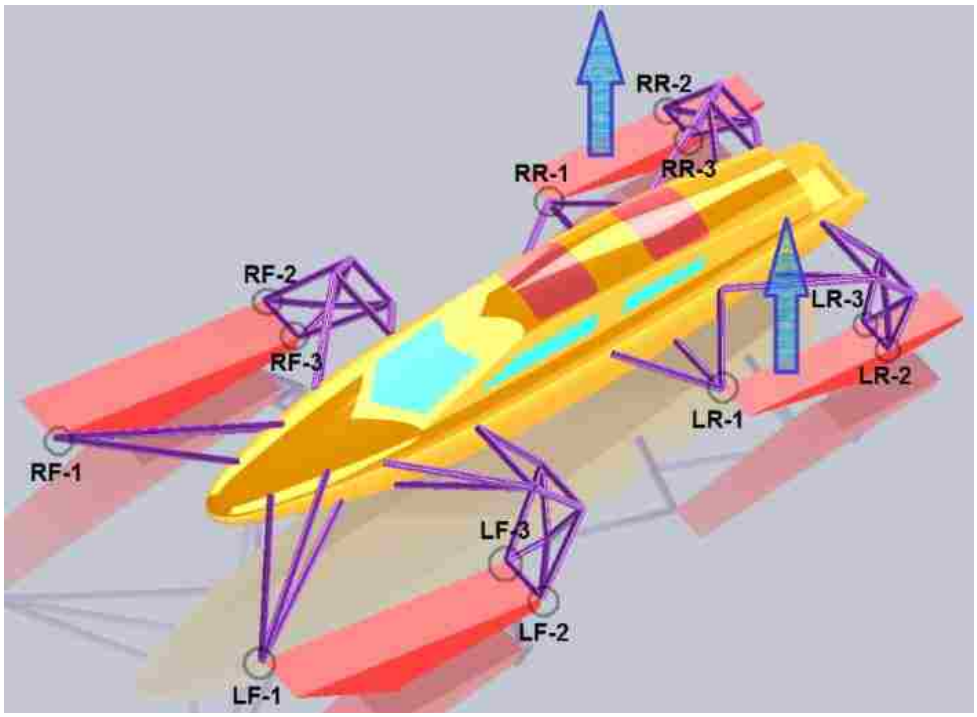

Figure 2.10-10: Illustration of Load Case 3 (the shock absorbers, which are assumed rigid for this load case, are not shown)

Load Case 3: vertical loads on the two rear sponsons			
	X-component of load	Y-component of load	Z-component of load
LF-1	0	0	0
LF-2	0	0	0
LF-3	0	0	0
LR-1	0	19090 N	0
LR-2	0	20000 N	0
LR-3	0	20000 N	0
RF-1	0	0	0
RF-2	0	0	0
RF-3	0	0	0
RR-1	0	19090 N	0
RR-2	0	20000 N	0
RR-3	0	20000 N	0

Table 2.10-5: Loads on sponsons for Load Case 3

Load Case 3: vertical loads on the two rear sponsons			
	X-component of load	Y-component of load	Z-component of load
L-A	0	0	0
L-B	0	0	0
L-C	0	0	0
L-D	0	0	0
L-E	0	0	0
L-F	0	0	0
L-G	-2839.7 N	2451.3 N	4648.7 N
L-H	-31451 N	12963 N	26757 N
L-I	24032 N	6099.1 N	4066.1 N
L-J	-47638 N	-10325 N	-14550 N
L-K	57897 N	47902 N	-20922 N
R-A	0	0	0
R-B	0	0	0
R-C	0	0	0
R-D	0	0	0
R-E	0	0	0
R-F	0	0	0
R-G	2839.7 N	2451.3 N	4648.7 N
R-H	31451 N	12963 N	26757 N
R-I	-24032 N	6099.1 N	4066.1 N
R-J	47638 N	-10325 N	-14550 N
R-K	-57897 N	47902 N	-20922 N

Table 2.10-6: Loads on fuselage for Load Case 3

V. Load Case 4: left front and right rear sponsons land on water, vertical loads only

This load case corresponds to the boat hitting a wave with the left front and the right rear sponsons at high speed. The total vertical load is 118000 N (10 g and total mass 1180 kg).

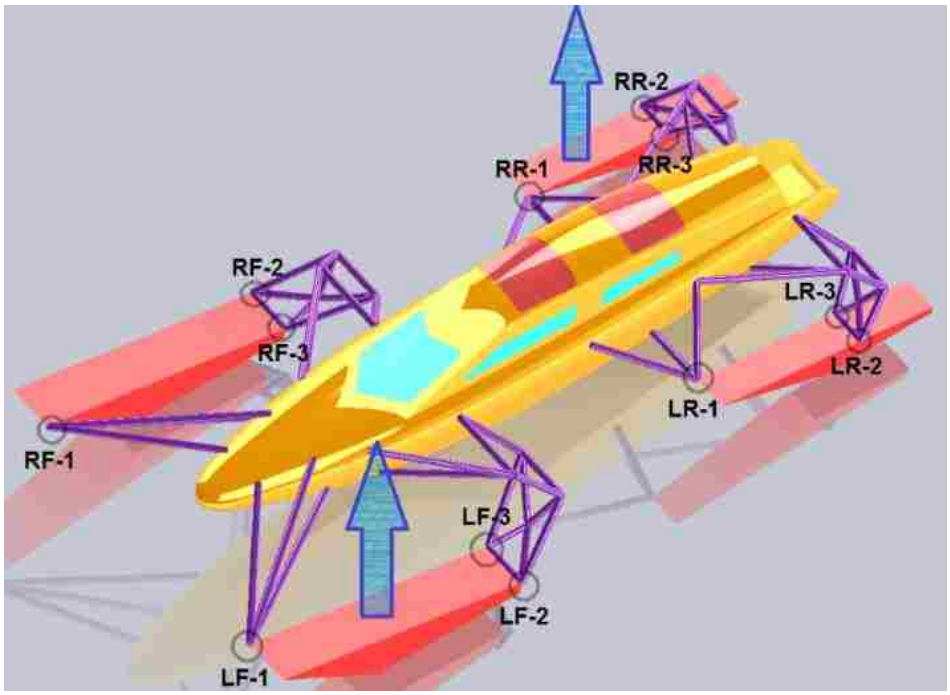

Figure 2.10-11: Illustration of Load Case 4 (the shock absorbers, which are assumed rigid for this load case, are not shown)

Load Case 4: vertical loads on the left front and right rear sponsons			
	X-component of load	Y-component of load	Z-component of load
LF-1	0	19090 N	0
LF-2	0	20000 N	0
LF-3	0	20000 N	0
LR-1	0	0	0
LR-2	0	0	0
LR-3	0	0	0
RF-1	0	0	0
RF-2	0	0	0
RF-3	0	0	0
RR-1	0	19090 N	0
RR-2	0	20000 N	0
RR-3	0	20000 N	0

Table 2.10-7: Loads on sponsons for Load Case 4

Load Case 4: vertical loads on the left front and right rear sponsons			
	X-component of load	Y-component of load	Z-component of load
L-A	46201 N	-11057 N	40947 N
L-B	-103130 N	31553 N	-151990 N
L-C	61246 N	-759.4 N	113910 N
L-D	-115860 N	6611 N	133520 N
L-E	-6238.2 N	-14000 N	-17838 N
L-F	117790 N	46743 N	-118550 N
L-G	0	0	0
L-H	0	0	0
L-I	0	0	0
L-J	0	0	0
L-K	0	0	0
R-A	0	0	0
R-B	0	0	0
R-C	0	0	0
R-D	0	0	0
R-E	0	0	0
R-F	0	0	0
R-G	2839.7 N	2451.3 N	4648.7 N
R-H	31451 N	12963 N	26757 N
R-I	-24032 N	6099.1 N	4066.1 N
R-J	47638 N	-10325 N	-14550 N
R-K	-57897 N	47902 N	-20922 N

Table 2.10-8: Loads on fuselage for Load Case 4

VI. Load Case 5: two left sponsons land on water, horizontal loads only

This load case corresponds for example to the boat yawing and hitting a wave with the two left sponsons at high speed. The total horizontal load is 236000 N (20 g and total mass 1180 kg).

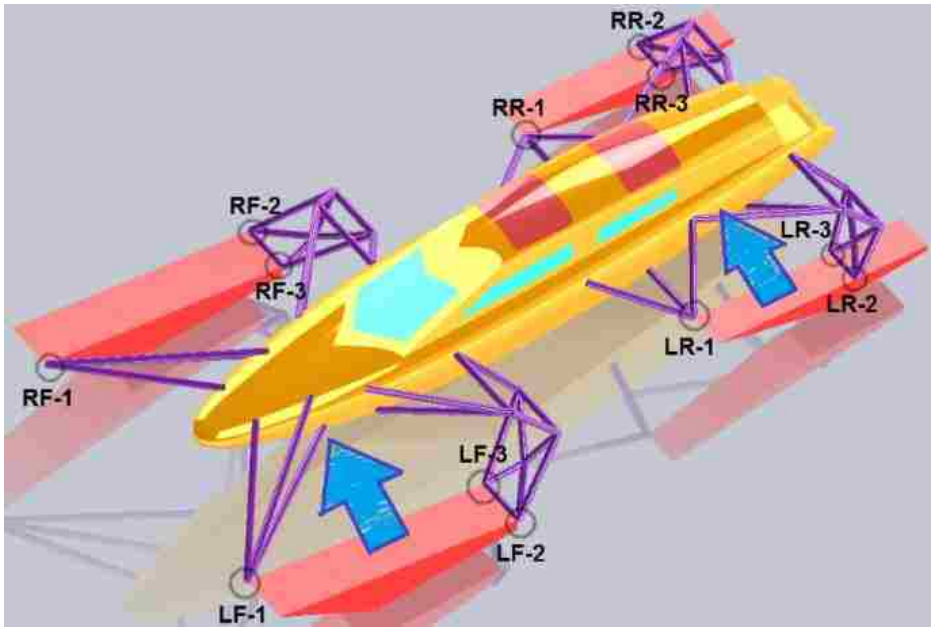

Figure 2.10-12: Illustration of Load Case 5 (the shock absorbers, which are assumed rigid for this load case, are not shown)

Load Case 5: horizontal loads on the two left sponsons			
	X-component of load	Y-component of load	Z-component of load
LF-1	0	0	0
LF-2	-59090 N	0	0
LF-3	-59090 N	0	0
LR-1	0	0	0
LR-2	-59090 N	0	0
LR-3	-59090 N	0	0
RF-1	0	0	0
RF-2	0	0	0
RF-3	0	0	0
RR-1	0	0	0
RR-2	0	0	0
RR-3	0	0	0

Table 2.10-9: Loads on sponsons for Load Case 5

Load Case 5: horizontal loads on the two left sponsons			
	X-component of load	Y-component of load	Z-component of load
L-A	-119500 N	28599 N	-105910 N
L-B	94198 N	-28819 N	138820 N
L-C	-17694 N	219.39 N	-32908 N
L-D	390500 N	-22281 N	-450000 N
L-E	-186850 N	132930 N	169370 N
L-F	-278830 N	-110650 N	280630 N
L-G	-5380.6 N	4644.8 N	8808.4 N
L-H	55660 N	-6203.8 N	-141720 N
L-I	-32258 N	-8186.8 N	-5457.9 N
L-J	-54595 N	77264 N	108880 N
L-K	-81606 N	-67519 N	29489 N
R-A	0	0	0
R-B	0	0	0
R-C	0	0	0
R-D	0	0	0
R-E	0	0	0
R-F	0	0	0
R-G	0	0	0
R-H	0	0	0
R-I	0	0	0
R-J	0	0	0
R-K	0	0	0

Table 2.10-10: Loads on fuselage for Load Case 5

VII. Load Case 6: the left front sponson lands on water, horizontal loads only

This load case corresponds to the boat hitting a wave horizontally with the left front sponson at high speed. The total horizontal load is 236000 N (20 g and total mass 1180 kg).

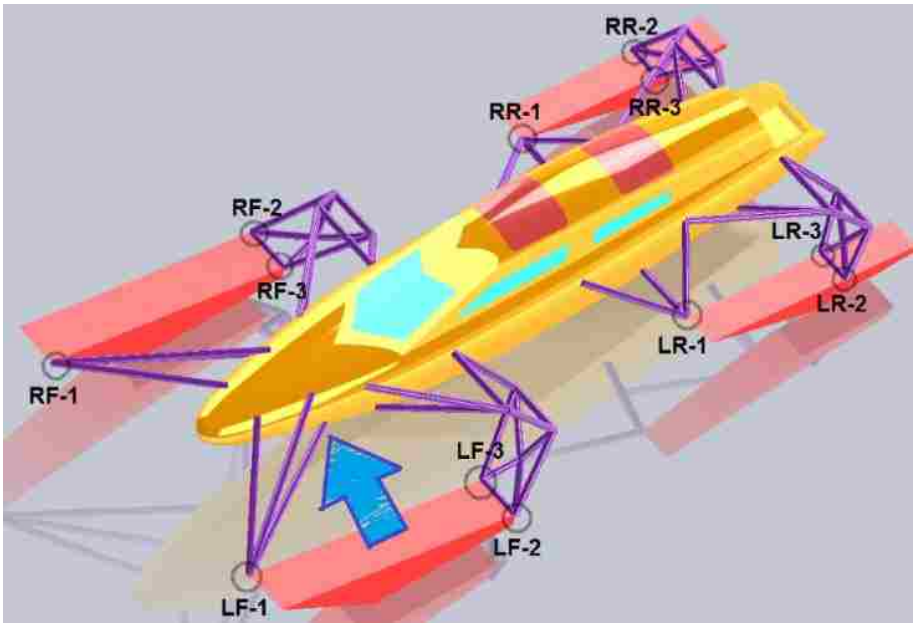

Figure 2.10-13: Illustration of Load Case 6 (the shock absorbers, which are assumed rigid for this load case, are not shown)

Load Case 6: horizontal loads on the left front sponson			
	X-component of load	Y-component of load	Z-component of load
LF-1	0	0	0
LF-2	-118180 N	0	0
LF-3	-118180 N	0	0
LR-1	0	0	0
LR-2	0	0	0
LR-3	0	0	0
RF-1	0	0	0
RF-2	0	0	0
RF-3	0	0	0
RR-1	0	0	0
RR-2	0	0	0
RR-3	0	0	0

Table 2.10-11: Loads on sponsons for Load Case 6

Load Case 6: horizontal loads on the left front sponson			
	X-component of load	Y-component of load	Z-component of load
L-A	-239000 N	57199 N	-211820 N
L-B	188400 N	-57638 N	277640 N
L-C	-35387 N	438.77 N	-65816 N
L-D	781000 N	-44563 N	-900000 N
L-E	-373710 N	265860 N	338730 N
L-F	-557660 N	-221300 N	561270 N
L-G	0	0	0
L-H	0	0	0
L-I	0	0	0
L-J	0	0	0
L-K	0	0	0
R-A	0	0	0
R-B	0	0	0
R-C	0	0	0
R-D	0	0	0
R-E	0	0	0
R-F	0	0	0
R-G	0	0	0
R-H	0	0	0
R-I	0	0	0
R-J	0	0	0
R-K	0	0	0

Table 2.10-12: Loads on fuselage for Load Case 6

VIII. Load Case 7: the left rear sponson lands on water, horizontal loads only

This load case corresponds to the boat hitting a wave horizontally with the left rear sponson at high speed. The total horizontal load is 236000 N (20 g and total mass 1180 kg).

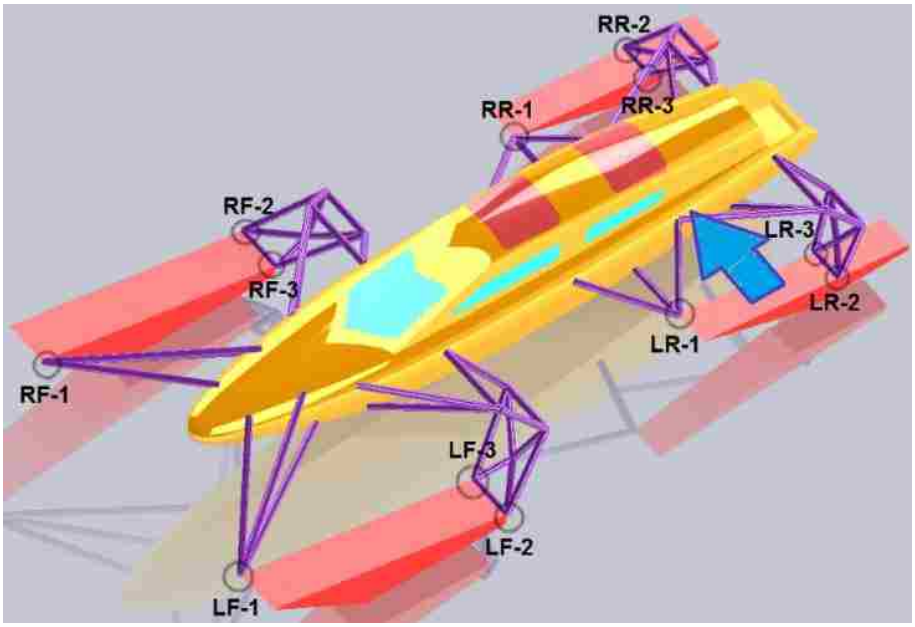

Figure 2.10-14: Illustration of Load Case 7 (the shock absorbers, which are assumed rigid for this load case, are not shown)

Load Case 7: horizontal loads on the left rear sponson			
	X-component of load	Y-component of load	Z-component of load
LF-1	0	0	0
LF-2	0	0	0
LF-3	0	0	0
LR-1	0	0	0
LR-2	-118180 N	0	0
LR-3	-118180 N	0	0
RF-1	0	0	0
RF-2	0	0	0
RF-3	0	0	0
RR-1	0	0	0
RR-2	0	0	0
RR-3	0	0	0

Table 2.10-13: Loads on sponsons for Load Case 7

Load Case 7: horizontal loads on the left rear sponson			
	X-component of load	Y-component of load	Z-component of load
L-A	0	0	0
L-B	0	0	0
L-C	0	0	0
L-D	0	0	0
L-E	0	0	0
L-F	0	0	0
L-G	-10761 N	9289.5 N	17617 N
L-H	111320 N	-12408 N	-283450 N
L-I	-64516 N	-16374 N	-10916 N
L-J	-109190 N	154530 N	217770 N
L-K	-163210 N	-135040 N	58979 N
R-A	0	0	0
R-B	0	0	0
R-C	0	0	0
R-D	0	0	0
R-E	0	0	0
R-F	0	0	0
R-G	0	0	0
R-H	0	0	0
R-I	0	0	0
R-J	0	0	0
R-K	0	0	0

Table 2.10-14: Loads on fuselage for Load Case 7

3. RESULTS AND OBSERVATIONS

A Viable Design of Bulkhead/Frame Layups and Window Panel Thicknesses

The final layup determined by the FEA-based analyses is shown in the figures below. The strain contour plots shown in the following sections are based on this layup.

I. Window panel thicknesses

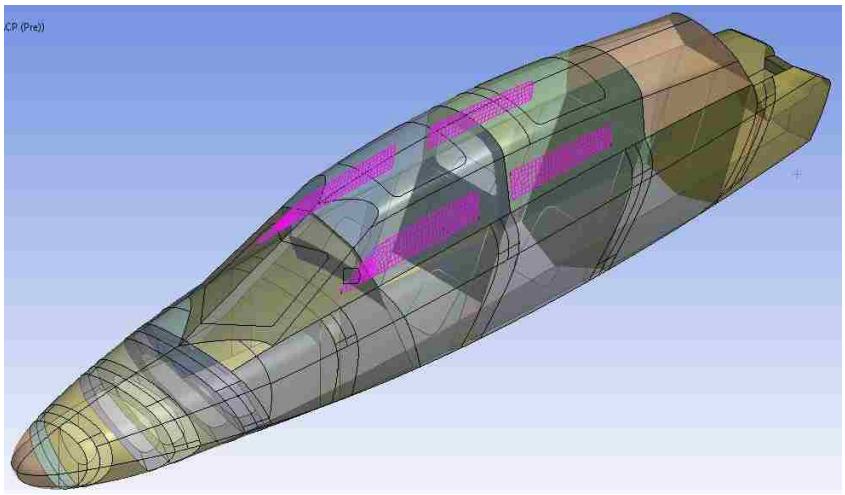

Figure 3.1-1: 12.7 mm PC window panels highlighted in purple

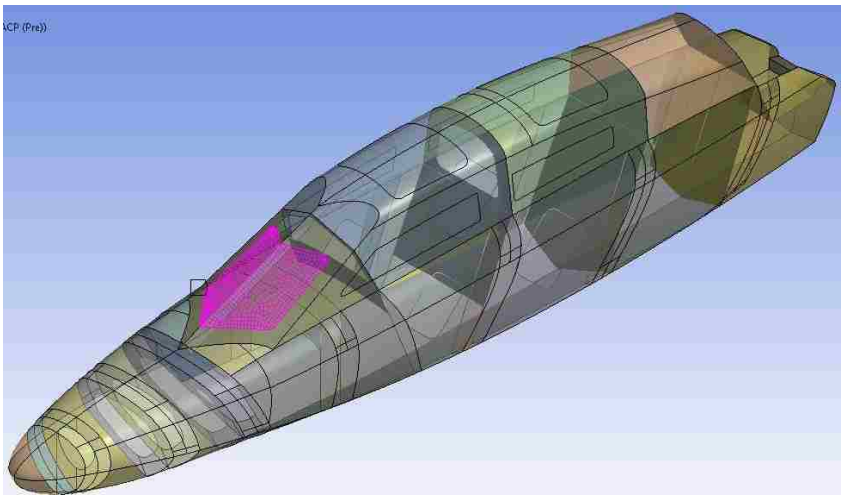

Figure 3.1-2: 15.9 mm PC window panels highlighted in purple

II. Layups of the cockpit frames and transverse bulkheads

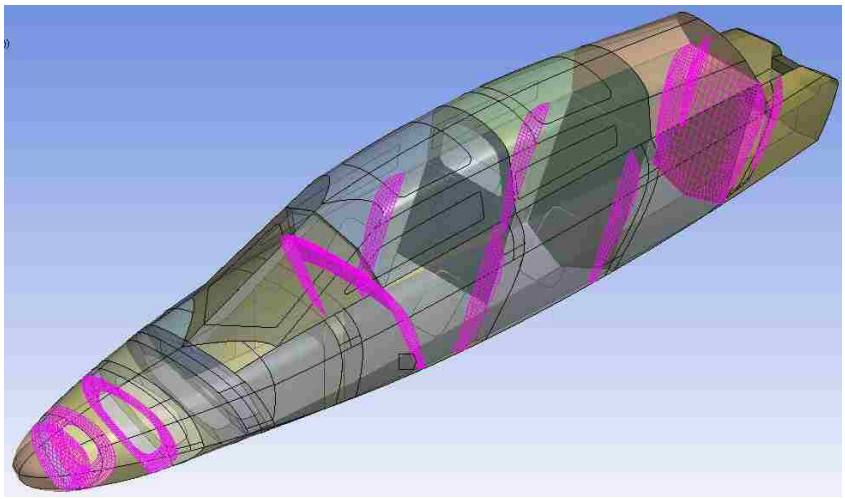

Figure 3.1-3: Bulkheads and frames with (45, -45, 0, 90) skins on each side of a 10mm H80 core highlighted in purple

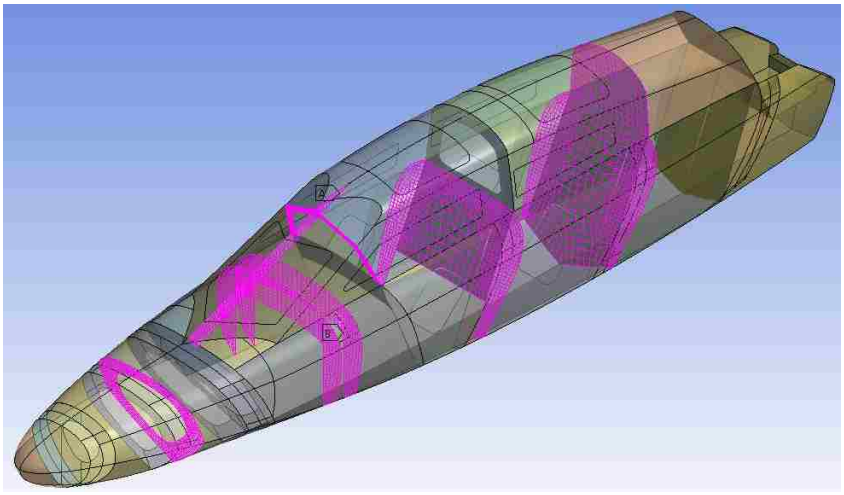

Figure 3.1-4: Bulkheads and frames with $(45, -45, 0, 90)_2$ skins on each side of a 10mm H80 core highlighted in purple

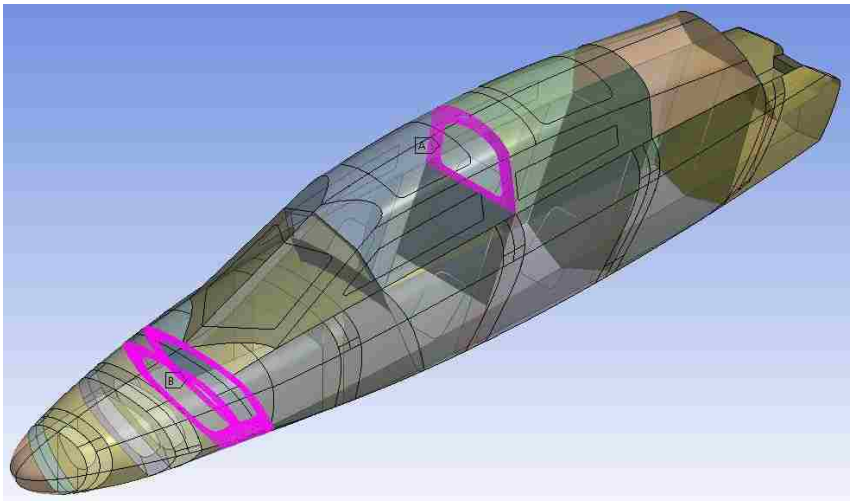

Figure 3.1-5: Bulkheads and frames with $(45, -45, 0, 90)_4$ skins on each side of a 15mm H80 core highlighted in purple

III. Layups of the longitudinal bulkheads

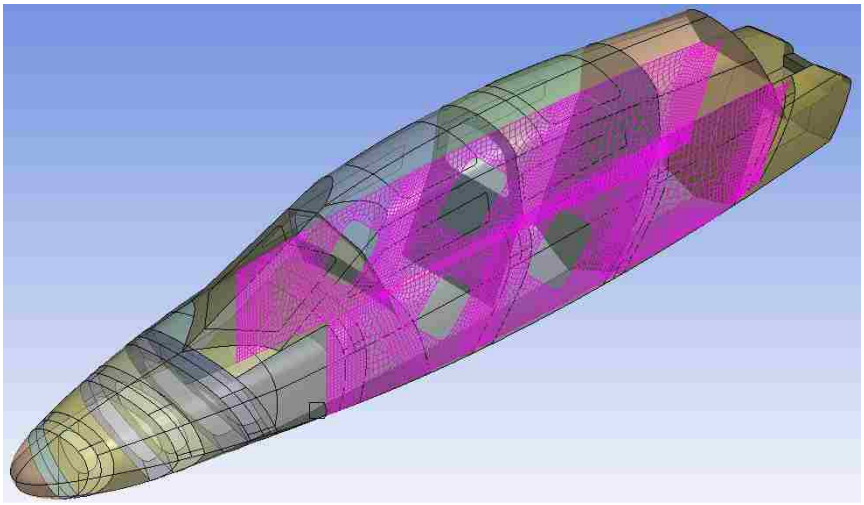

Figure 3.1-6: Longitudinal bulkheads with (45, -45) skins on each side of a 10mm H80 core highlighted in purple

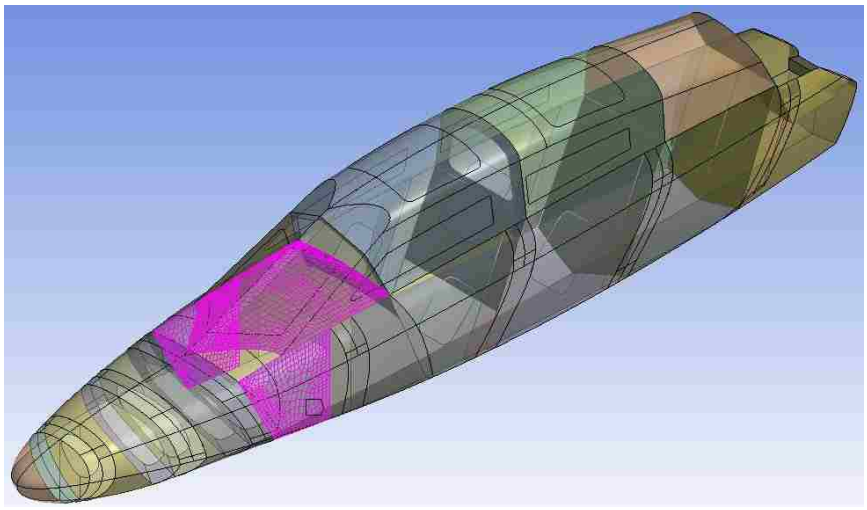

Figure 3.1-7: Longitudinal bulkheads with $(45, -45)_2$ skins on each side of a 10mm H80 core highlighted in purple

Results for Crash Scenario – Front under Hydrodynamic Load

The internal bulkheads and frames as well as the front window panels were overall strong enough to withstand the loads in this crash scenario. Some grey spots (excessive compression) shown in Figure 3.2-1 may need some further reinforcements.

The strain contour plots for the external composite structure, however, suggest that the composite structure at the front end of cockpit needs some serious reinforcement. Figure 3.2-5 and Figure 3.2-6 indicates that even the CFRP compressive strains at elements relatively far away from sharp corners substantially exceeded the failure criteria. Figure 3.2-7 and Figure 3.2-8 also suggests severe risk of core failure at the same areas.

I. Contour plots for the internal structure:

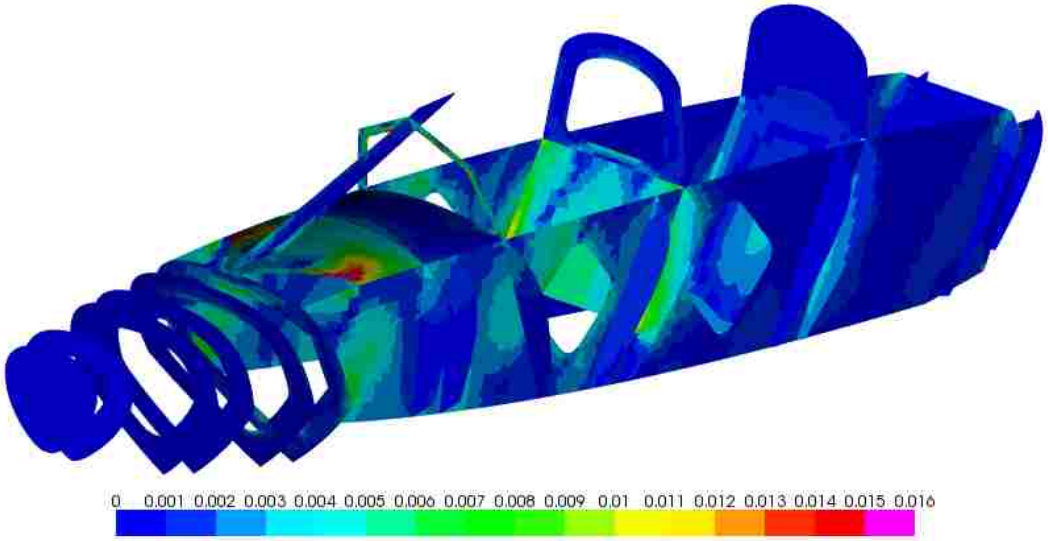

Figure 3.2-1: Maximum principal strains of CFRP, internal structure, front under hydrodynamic load

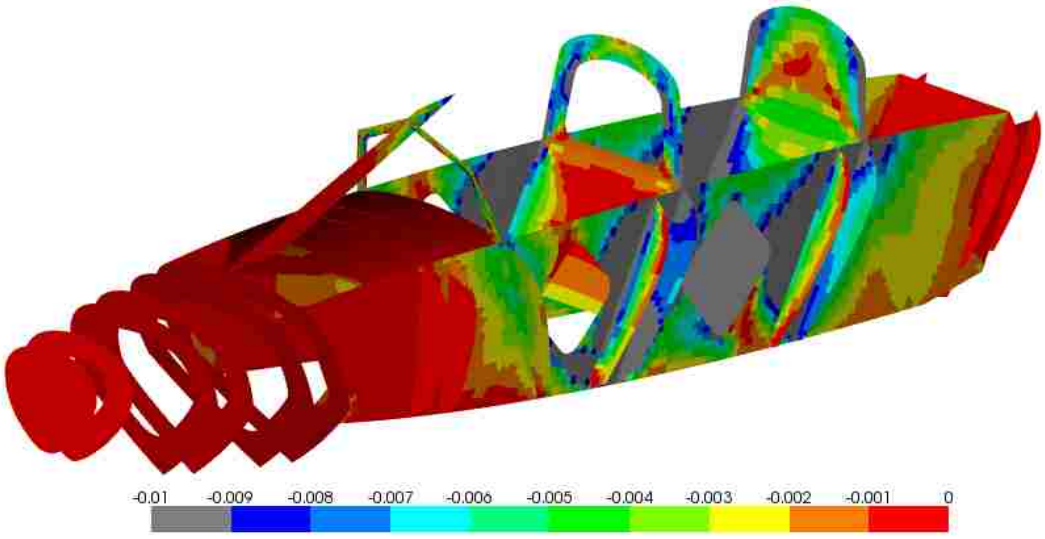

Figure 3.2-2: Minimum principal strains of CFRP, internal structure, front under hydrodynamic load

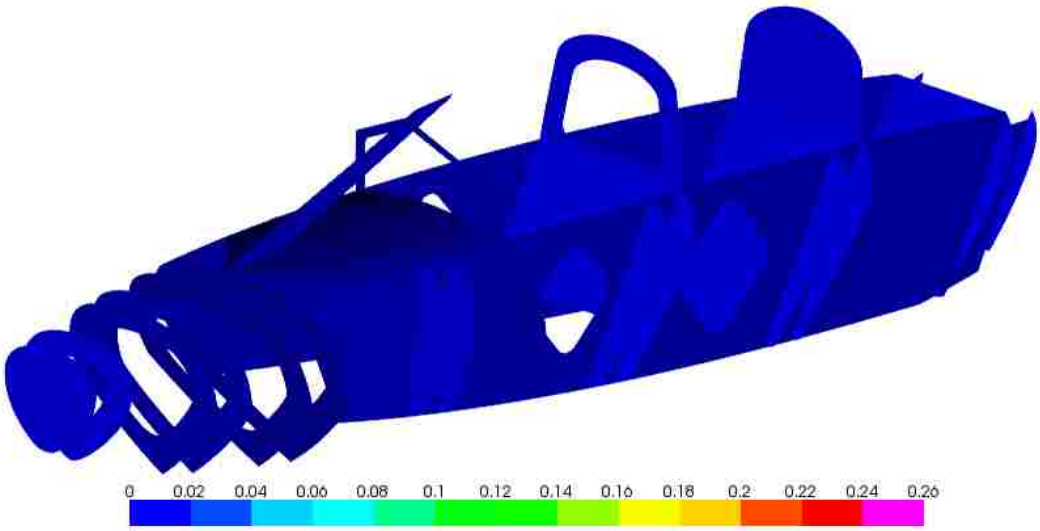

Figure 3.2-3: Out-of-plane shear strains of cores, internal structure, front under hydrodynamic load

II. Contour plots for the external composite structure:

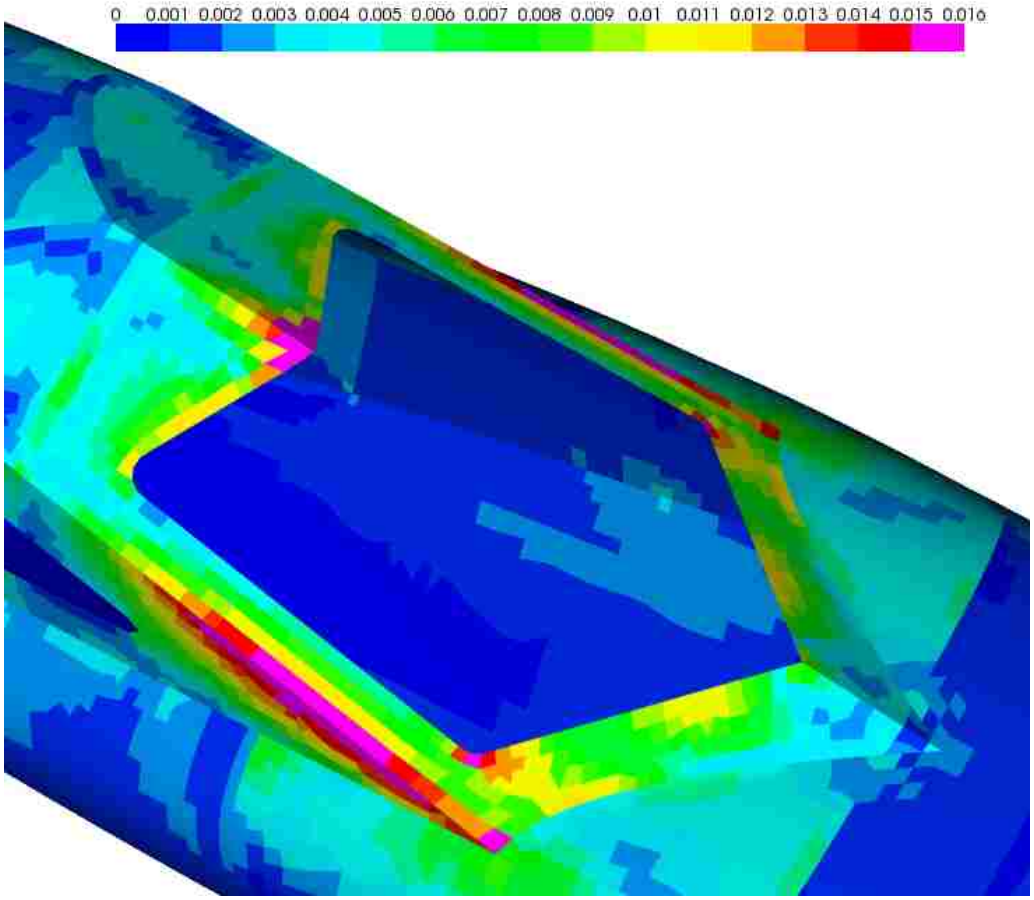

Figure 3.2-4: Maximum principal strains of CFRP, external composite structure, front under hydrodynamic load

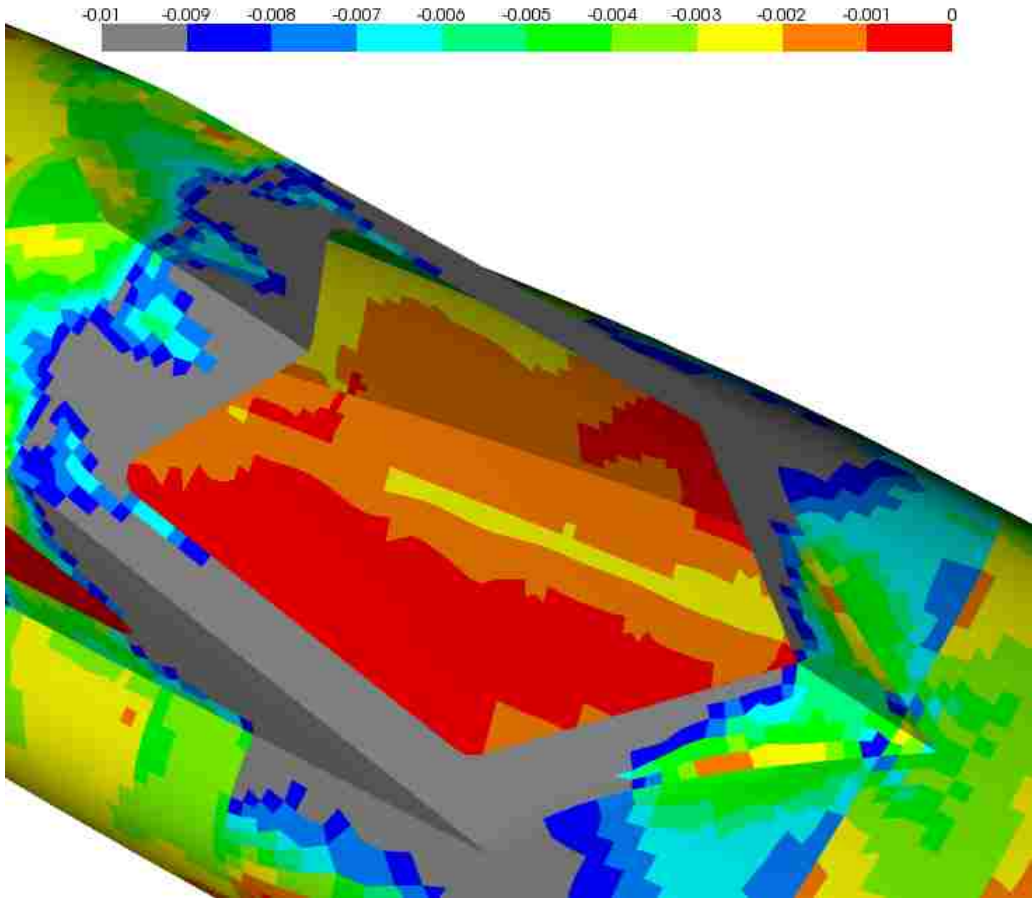

Figure 3.2-5: Minimum principal strains of CFRP, external composite structure, front under hydrodynamic load, very large strains shown in grey

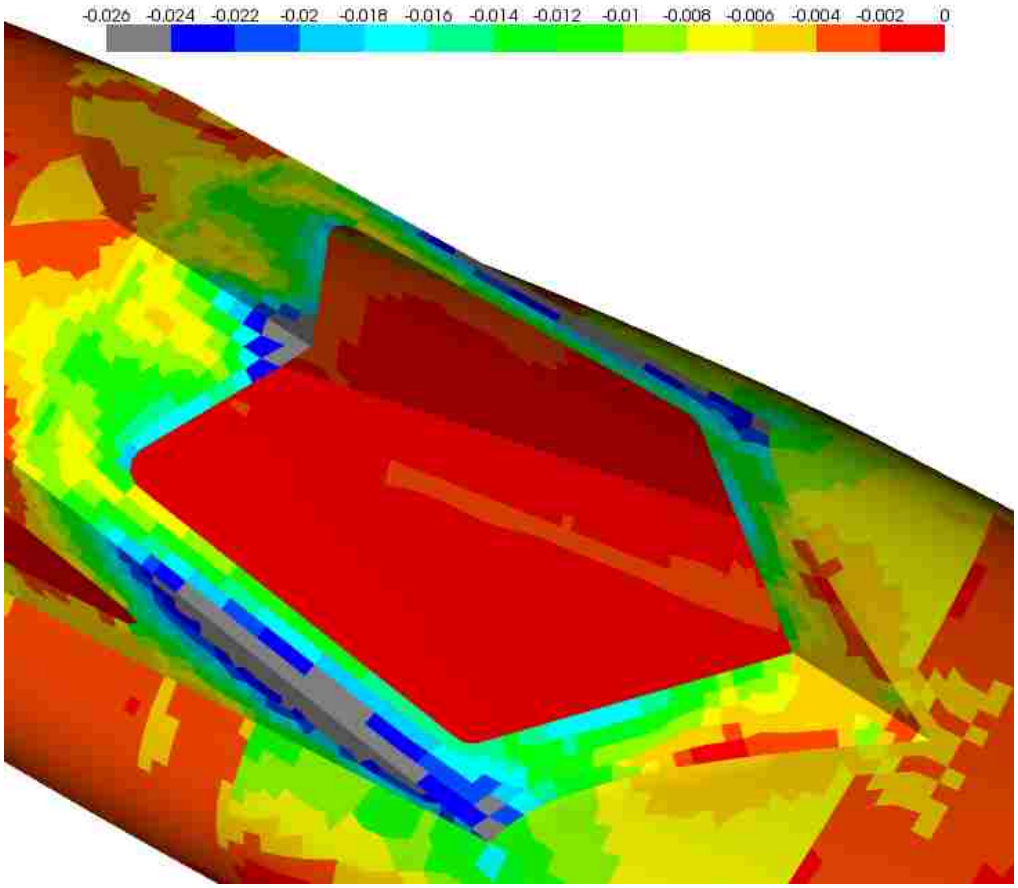

Figure 3.2-6: Minimum principal strains of CFRP, external composite structure, front under hydrodynamic load, showing the full spectrum of values

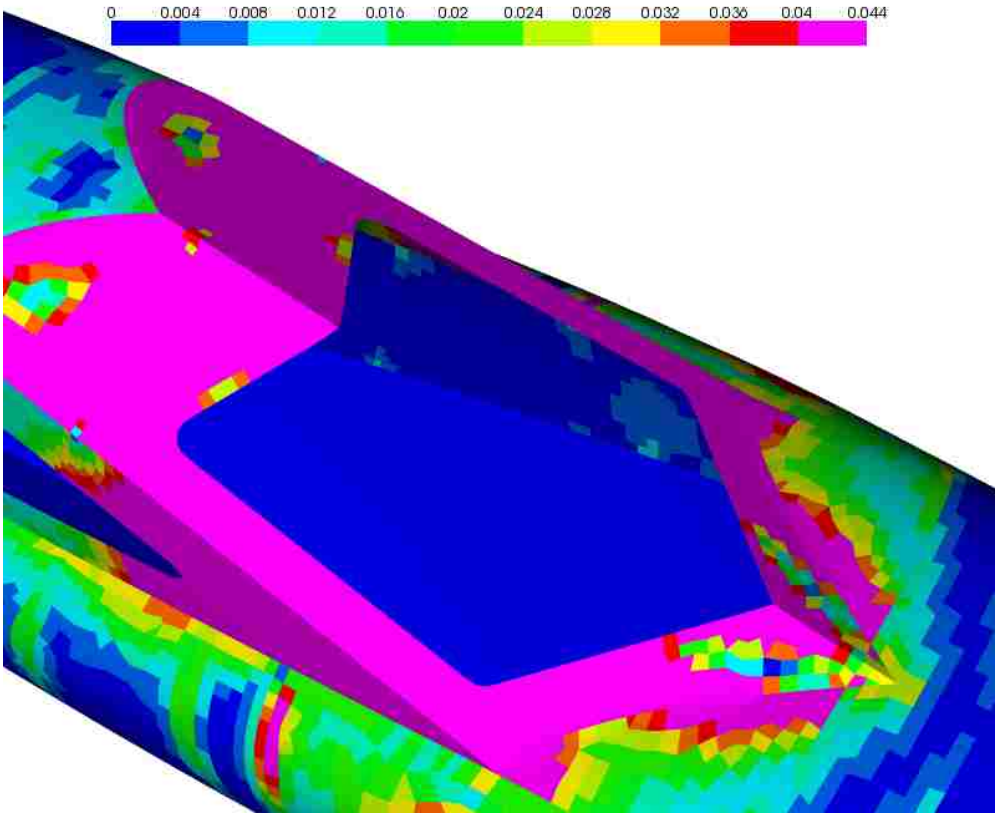

Figure 3.2-7: Out-of-plane shear strains of cores, external composite structure, front under hydrodynamic load, very large strains shown in violet

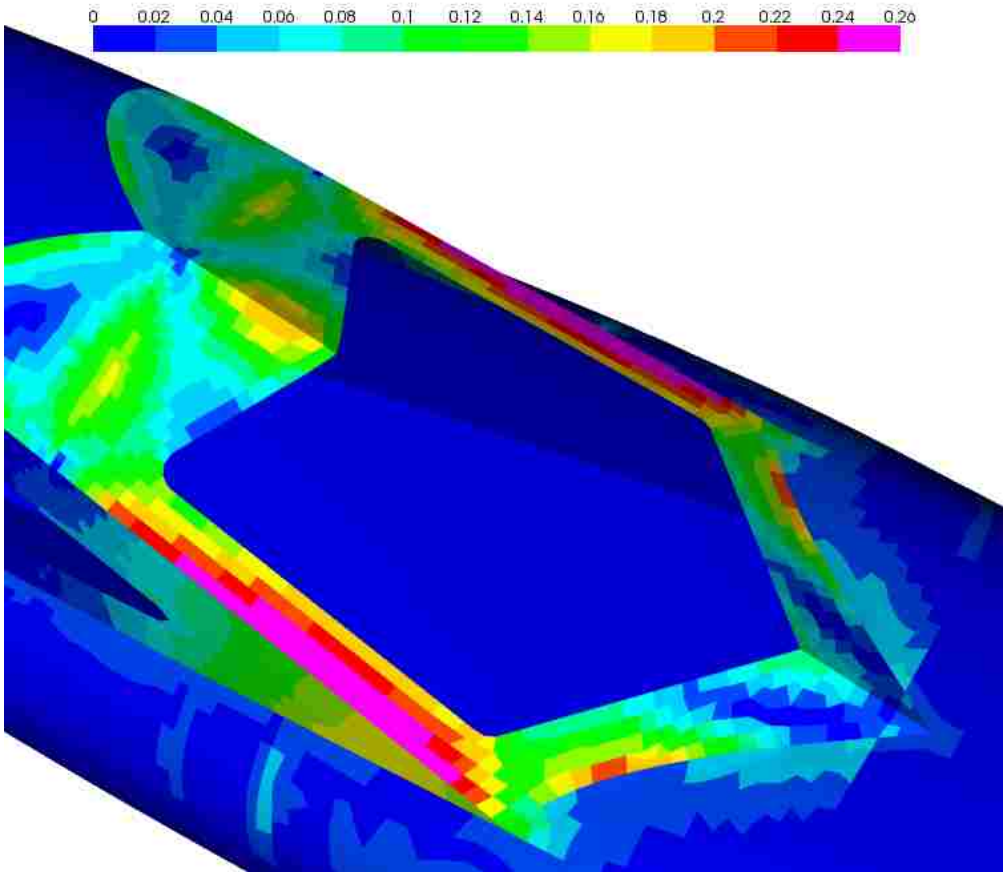

Figure 3.2-8: Out-of-plane shear strains of cores, external composite structure, front under hydrodynamic load, showing the full spectrum of values

III. Contour plots for the front PC window panels:

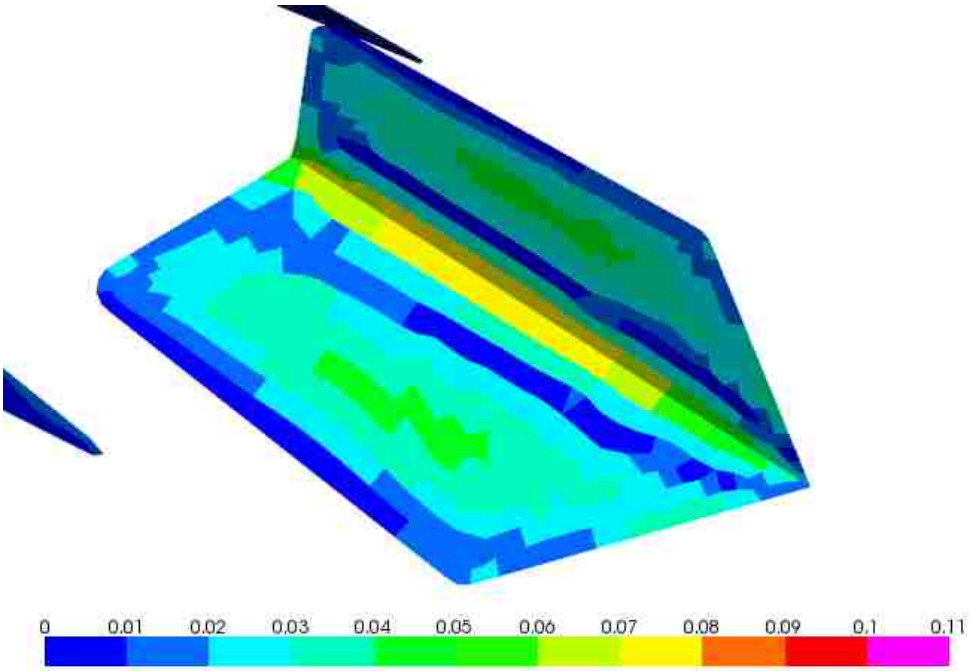

Figure 3.2-9: Maximum principal strains of PC, front under hydrodynamic load

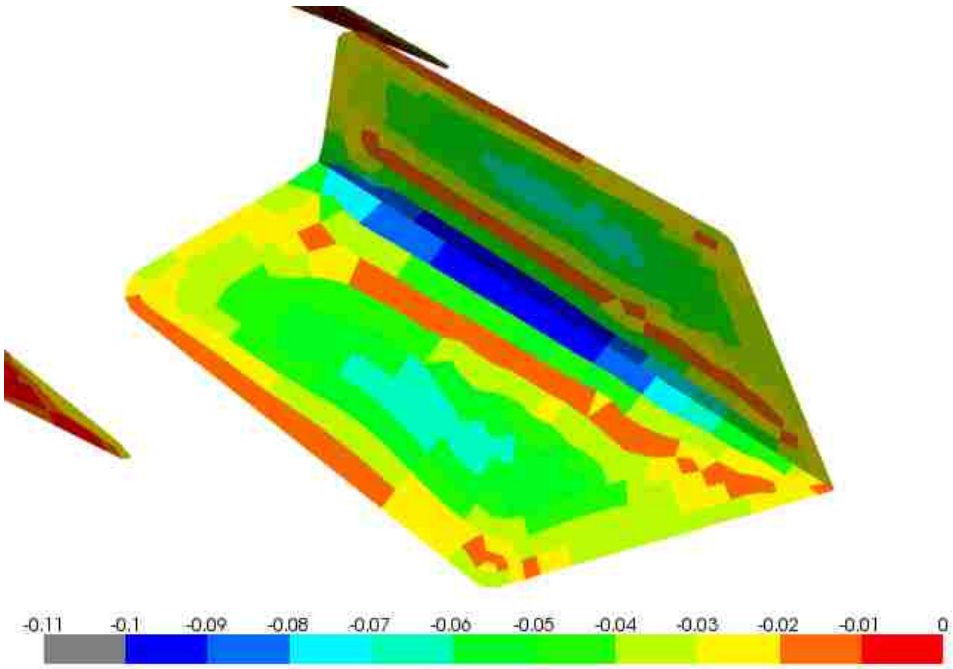

Figure 3.2-10: Minimum principal strains of PC, front under hydrodynamic load

Results for Crash Scenario –Top under Hydrodynamic Load

For the internal bulkheads and frames, the small violet spots (excessive tension) in Figure 3.3-1 and grey spots (excessive compression) in Figure 3.3-2 indicate that local reinforcements might be needed. More importantly, Figure 3.3-2 shows significant grey areas where the longitudinal shear panels join the transverse bulkheads, this suggests that the shear panels at these locations were also taking the vertical loads transferred through the neighboring transverse bulkheads so the future task on reinforcing these areas must take this as well as the complex structure of the actual joints of composite panels into account. Figure 3.3-2 also shows a large grey area on the lower part of the transverse bulkhead where the second pilot would sit. This area will be constructed differently for the real boat, with discrete attachments to an off-the-shelf commercial racing seat.

Judging from Figure 3.3-5 and Figure 3.3-6, the outside skin of the top of the cockpit, which was in compression in this case, needs to be reinforced with some extra plies of CFRP. Figure 3.3-7 and Figure 3.3-8 also suggest that local reinforcements at the

locations where the cockpit frames join the cockpit external structure would be necessary to prevent core failure.

I. Contour plots for the internal composite structure:

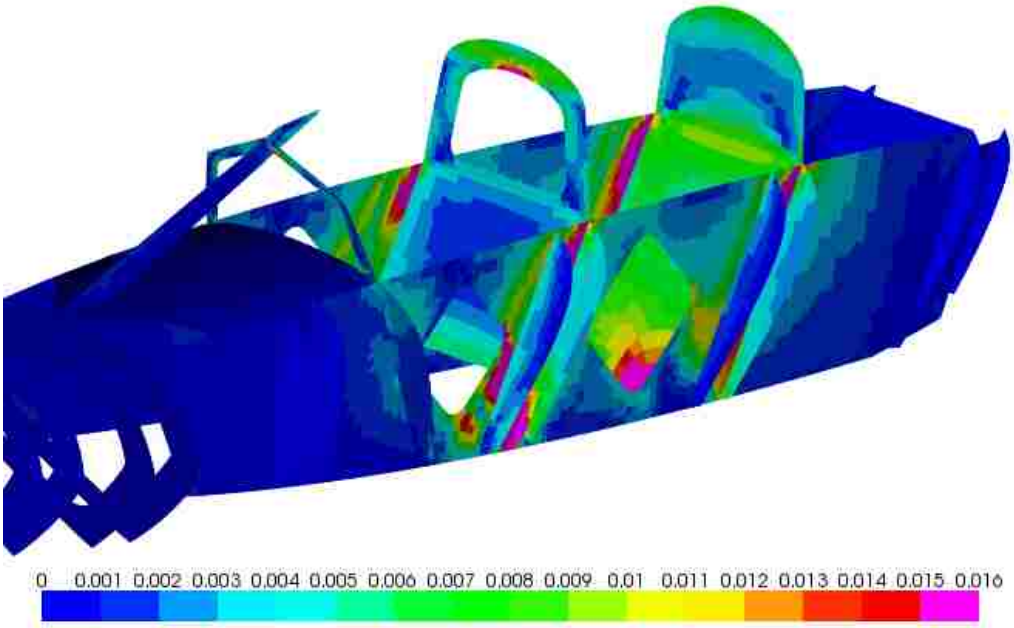

Figure 3.3-1: Maximum principal strains of CFRP, internal structure, top under hydrodynamic load

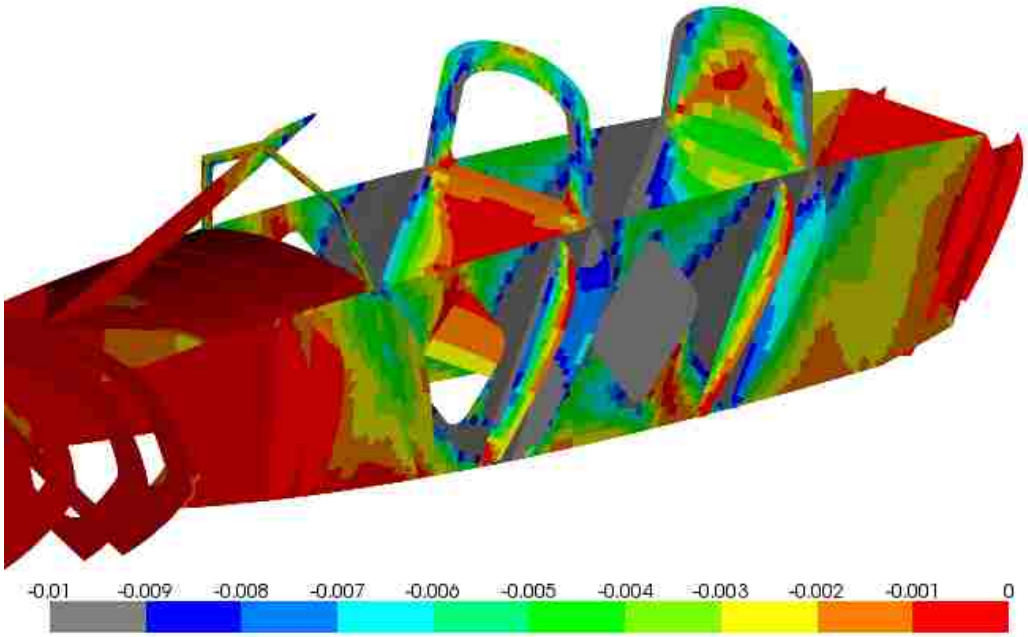

Figure 3.3-2: Minimum principal strains of CFRP, internal structure, top under hydrodynamic load

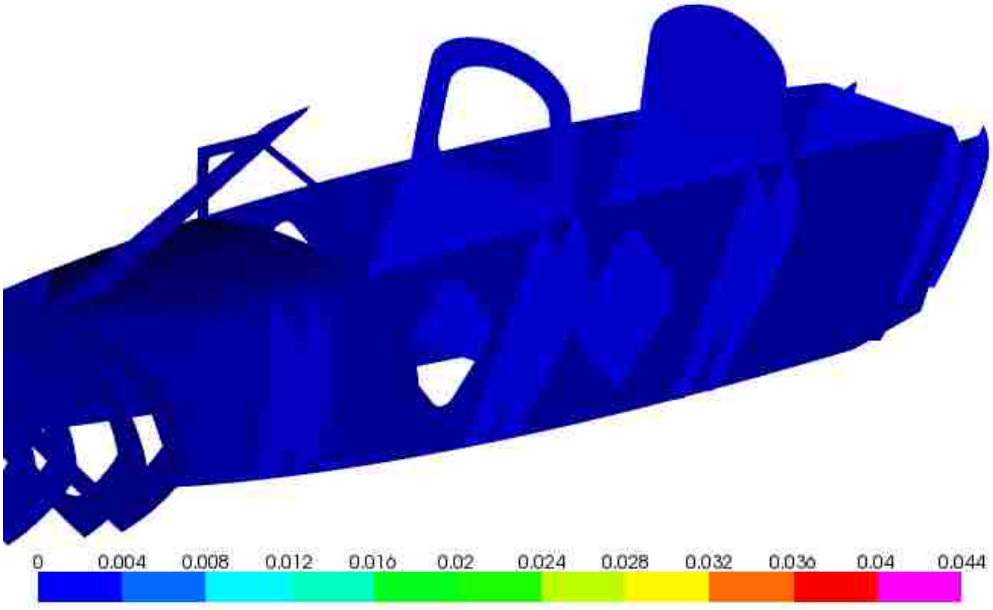

Figure 3.3-3: Out-of-plane shear strains of cores, internal structure, top under hydrodynamic load

II. Contour plots for the external composite structure:

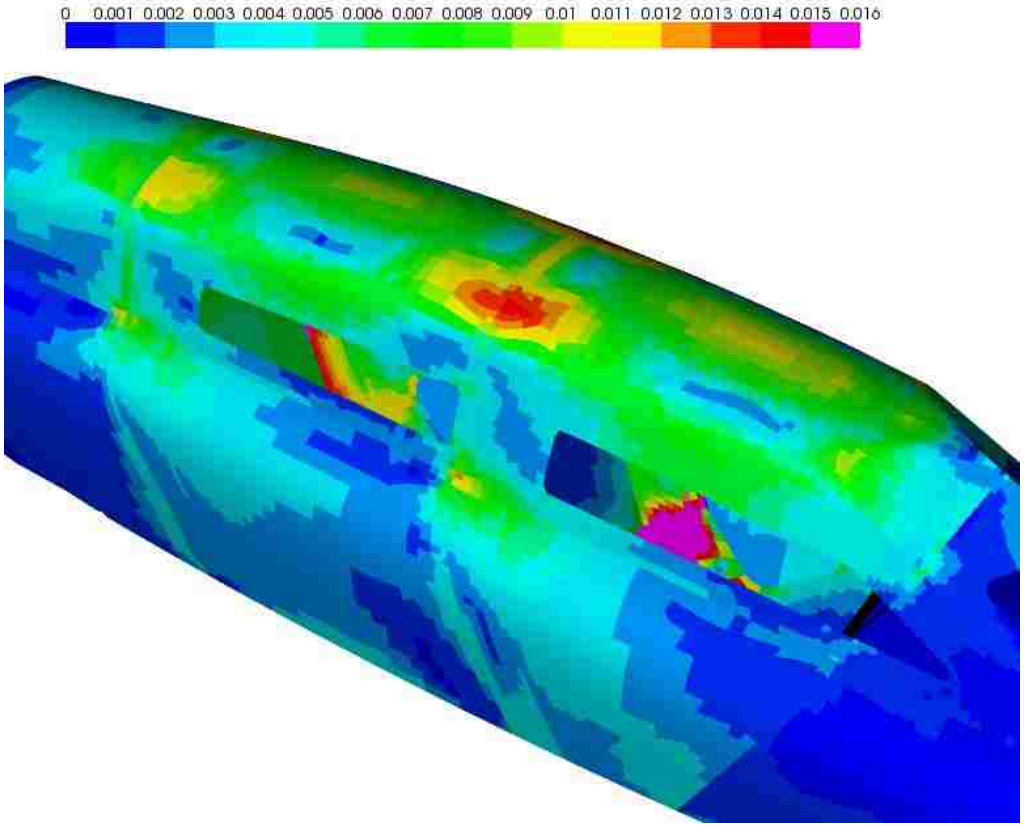

Figure 3.3-4: Maximum principal strains of CFRP, external composite structure, top under hydrodynamic load

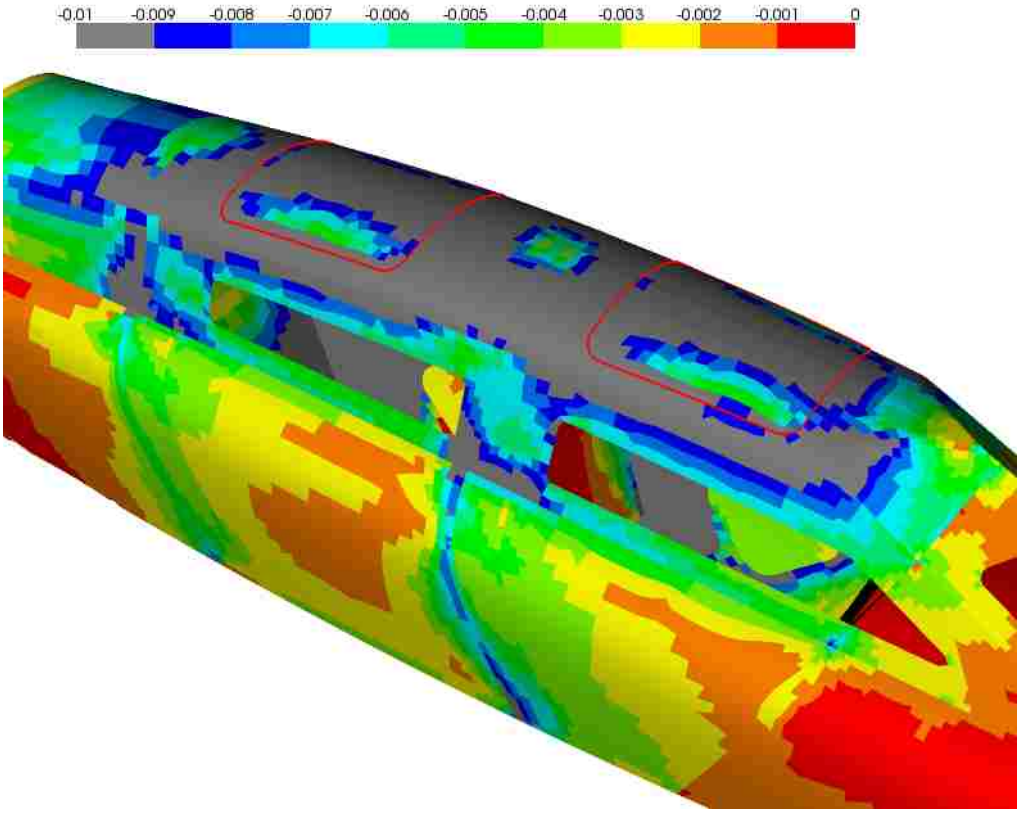

Figure 3.3-5: Minimum principal strains of CFRP, external composite structure, top under hydrodynamic load, very large strains shown in grey. The high compression strains occur in the outer skin of the sandwich.

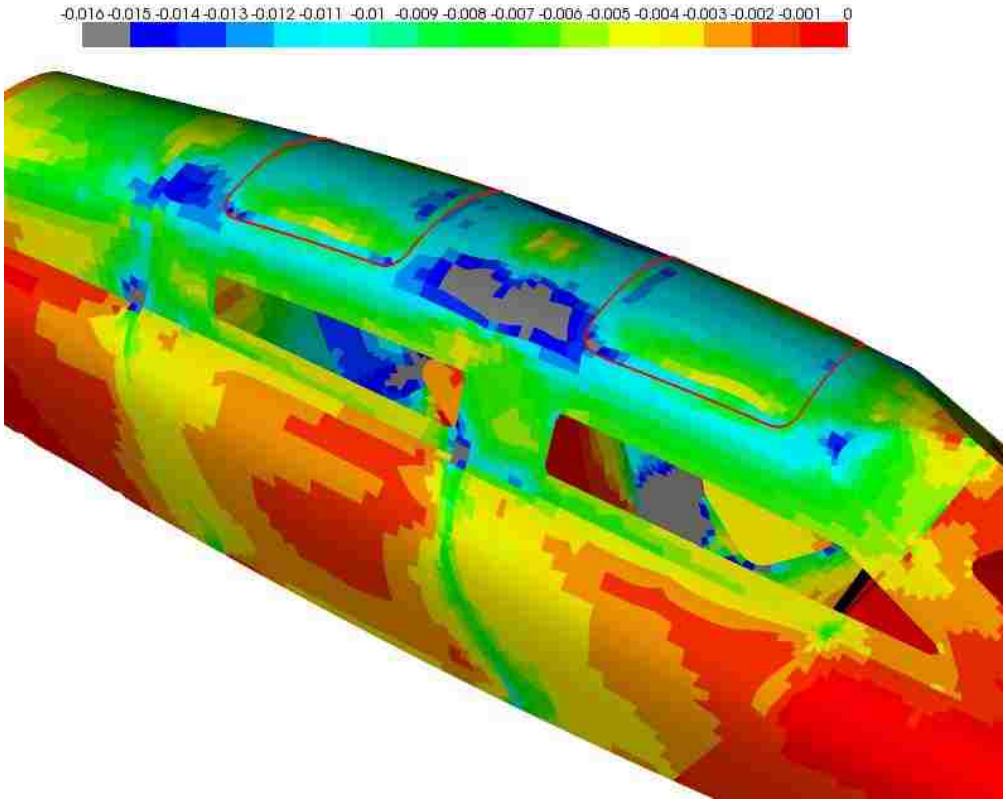

Figure 3.3-6: Minimum principal strains of CFRP, external composite structure, top under hydrodynamic load, showing the full spectrum of values

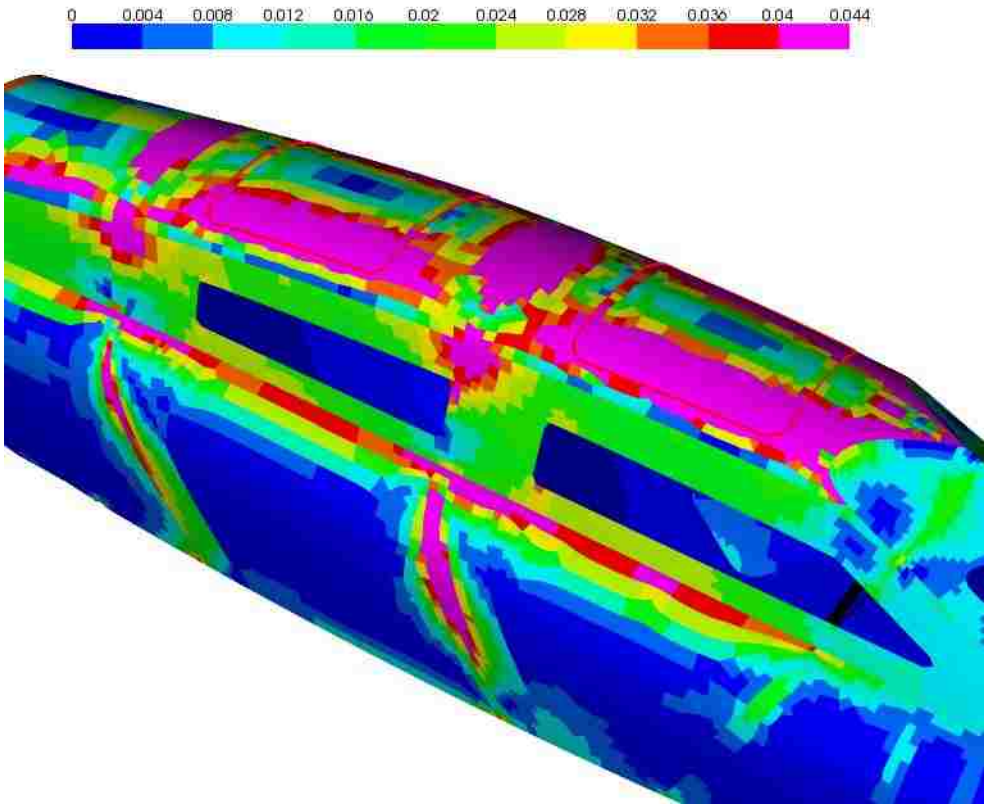

Figure 3.3-7: Out-of-plane shear strains of cores, external composite structure, top under hydrodynamic load, very large strains shown in violet

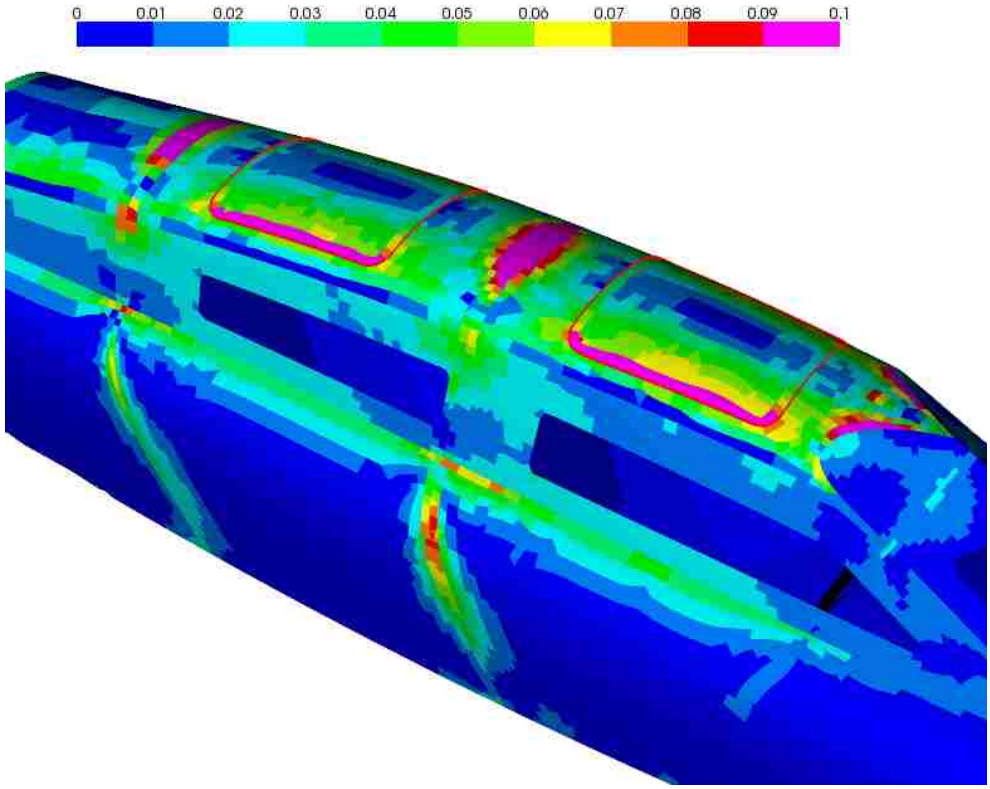

Figure 3.3-8: Out-of-plane shear strains of cores, external composite structure, top under hydrodynamic load, showing the full spectrum of values

Results for Side Window Panels under Hydrodynamic Load Case

The side PC window panels have enough strength to survive the loads in this case.

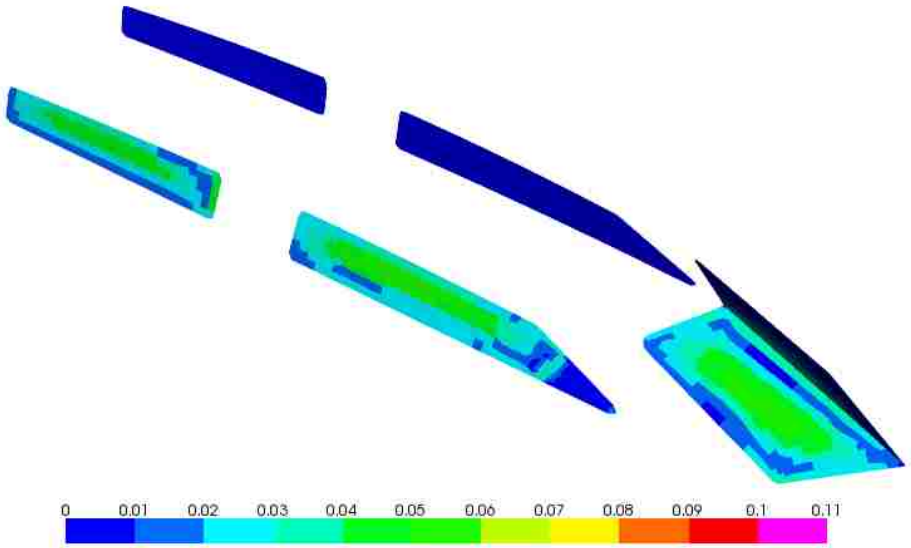

Figure 3.4-1: Maximum principal strains of PC,
right side window panels under hydrodynamic load

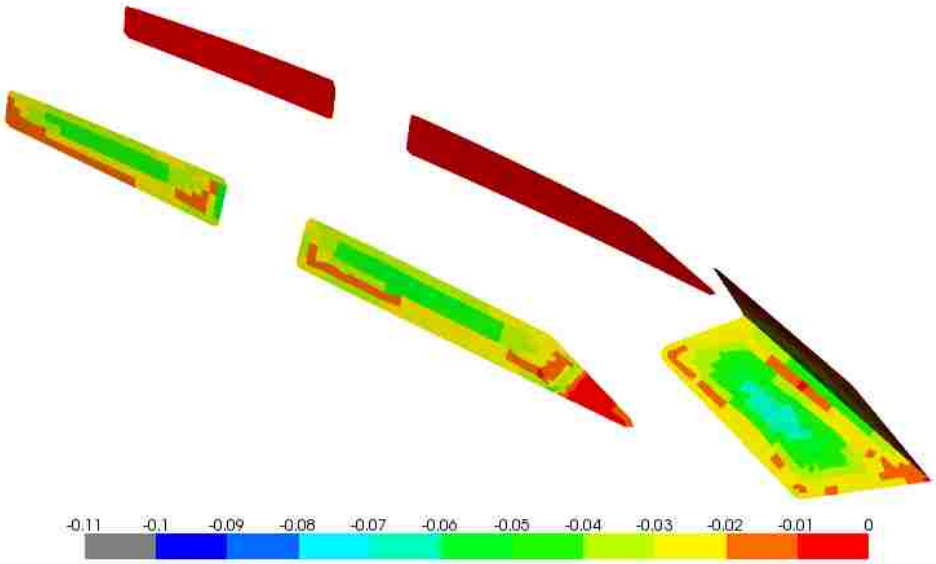

Figure 3.4-2: Minimum principal strains of PC,
right side window panels under hydrodynamic load

Results for Suspension-Introduced Loading Cases

The internal bulkheads and frames overall had adequate strength to withstand the loads in the seven cases. Several spots showing in grey (excessive compression) or violet (excessive tension) were identified and they will be locally reinforced when the boat is built.

Due to the lack of local reinforcement at the neighborhoods of the hardpoints in this FE shell element model, local strains were very high on the external composite structure at those areas. The severity of the strains at these areas provide insight into where local reinforcements should be and how strong they need to be to withstand the loads.

I. Contour plots for Load Case 1: all four sponsons taking vertical loads

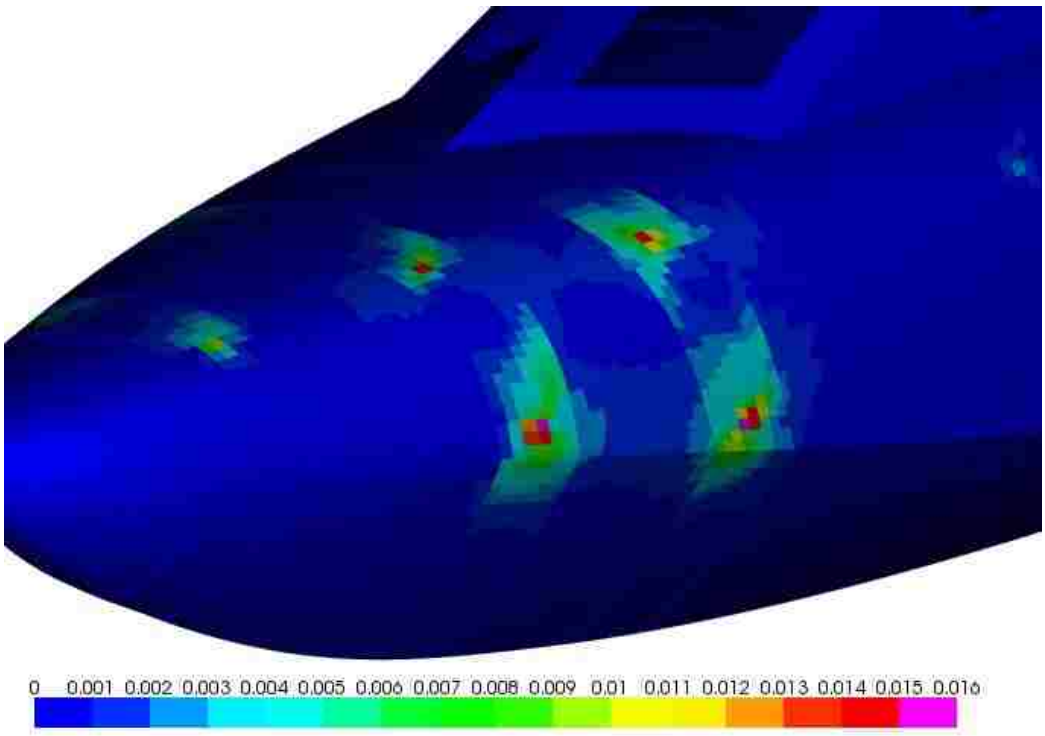

Figure 3.5-1: Front view of maximum principal strains of CFRP, external composite structure

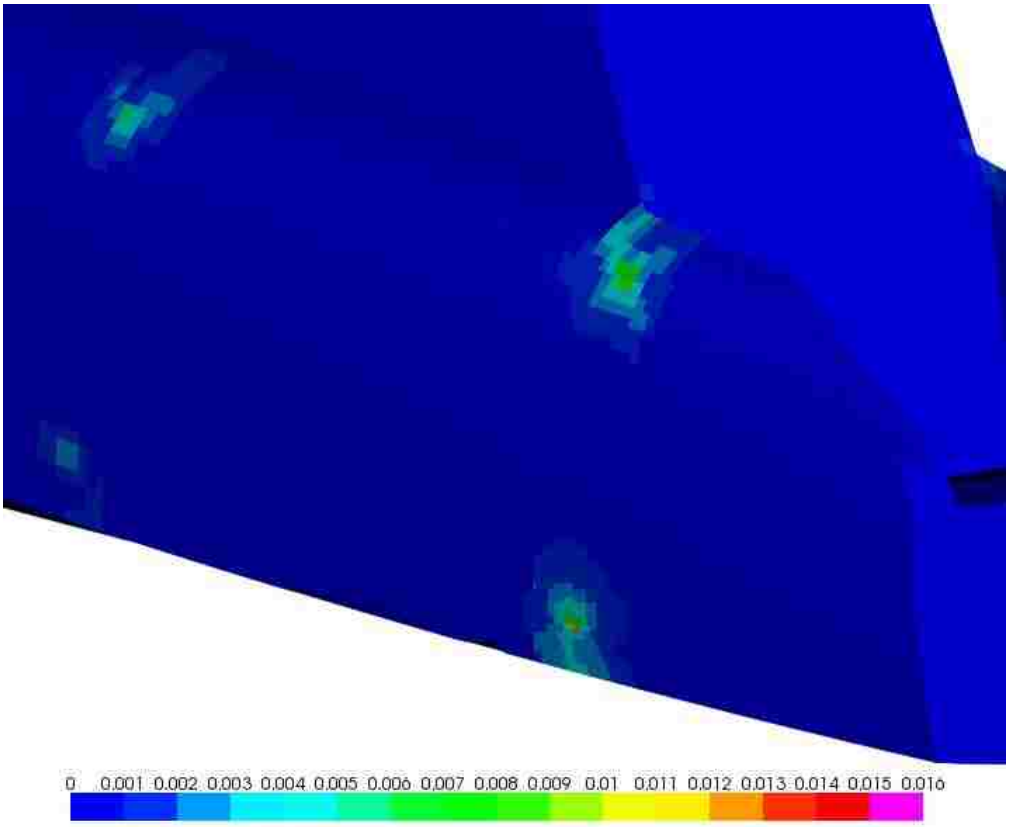

Figure 3.5-2: Rear view of maximum principal strains of CFRP, external composite structure

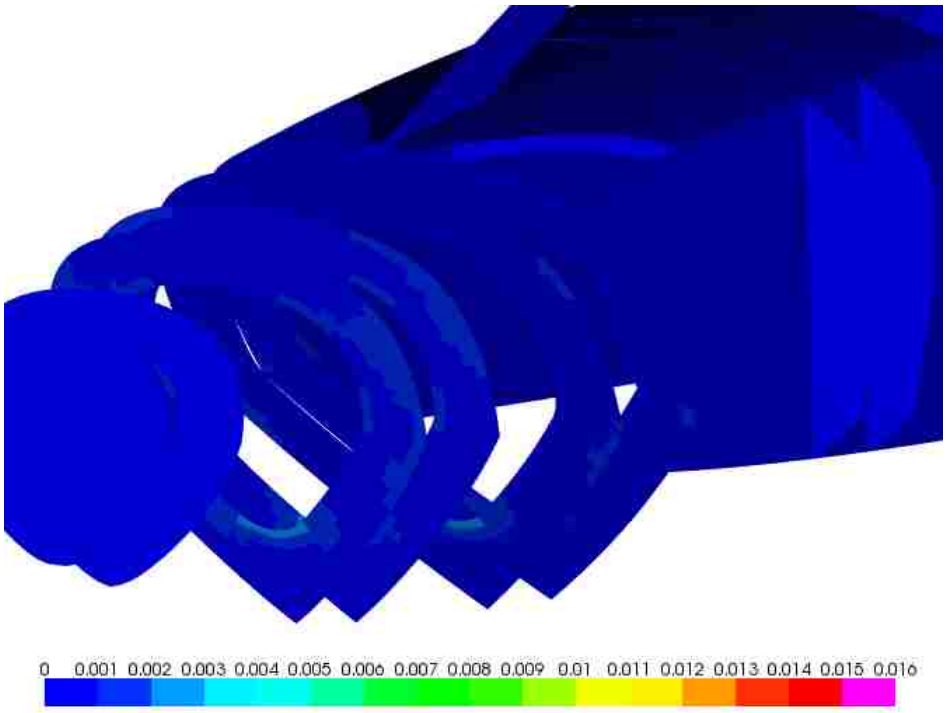

Figure 3.5-3: Front view of maximum principal strains of CFRP, internal composite structure

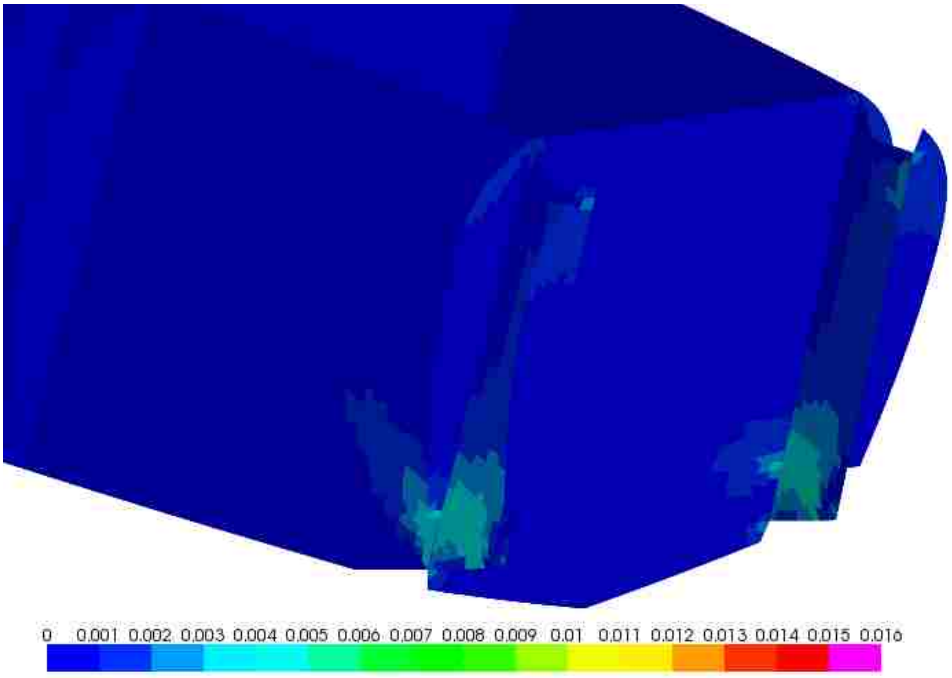

Figure 3.5-4: Rear view of maximum principal strains of CFRP, internal composite structure

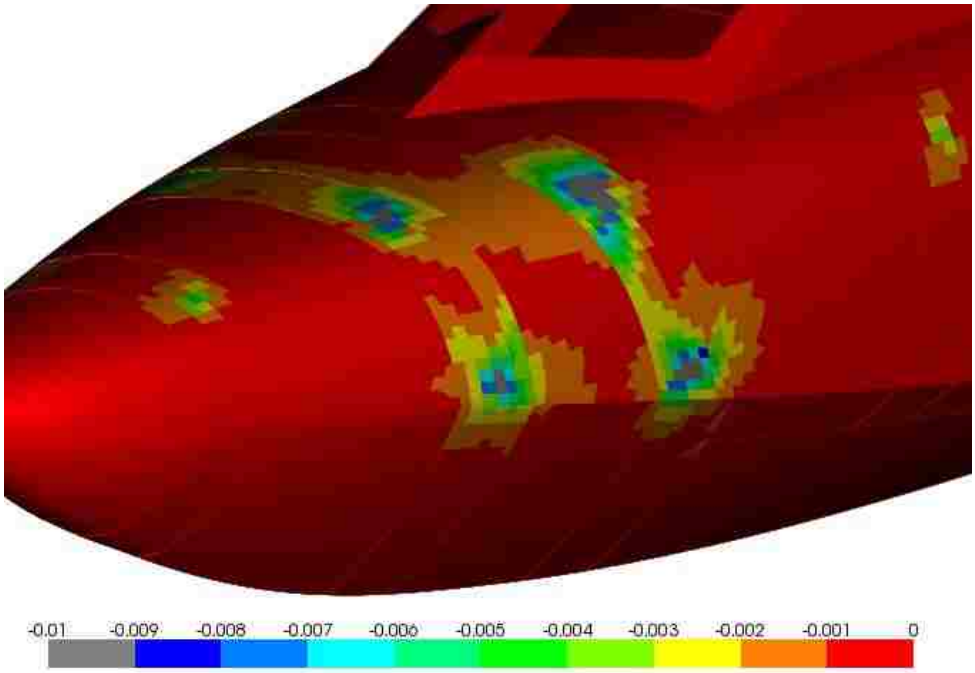

Figure 3.5-5: Front view of minimum principal strains of CFRP, external composite structure

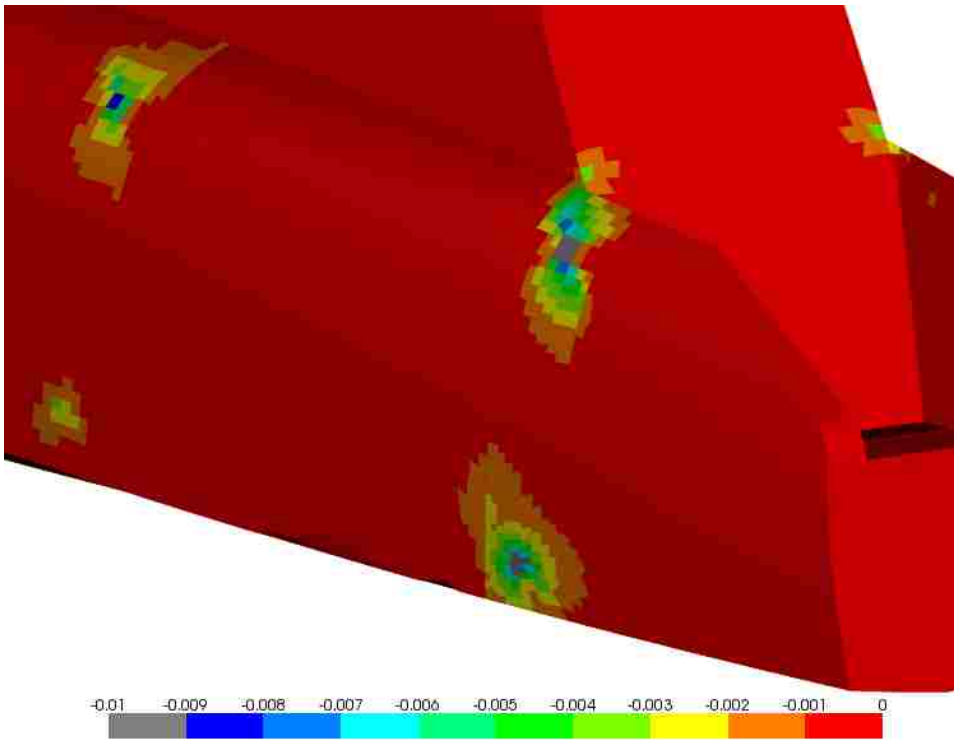

Figure 3.5-6: Rear view of minimum principal strains of CFRP, external composite structure

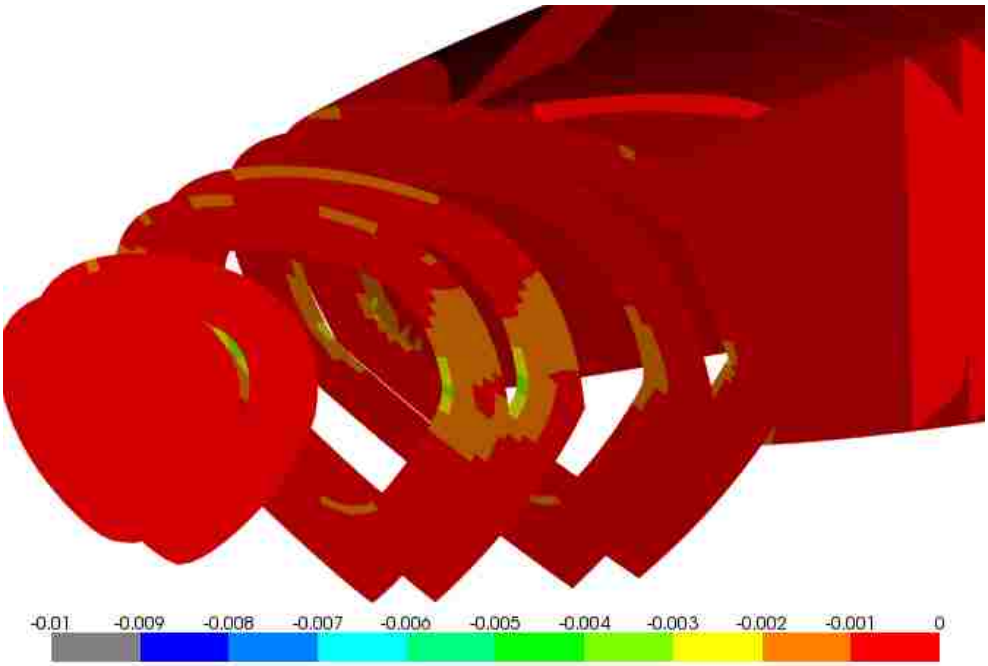

Figure 3.5-7: Front view of minimum principal strains of CFRP, internal composite structure

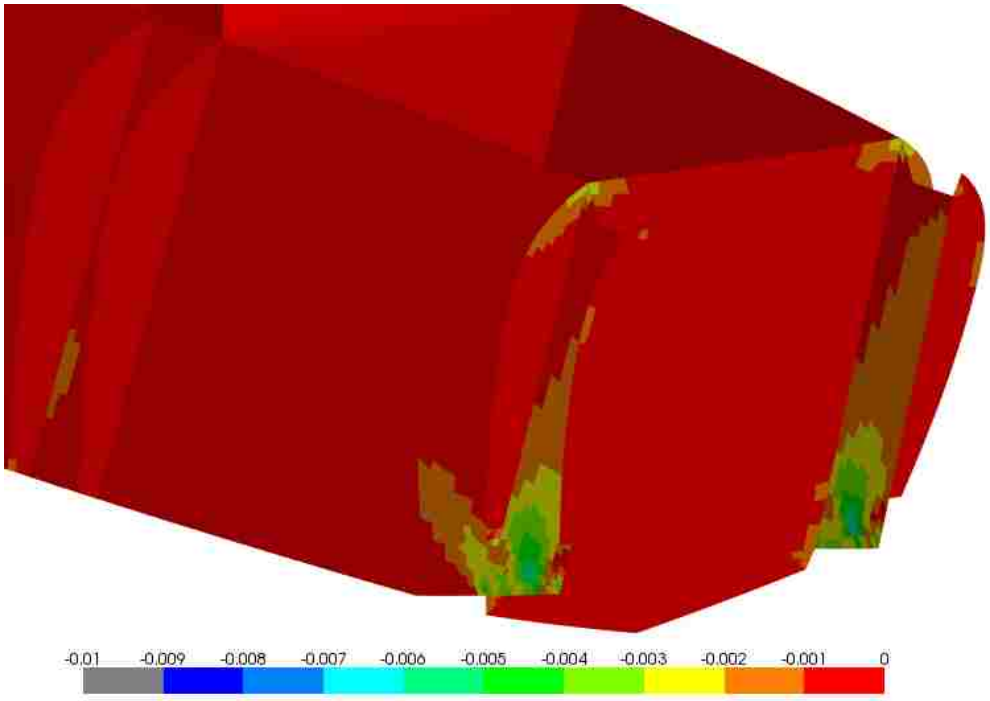

Figure 3.5-8: Rear view of minimum principal strains of CFRP, internal composite structure

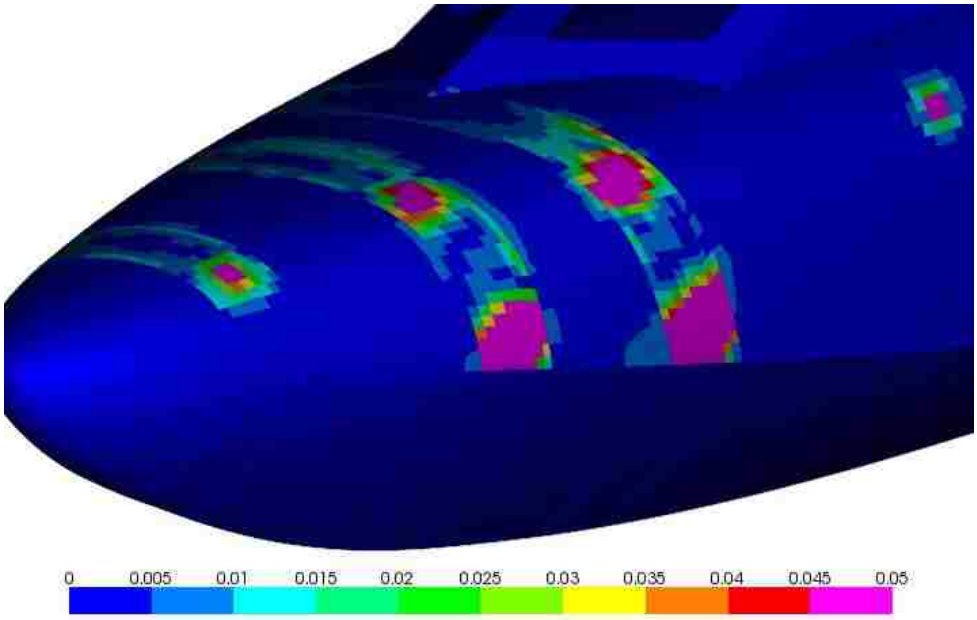

Figure 3.5-9: Front view of out-of-plane shear strains of cores, external composite structure

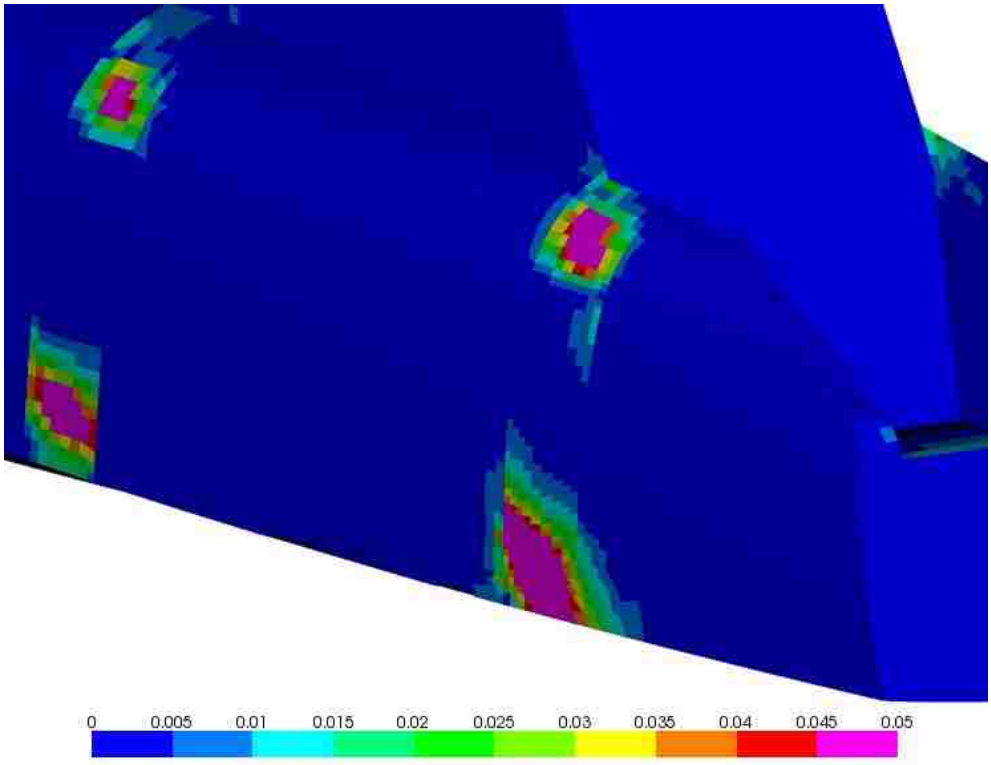

Figure 3.5-10: Rear view of out-of-plane shear strains of cores, external composite structure

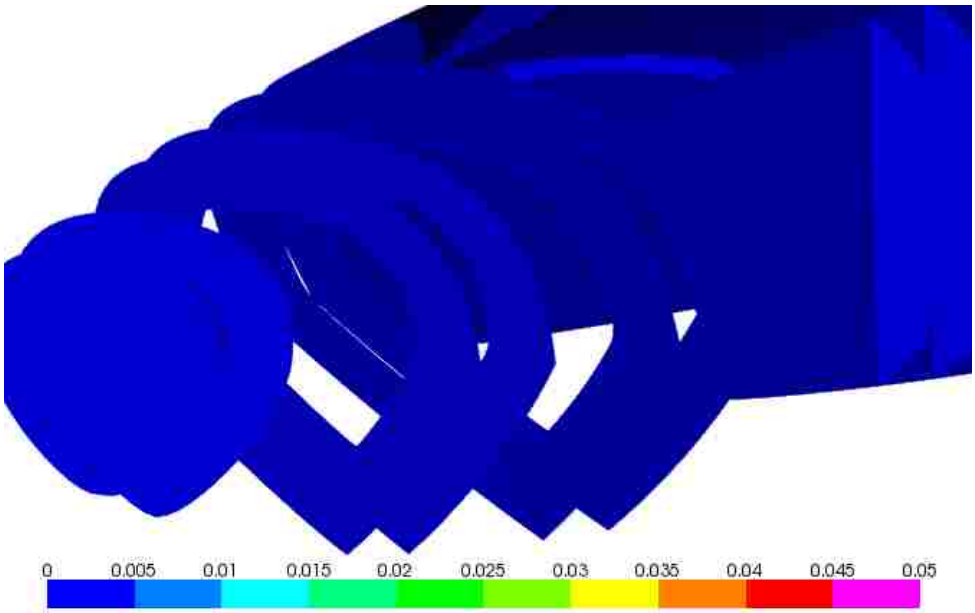

Figure 3.5-11: Front view of out-of-plane shear strains of cores, internal composite structure

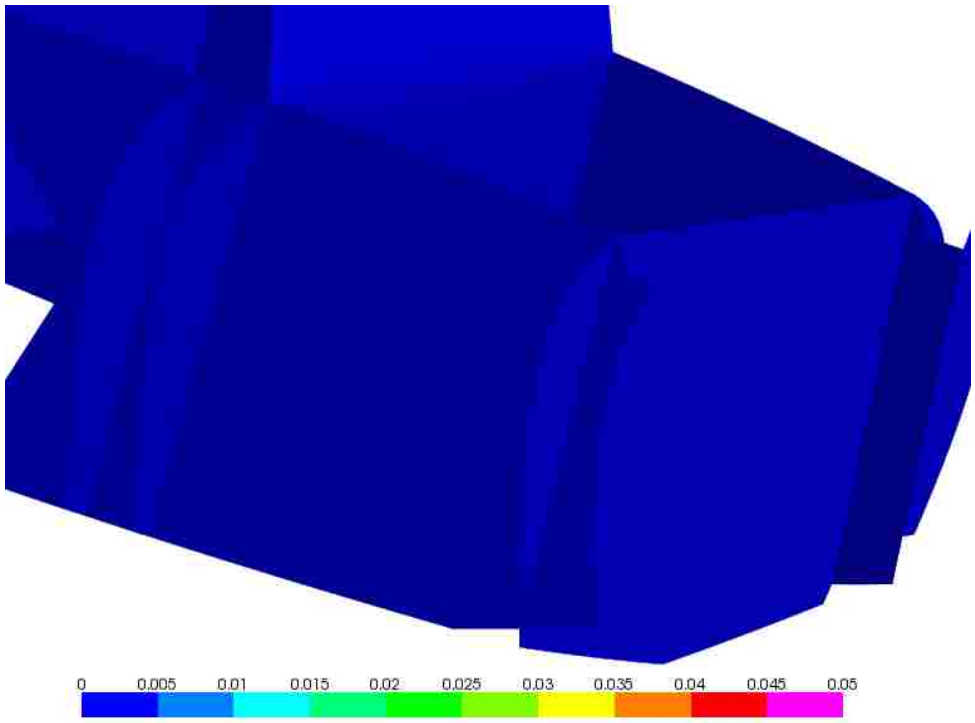

Figure 3.5-12: Rear view of out-of-plane shear strains of cores, internal composite structure

II. Contour plots for Load Case 2: two front sponsons taking vertical loads

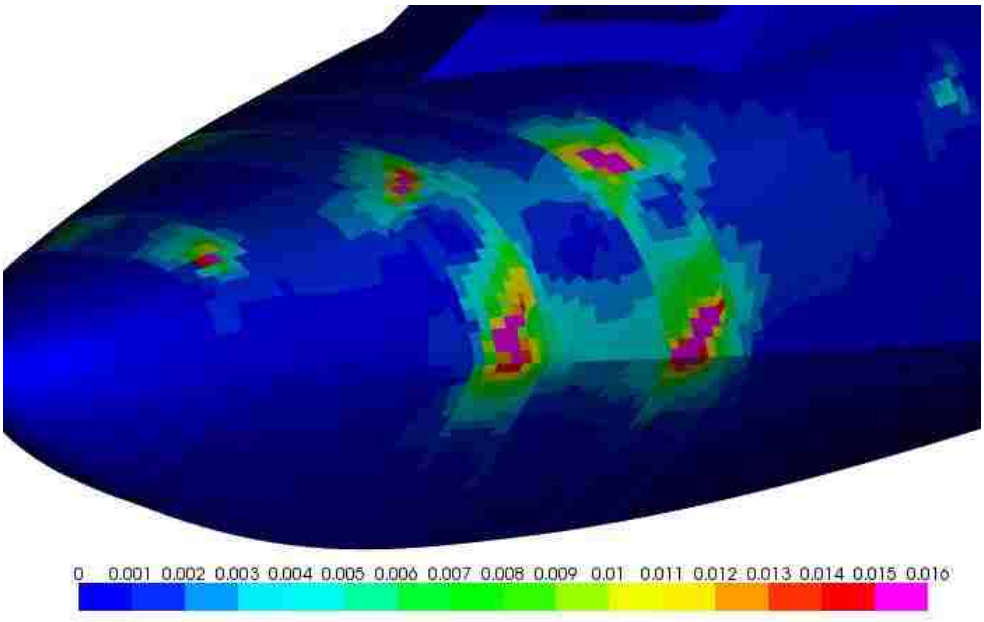

Figure 3.5-13: Front view of maximum principal strains of CFRP, external composite structure

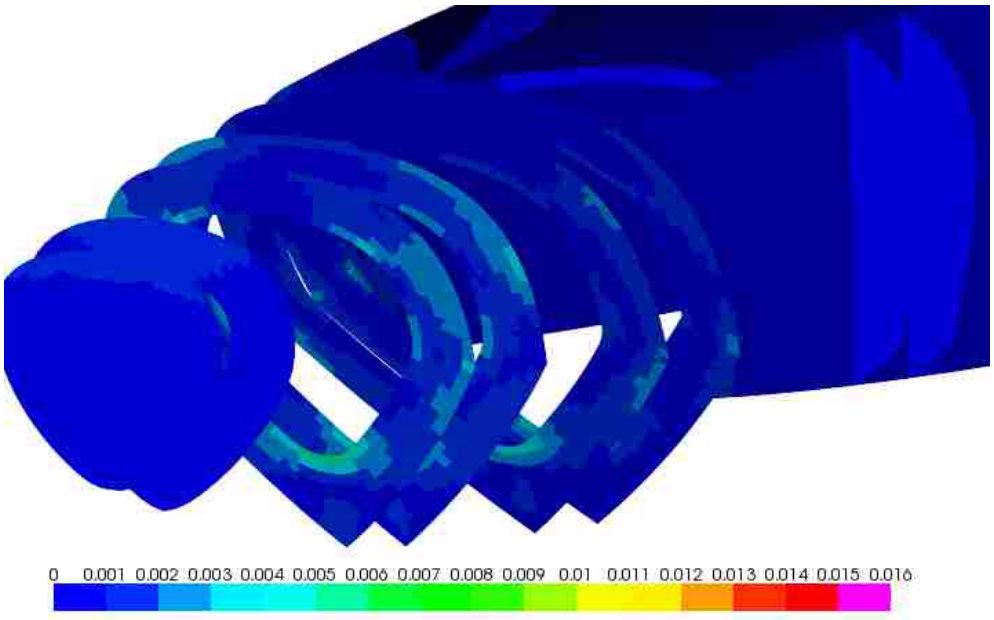

Figure 3.5-14: Front view of maximum principal strains of CFRP, internal composite structure

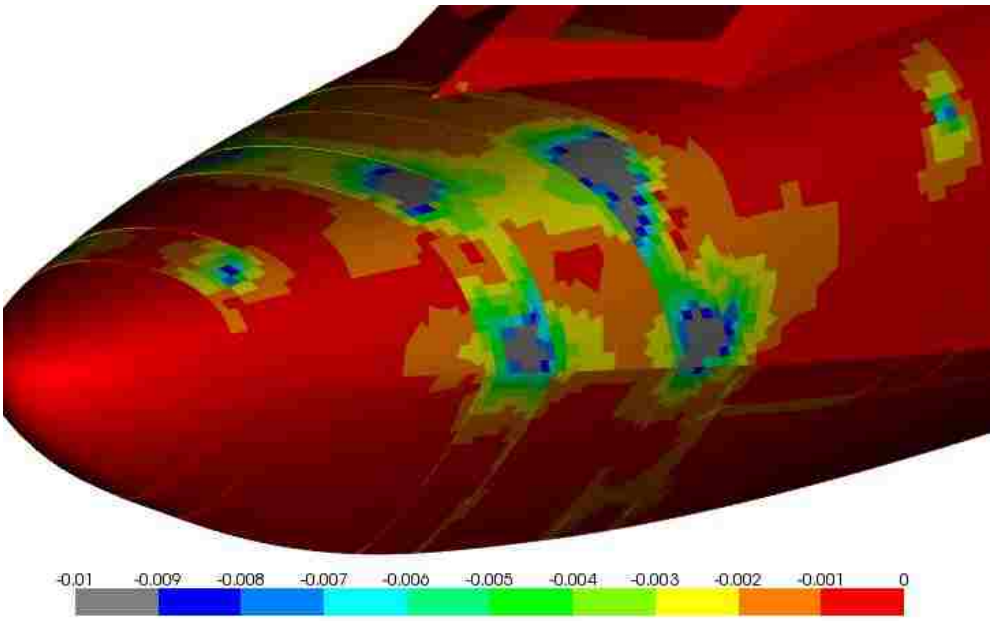

Figure 3.5-15: Front view of minimum principal strains of CFRP, external composite structure

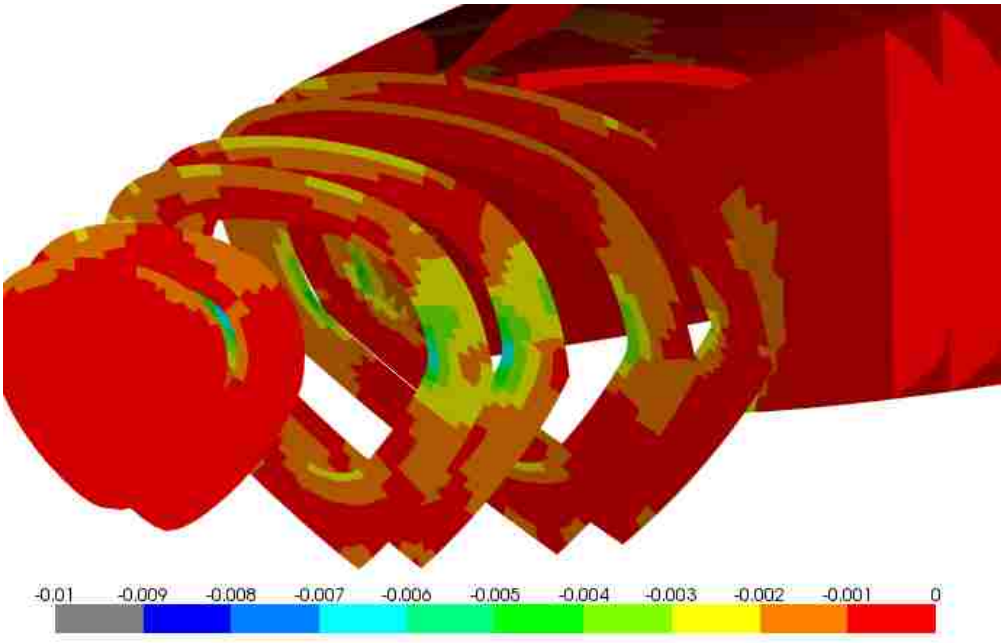

Figure 3.5-16: Front view of minimum principal strains of CFRP, internal composite structure

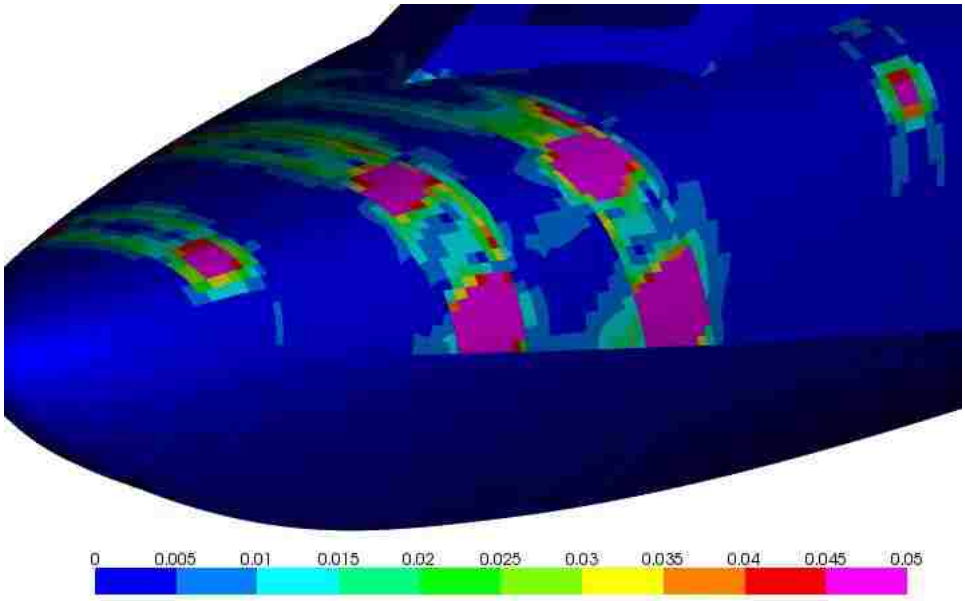

Figure 3.5-17: Front view of out-of-plane shear strains of cores, external composite structure

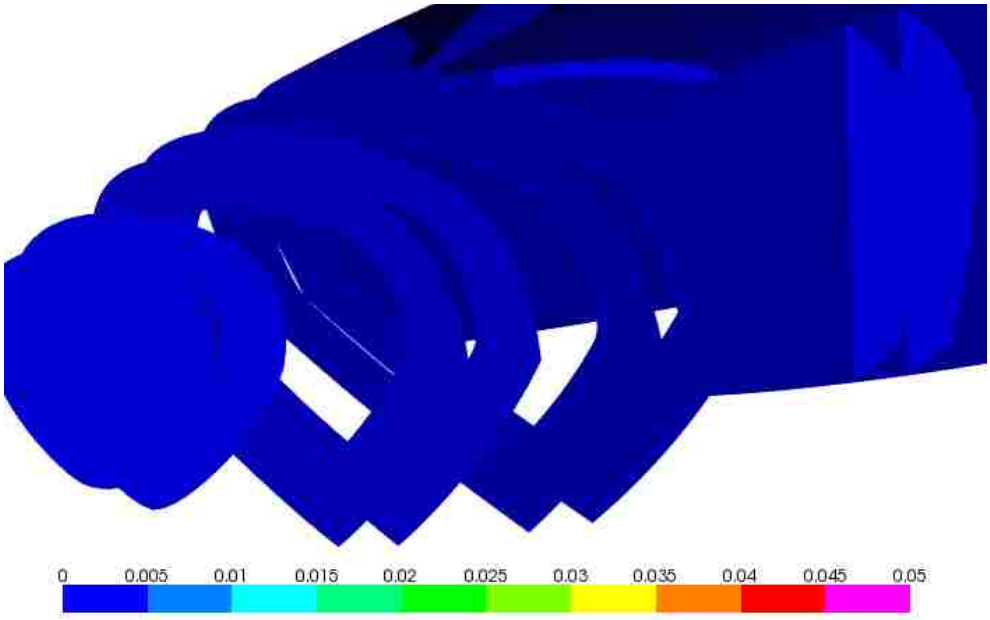

Figure 3.5-18: Front view of out-of-plane shear strains of cores, internal composite structure

III. Contour plots for Load Case 3: two rear sponsons taking vertical loads

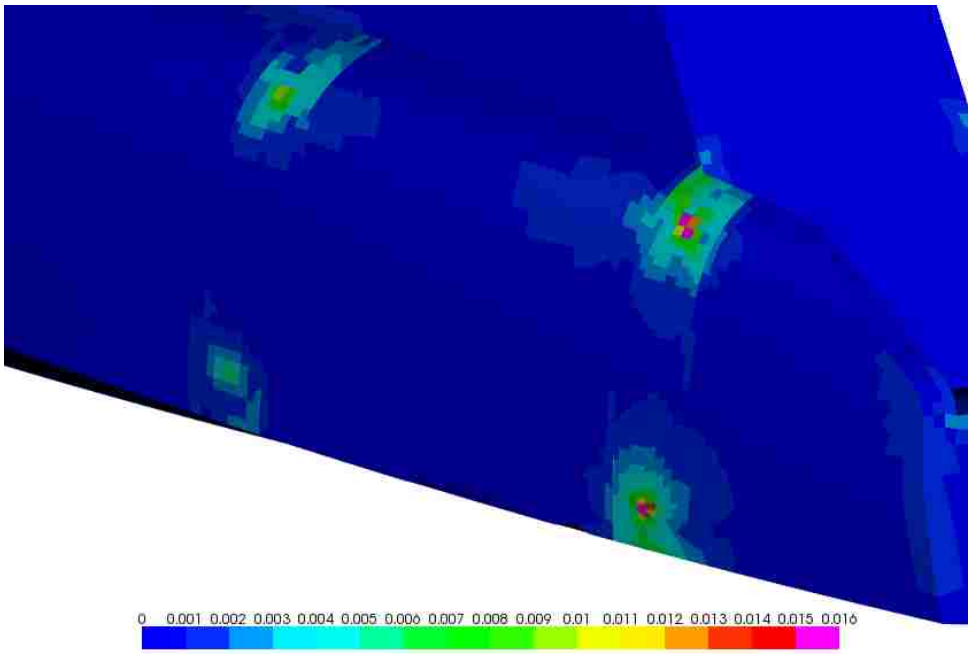

Figure 3.5-19: Rear view of maximum principal strains of CFRP, external composite structure

\

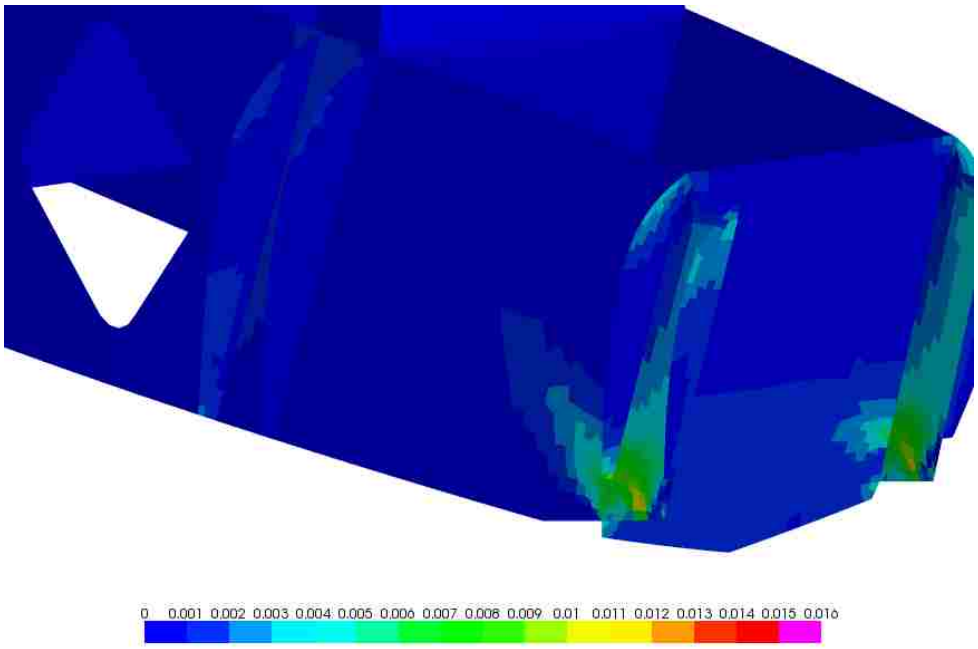

Figure 3.5-20: Rear view of maximum principal strains of CFRP, internal composite structure

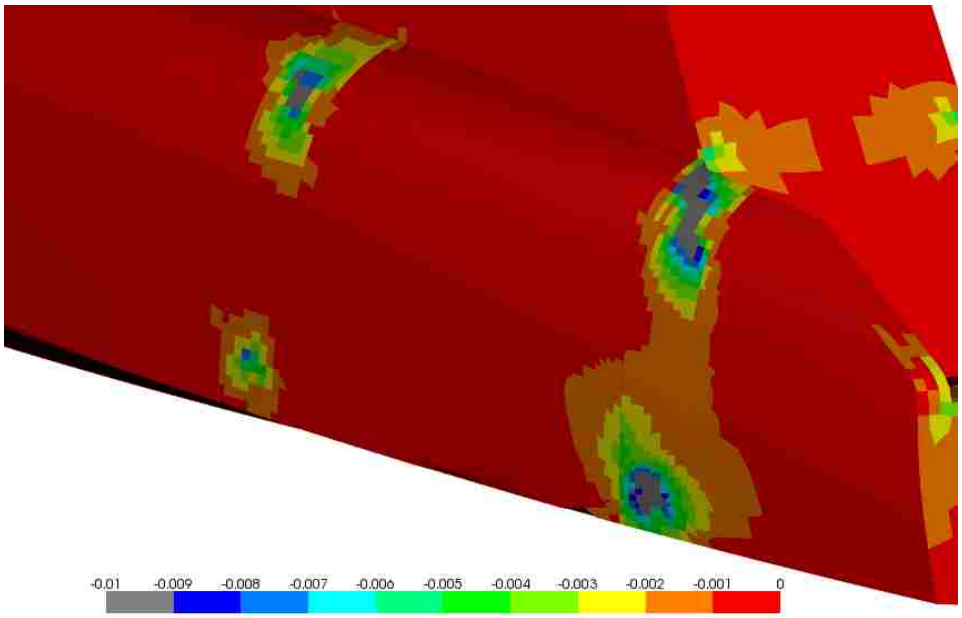

Figure 3.5-21: Rear view of minimum principal strains of CFRP, external composite structure

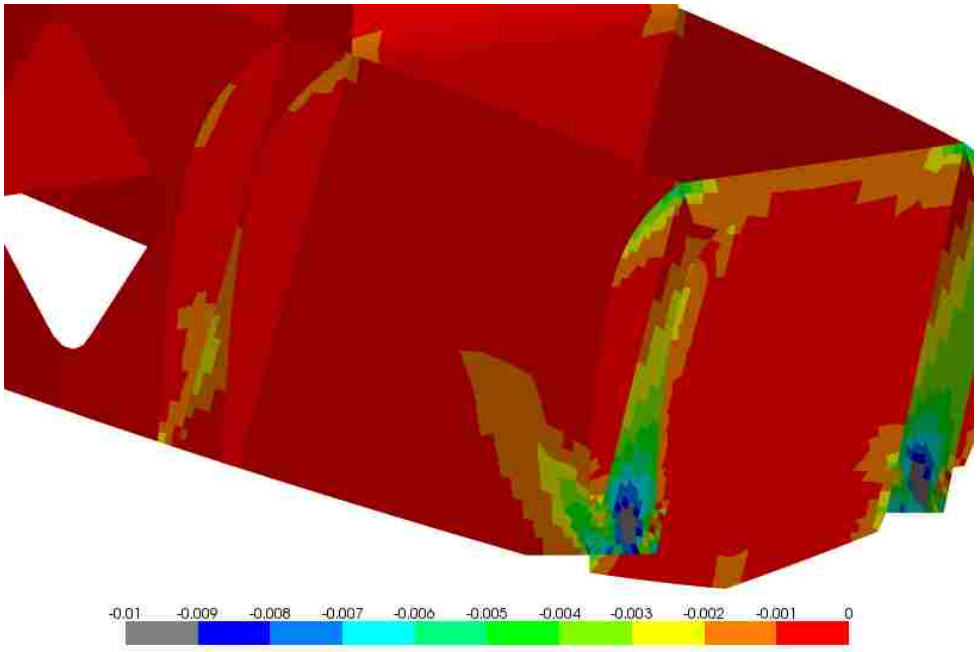

Figure 3.5-22: Rear view of minimum principal strains of CFRP, internal composite structure

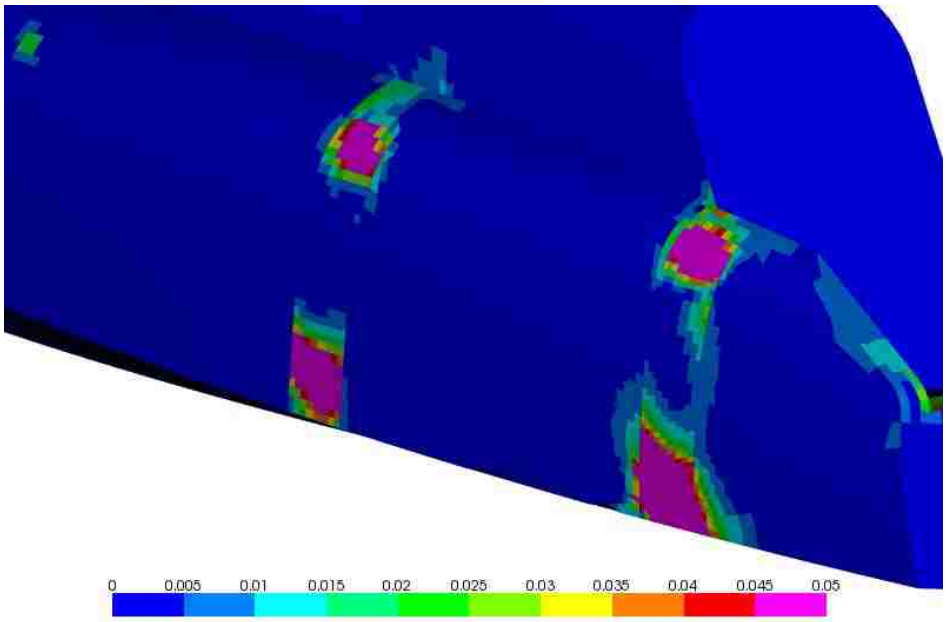

Figure 3.5-23: Rear view of out-of-plane shear strains of cores, external composite structure

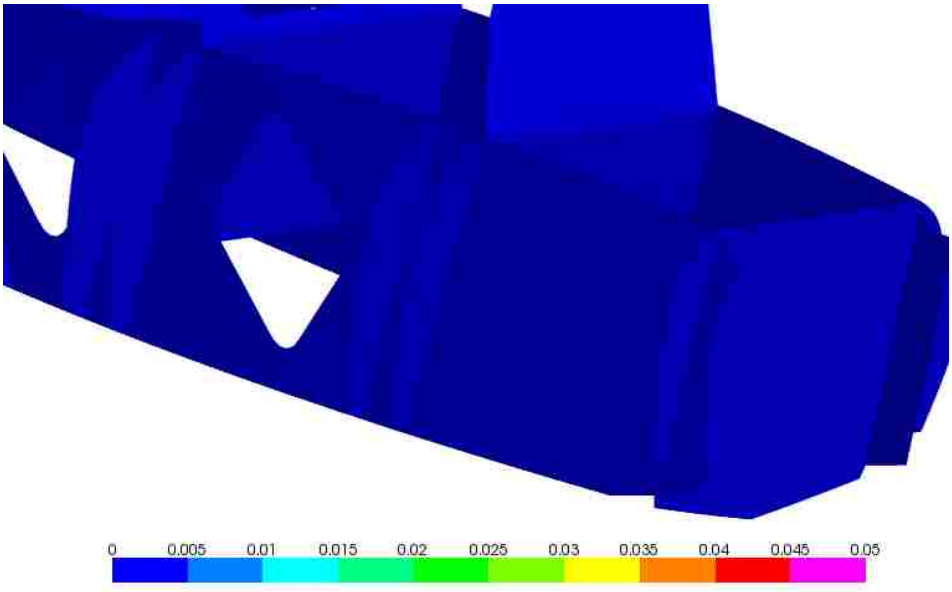

Figure 3.5-24: Rear view of out-of-plane shear strains of cores, internal composite structure

IV. Contour plots for Load Case 4: left front and right rear sponsons taking vertical loads

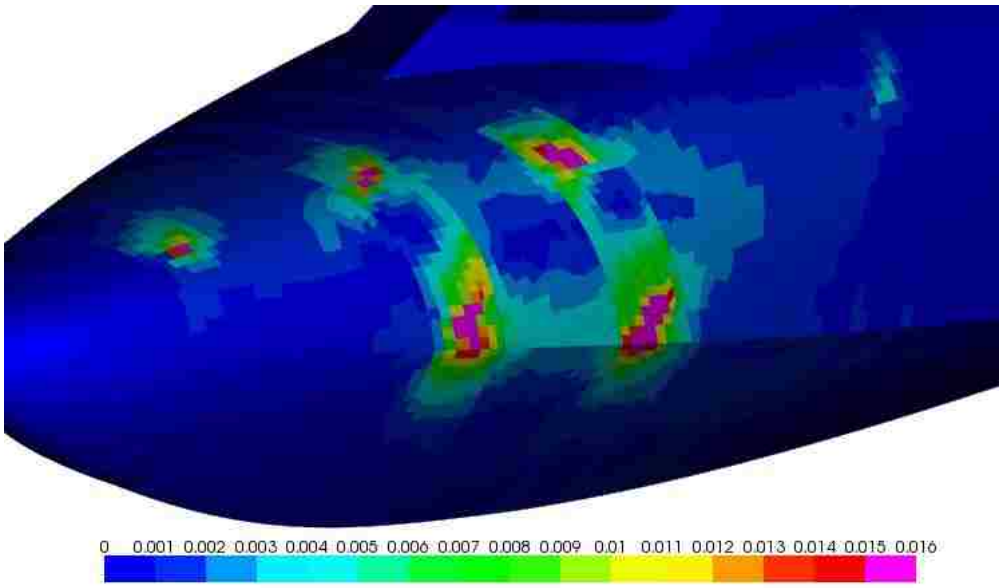

Figure 3.5-25: Front view of maximum principal strains of CFRP, external composite structure

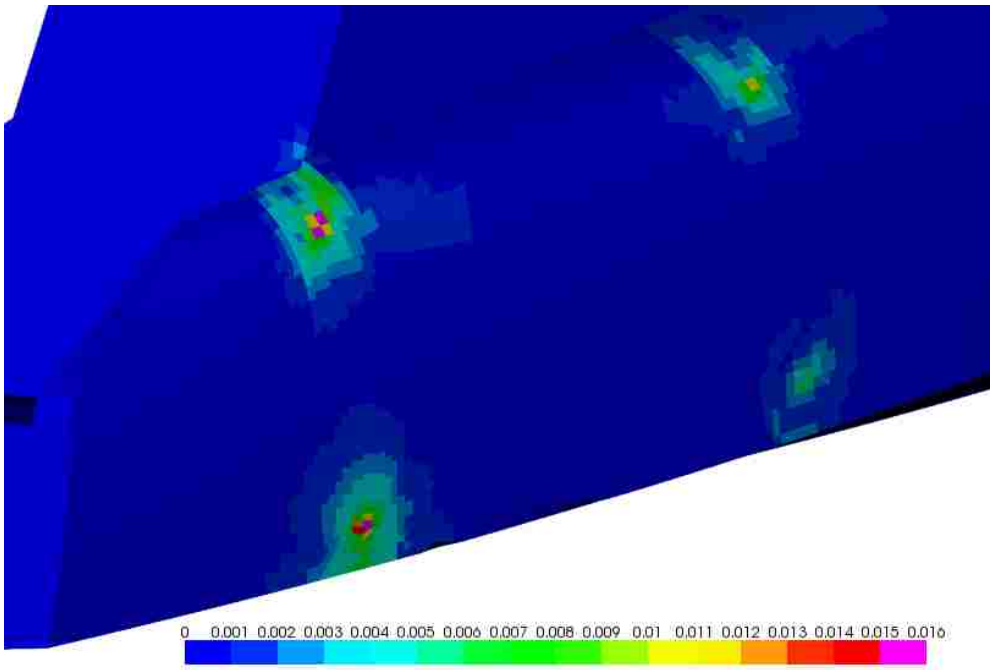

Figure 3.5-26: Rear view of maximum principal strains of CFRP, external composite structure

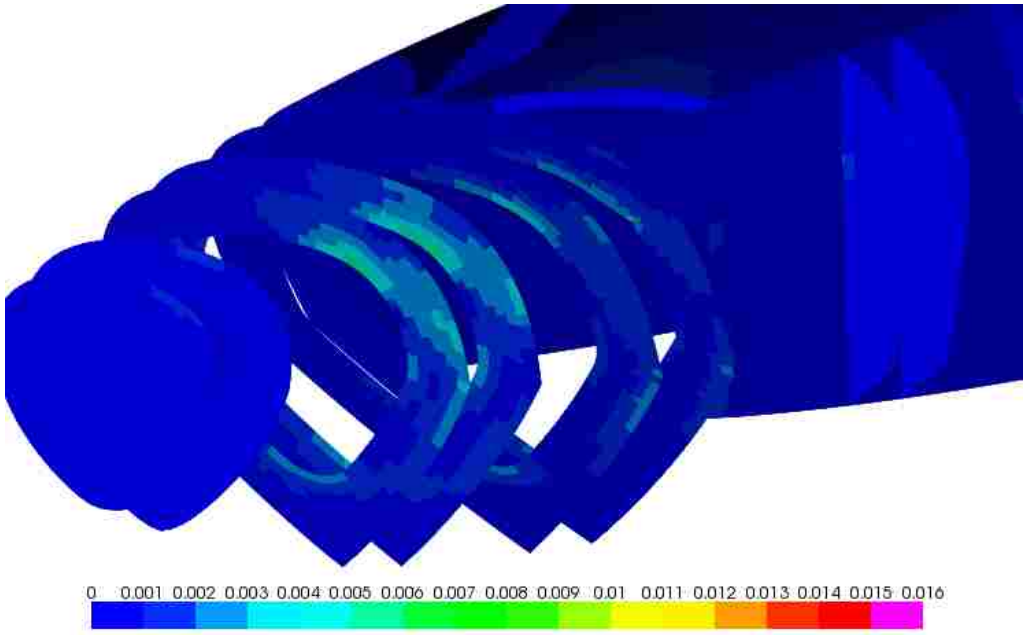

Figure 3.5-27: Front view of maximum principal strains of CFRP, internal composite structure

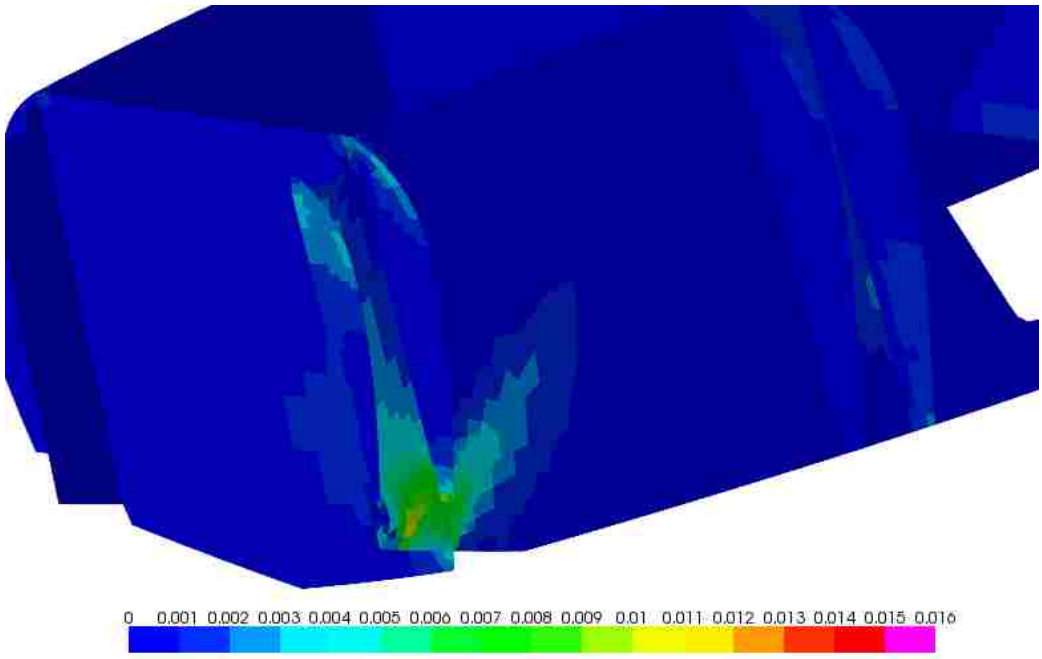

Figure 3.5-28: Rear view of maximum principal strains of CFRP, internal composite structure

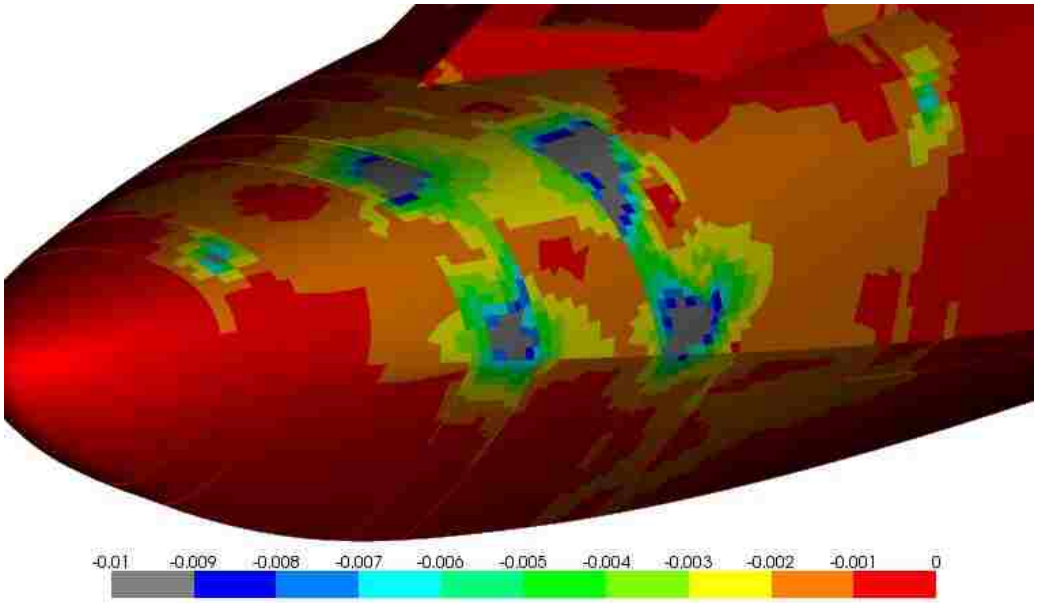

Figure 3.5-29: Front view of minimum principal strains of CFRP, external composite structure

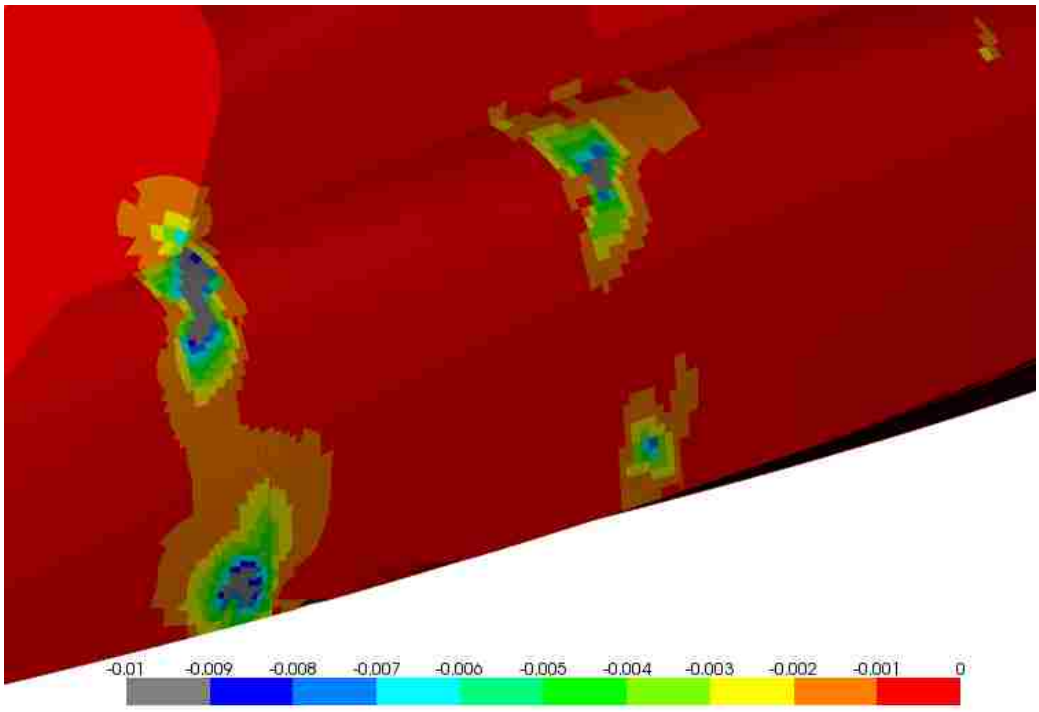

Figure 3.5-30: Rear view of minimum principal strains of CFRP, external composite structure

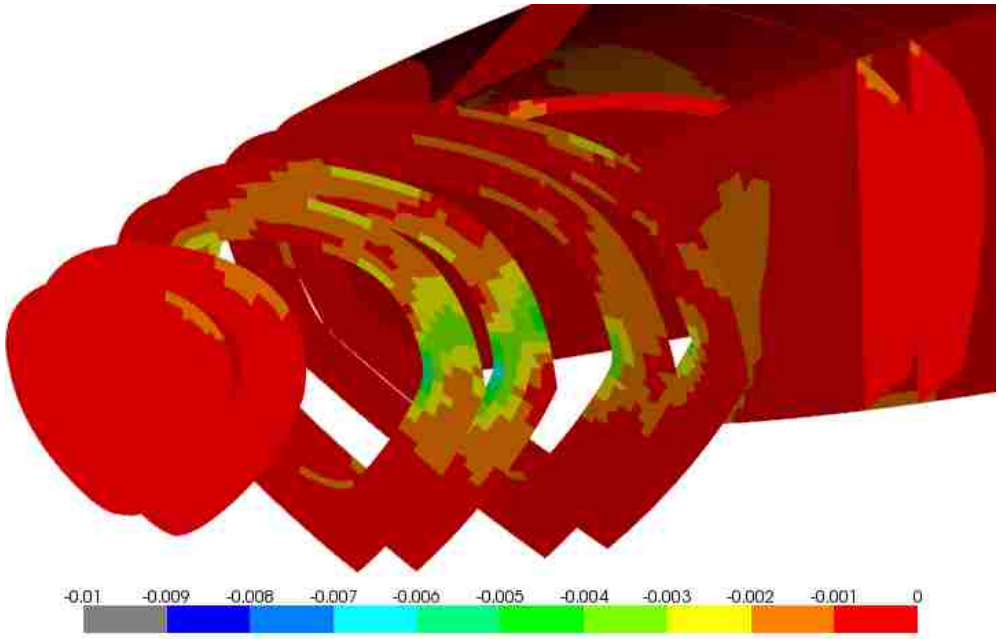

Figure 3.5-31: Front view of minimum principal strains of CFRP, internal composite structure

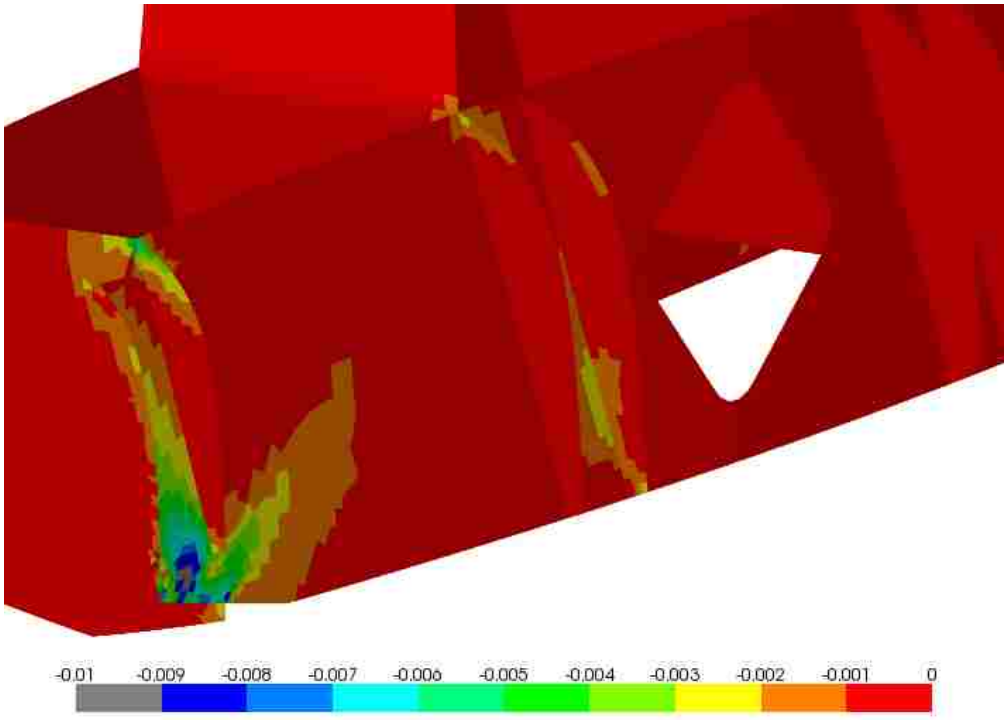

Figure 3.5-32: Rear view of minimum principal strains of CFRP, internal composite structure

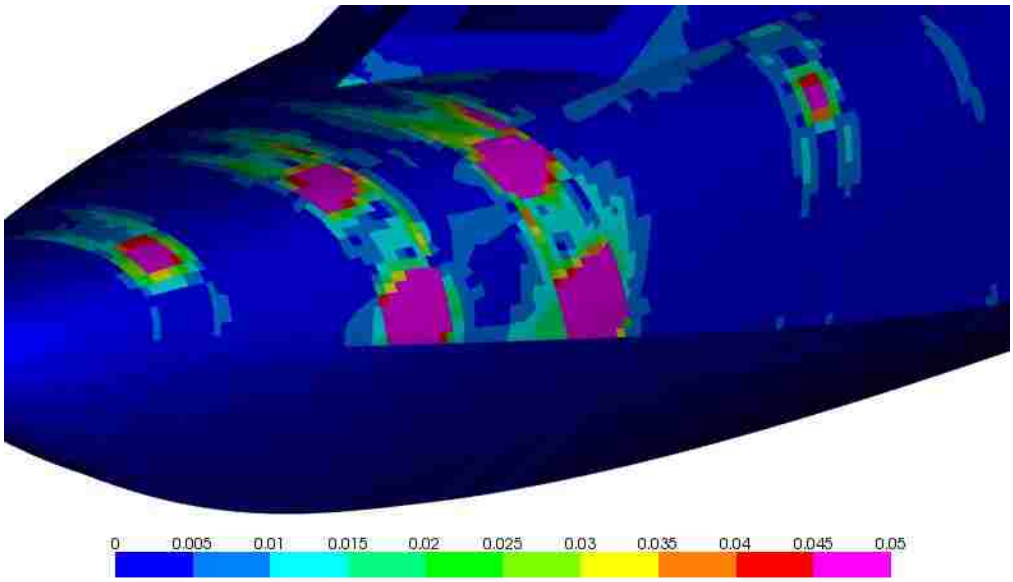

Figure 3.5-33: Front view of out-of-plane shear strains of cores, external composite structure

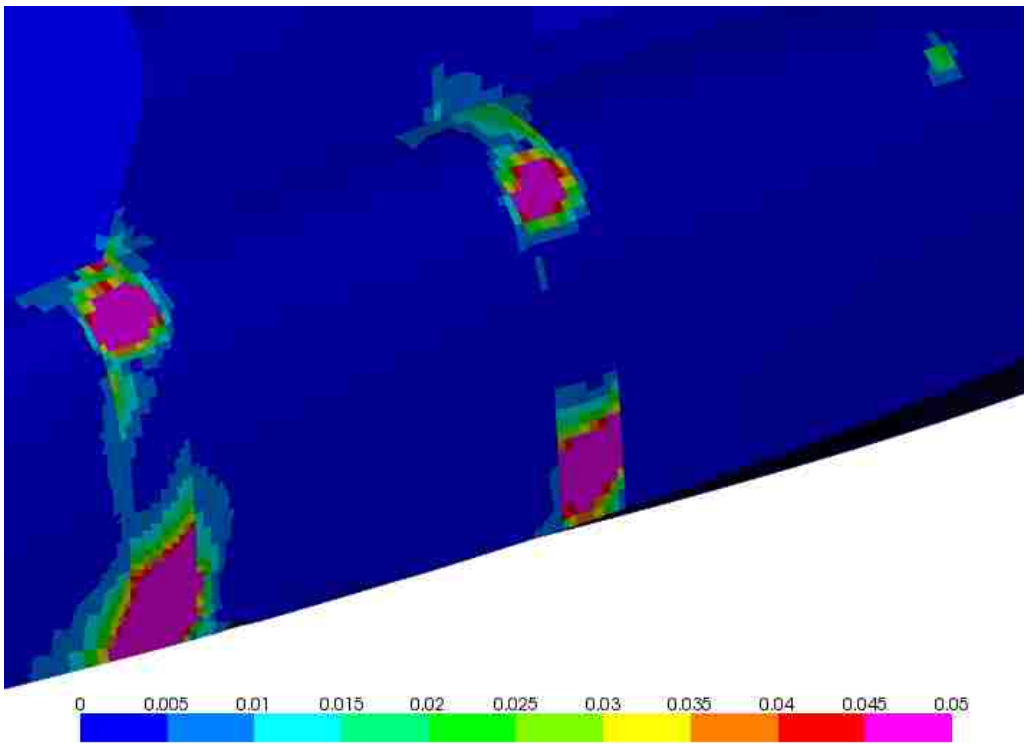

Figure 3.5-34: Rear view of out-of-plane shear strains of cores, external composite structure

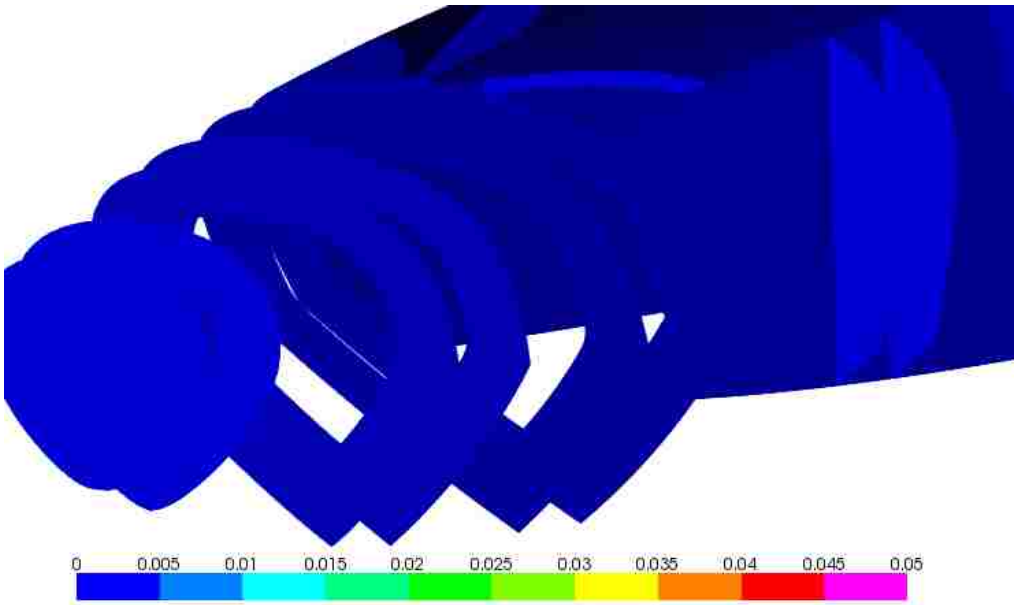

Figure 3.5-35: Front view of out-of-plane shear strains of cores, internal composite structure

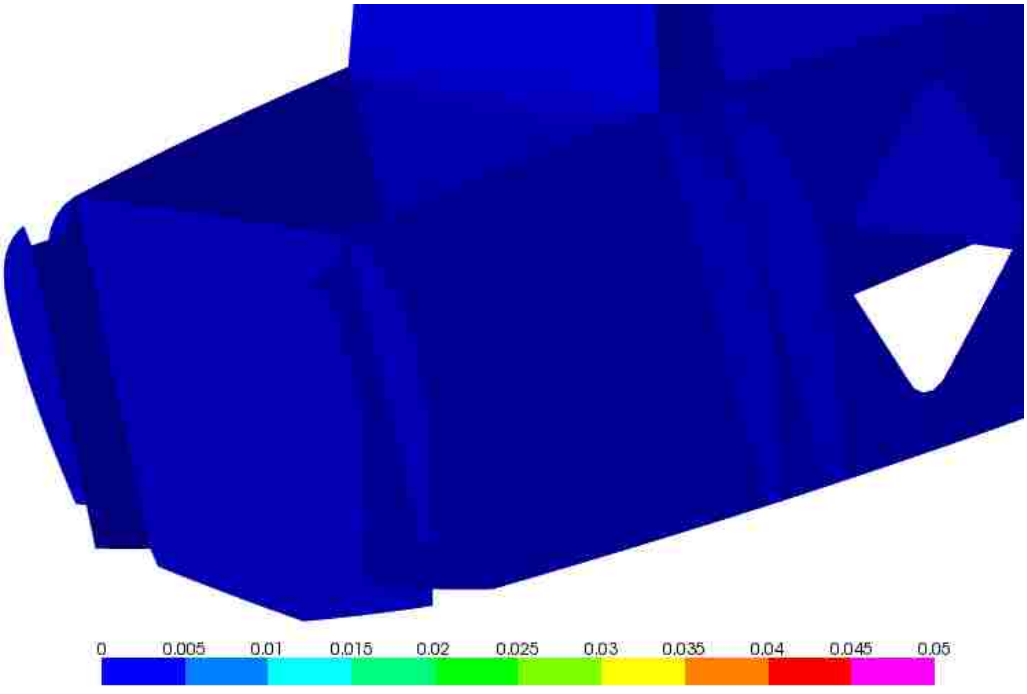

Figure 3.5-36: Rear view of out-of-plane shear strains of cores, internal composite structure

V. Contour plots for Load Case 5: two left sponsons taking horizontal loads

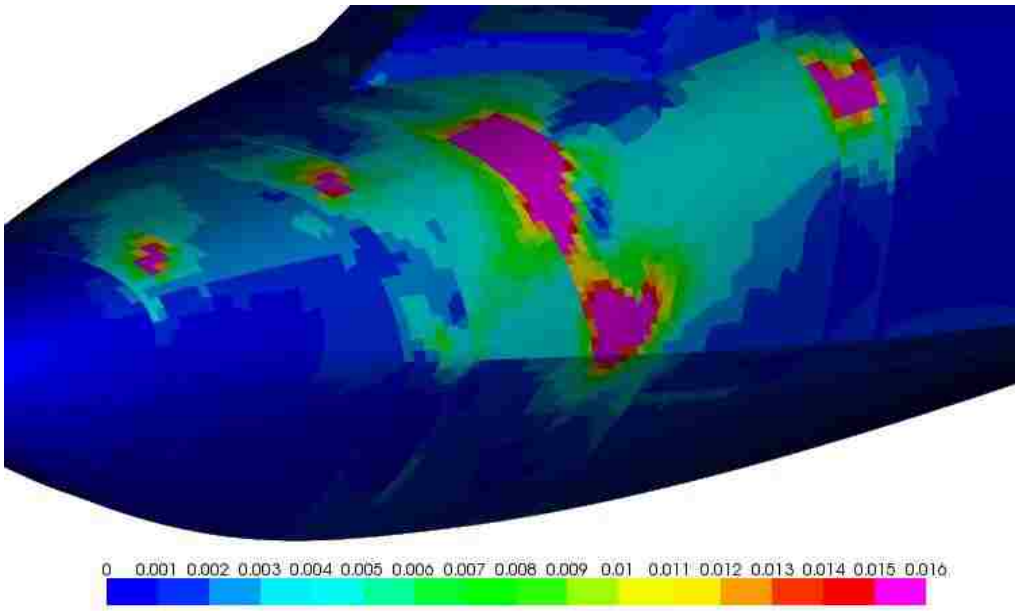

Figure 3.5-37: Front view of maximum principal strains of CFRP, external composite structure

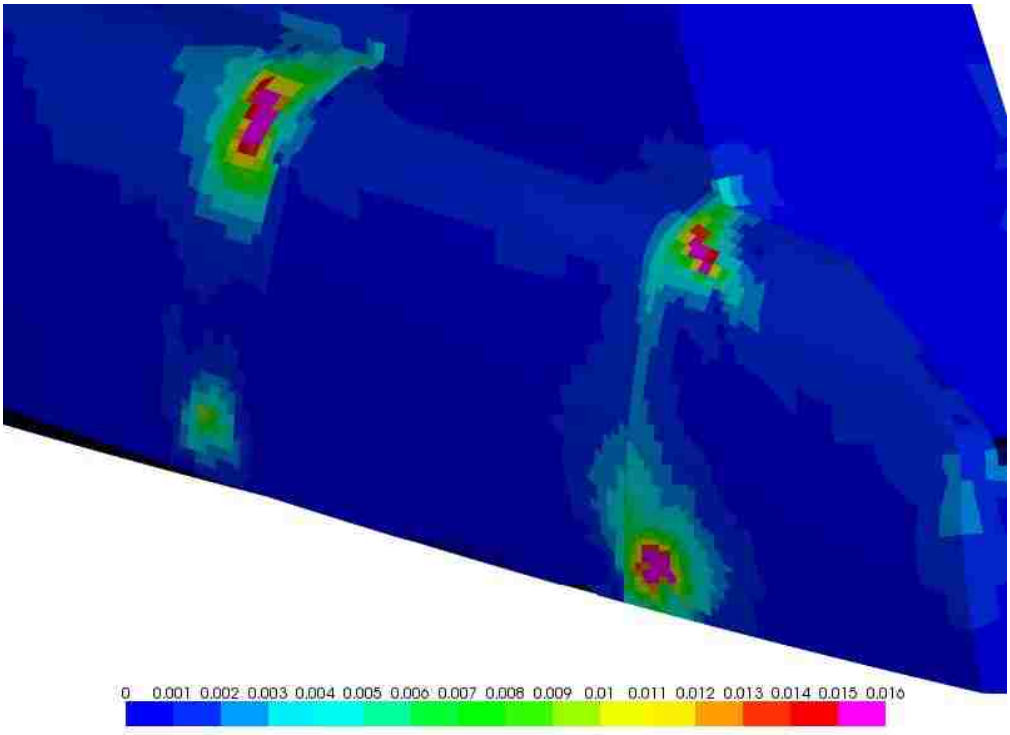

Figure 3.5-38: Rear view of maximum principal strains of CFRP, external composite structure

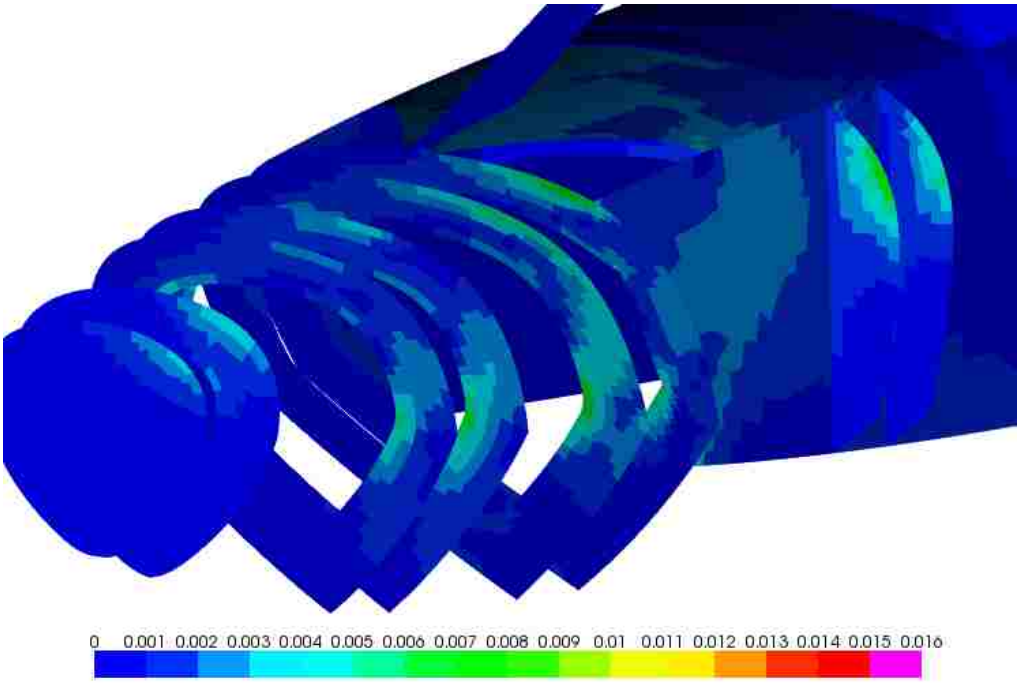

Figure 3.5-39: Front view of maximum principal strains of CFRP, internal composite structure

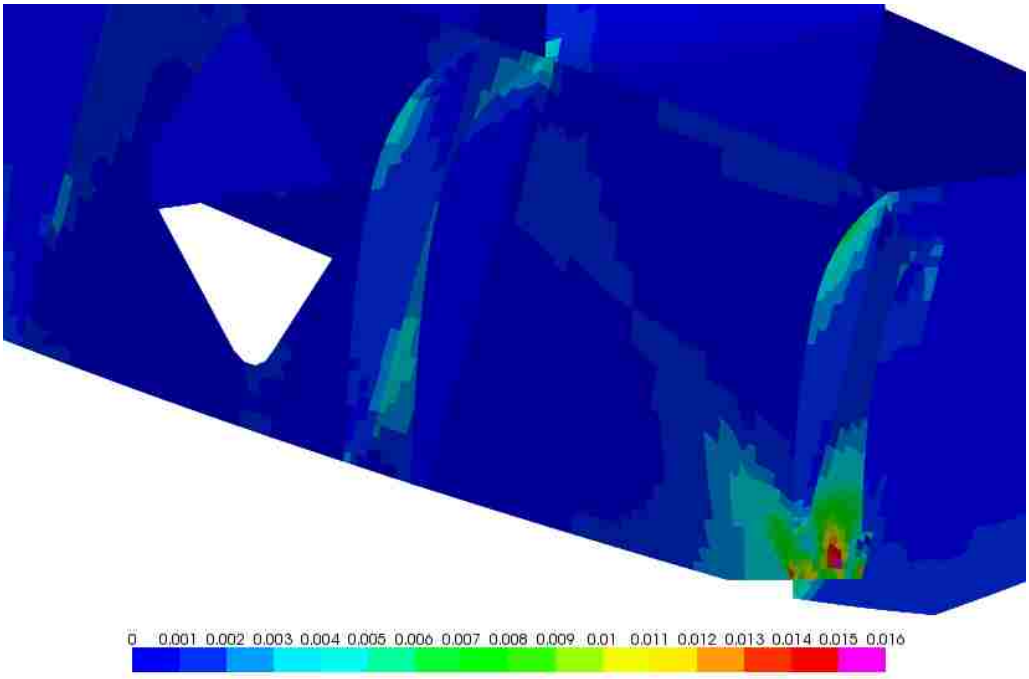

Figure 3.5-40: Rear view of maximum principal strains of CFRP, internal composite structure

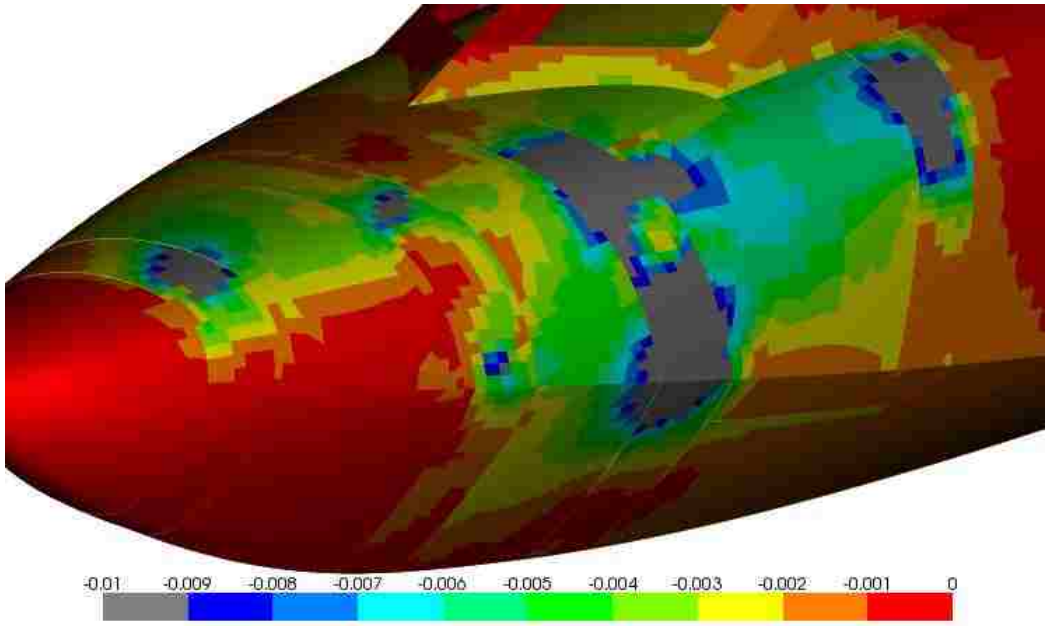

Figure 3.5-41: Front view of minimum principal strains of CFRP, external composite structure

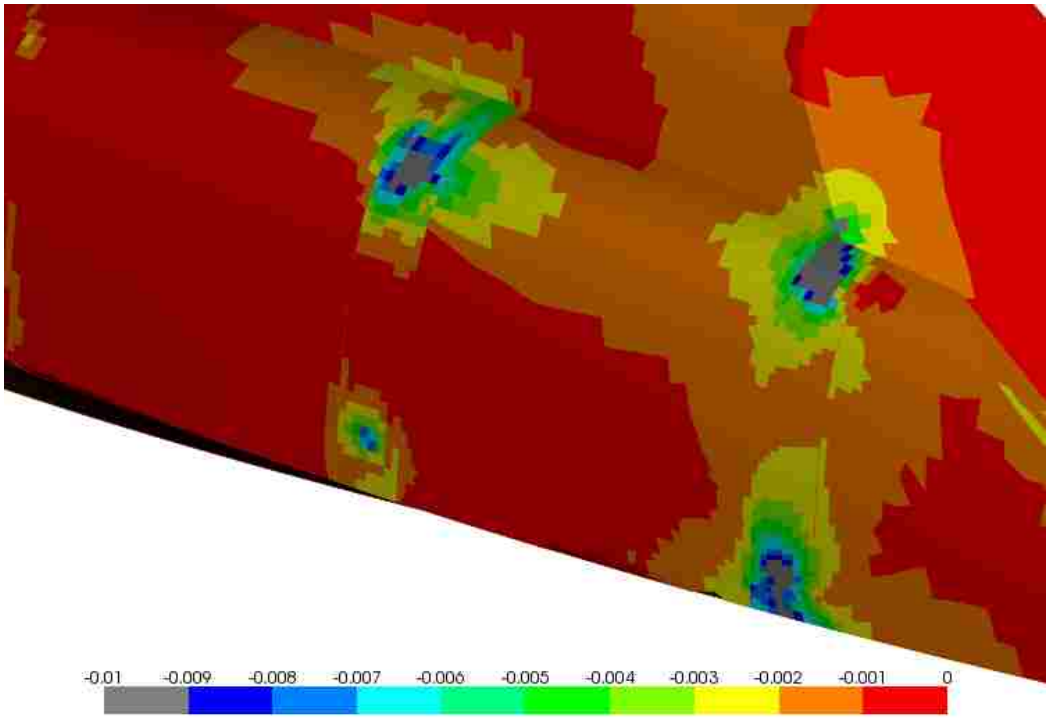

Figure 3.5-42: Rear view of minimum principal strains of CFRP, external composite structure

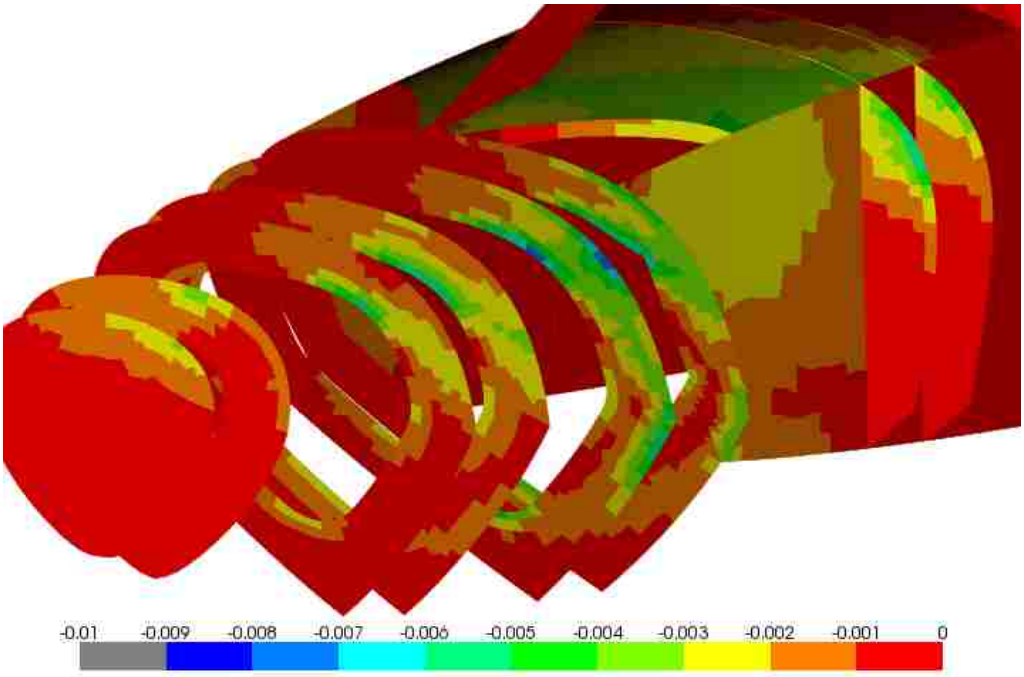

Figure 3.5-43: Front view of minimum principal strains of CFRP, internal composite structure

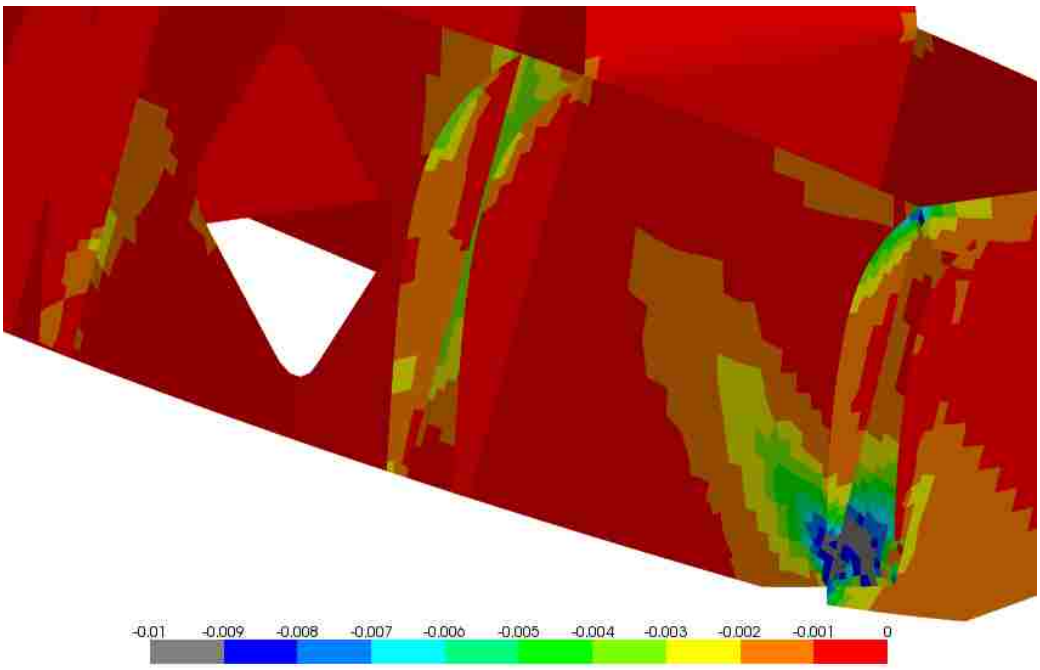

Figure 3.5-44: Rear view of minimum principal strains of CFRP, internal composite structure

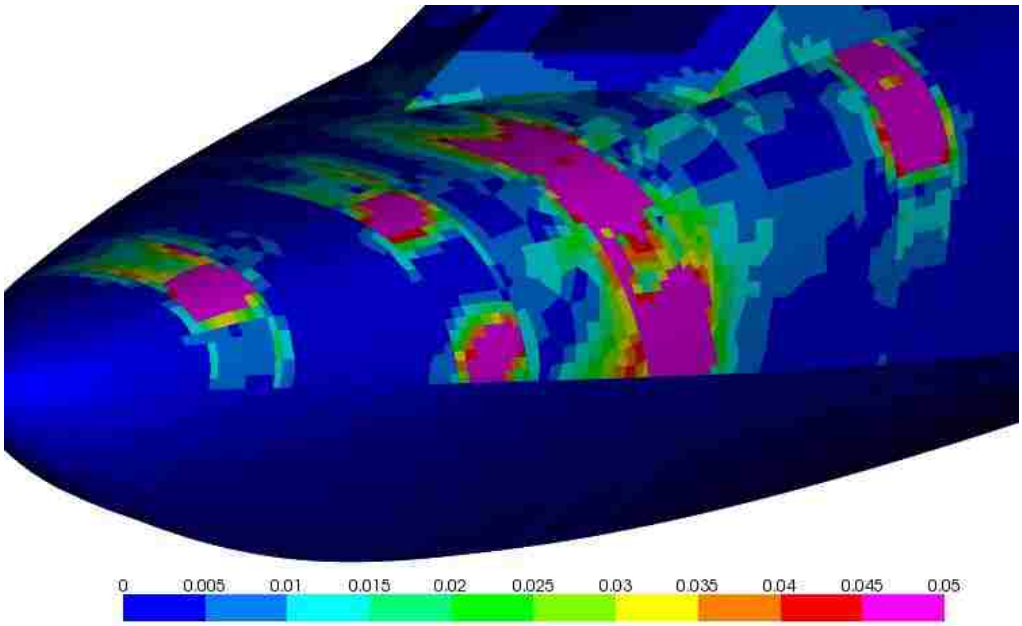

Figure 3.5-45: Front view of out-of-plane shear strains of cores, external composite structure

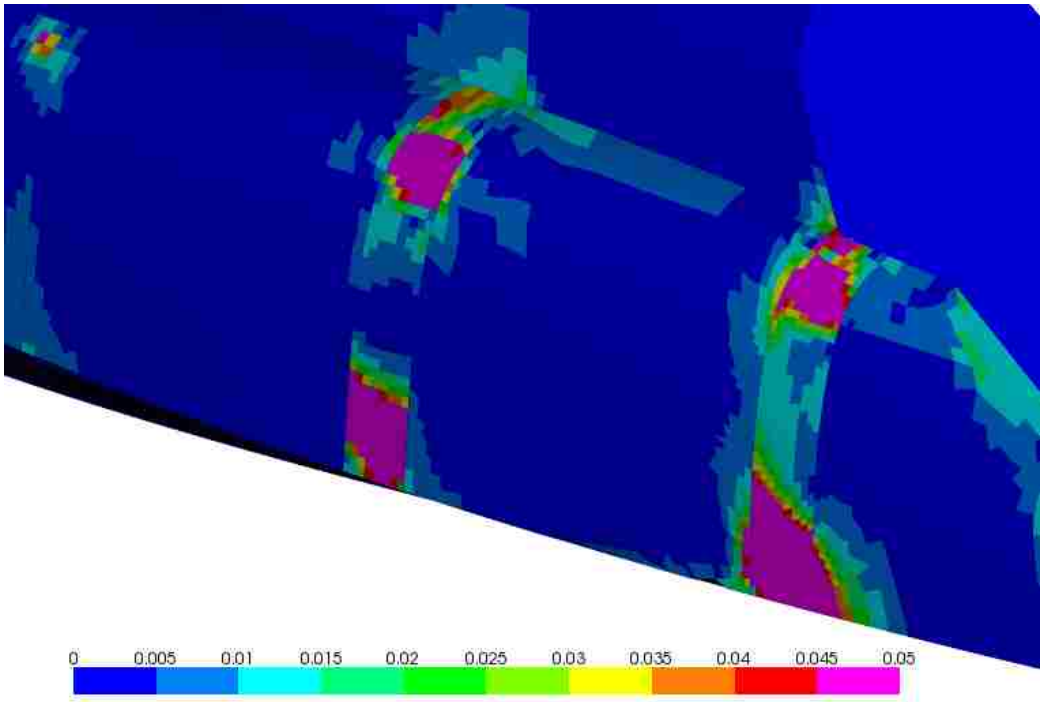

Figure 3.5-46: Rear view of out-of-plane shear strains of cores, external composite structure

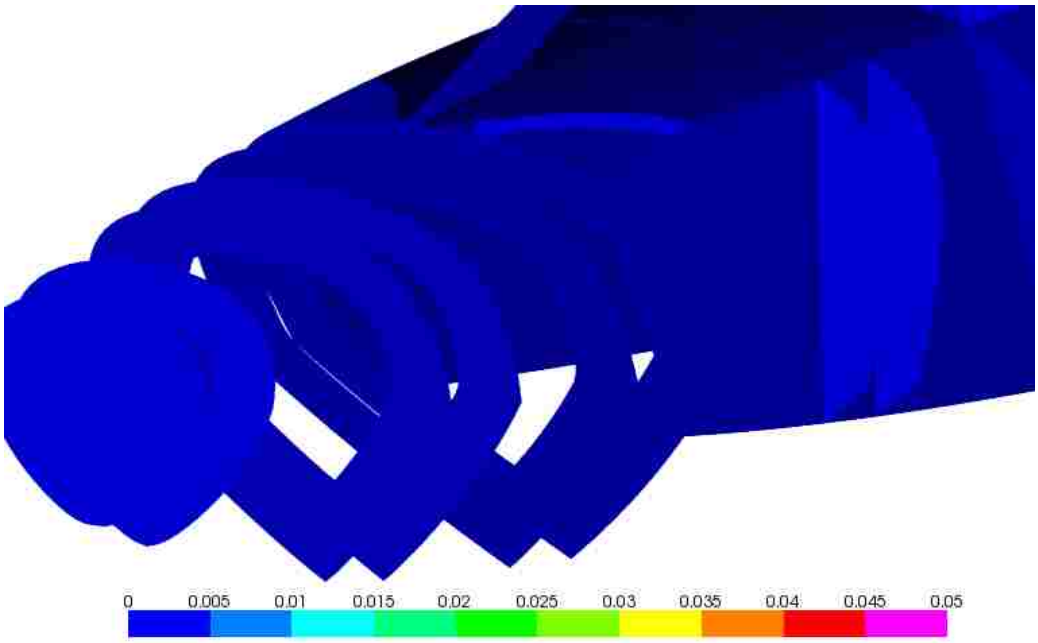

Figure 3.5-47: Front view of out-of-plane shear strains of cores, internal composite structure

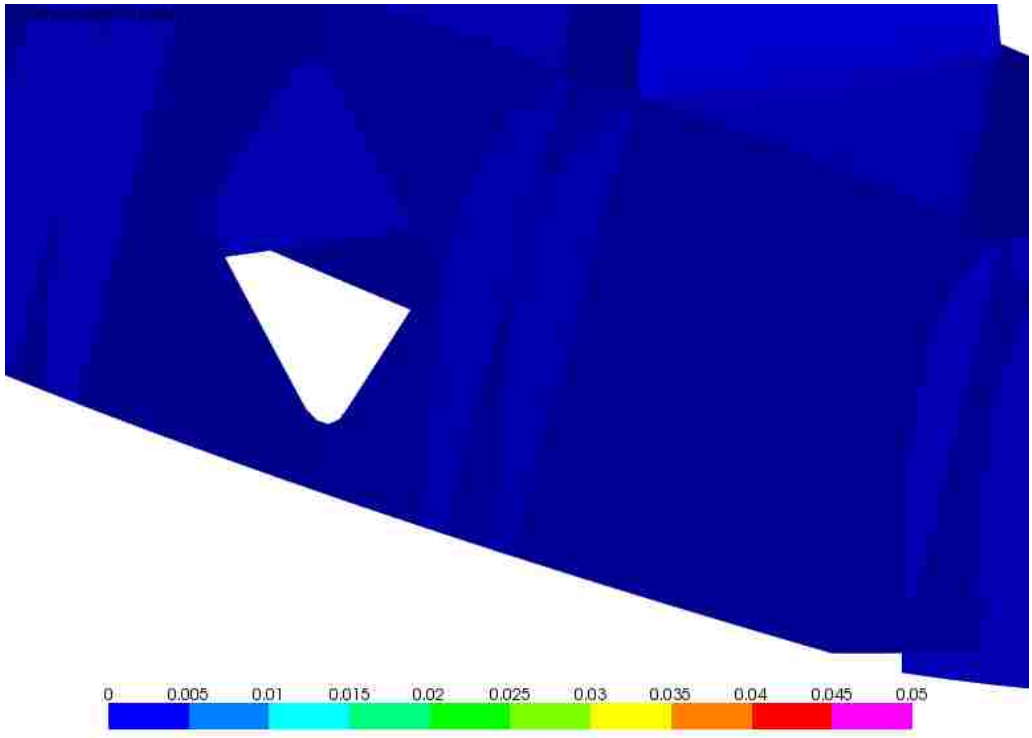

Figure 3.5-48: Rear view of out-of-plane shear strains of cores, internal composite structure

VI. Contour plots for Load Case 6: left front sponson taking horizontal loads

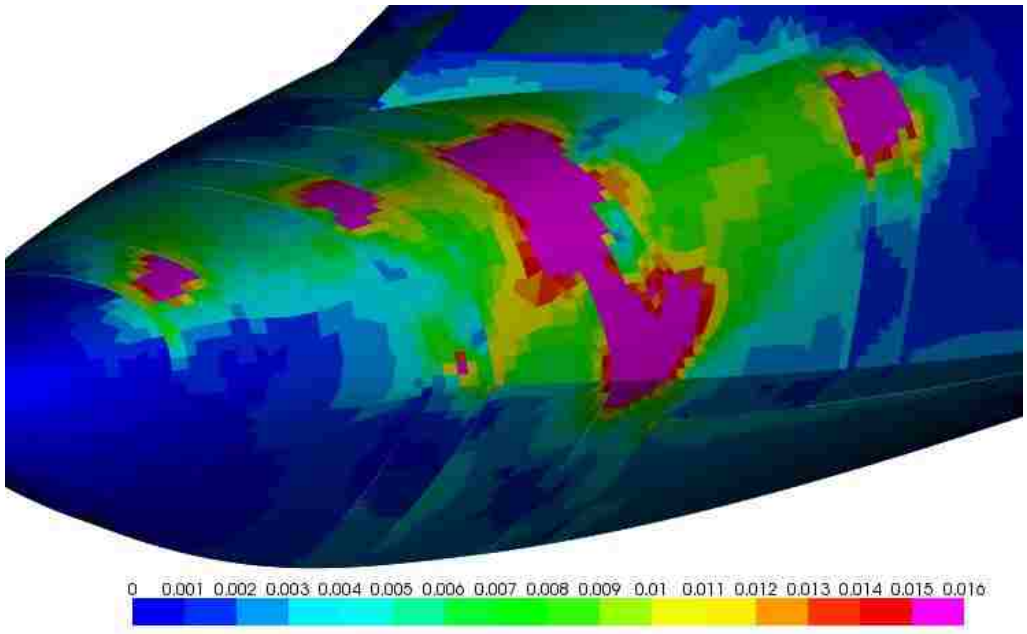

Figure 3.5-49: Front view of maximum principal strains of CFRP, external composite structure

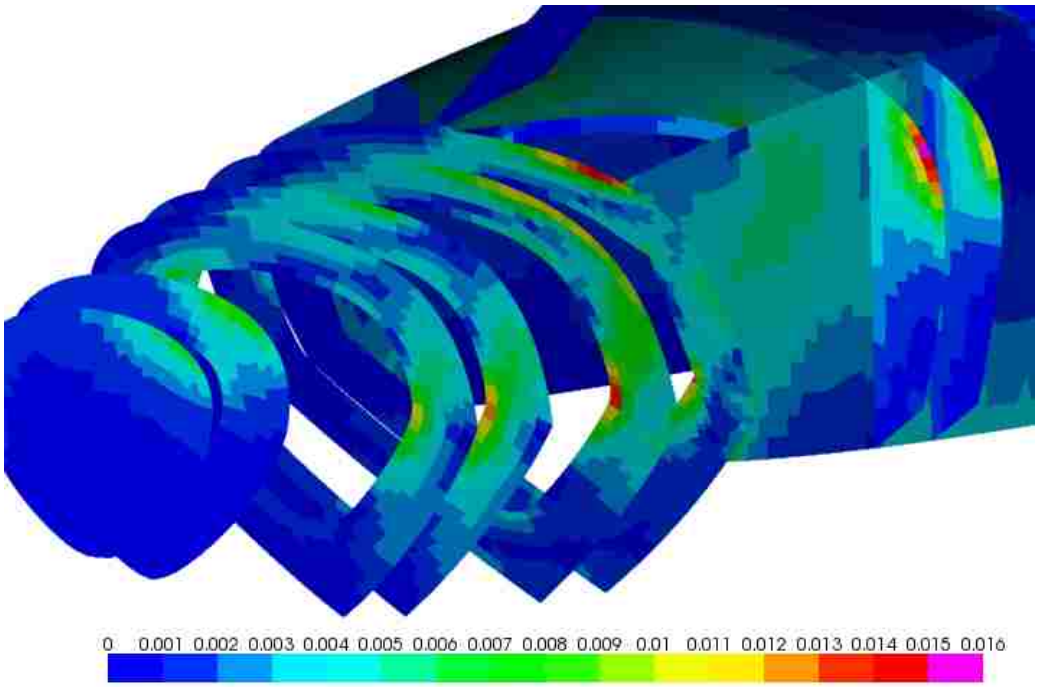

Figure 3.5-50: Front view of maximum principal strains of CFRP, internal composite structure

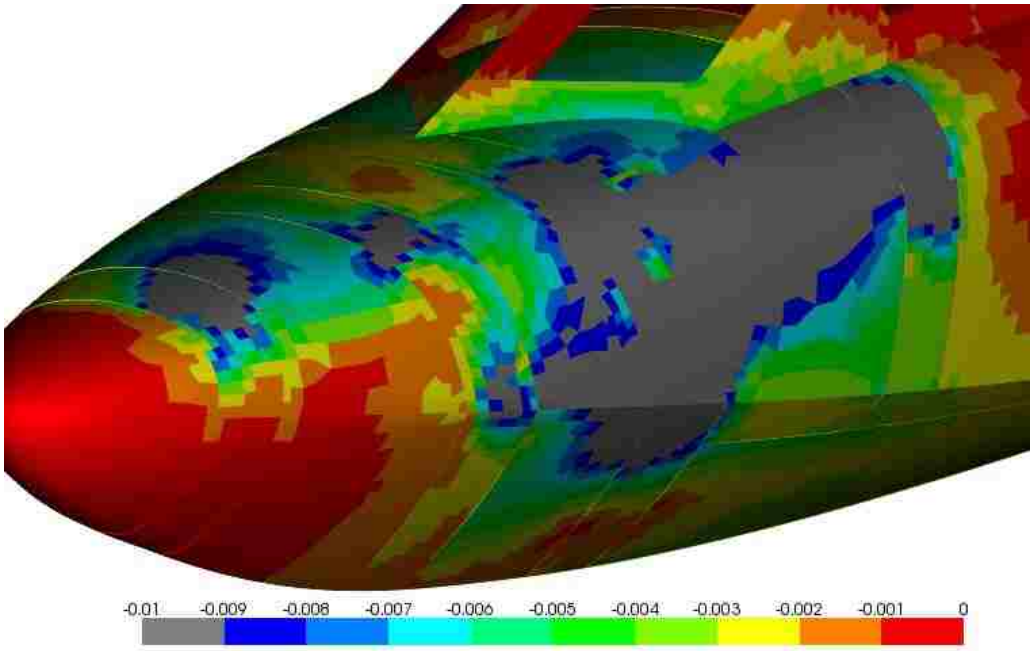

Figure 3.5-51: Front view of minimum principal strains of CFRP, external composite structure

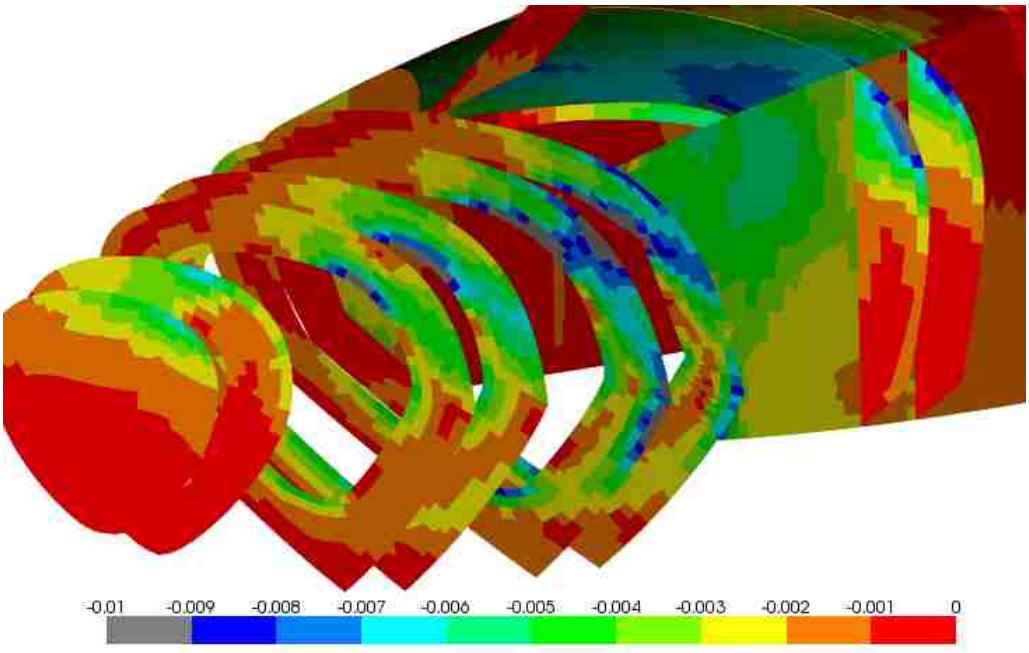

Figure 3.5-52: Front view of minimum principal strains of CFRP, internal composite structure

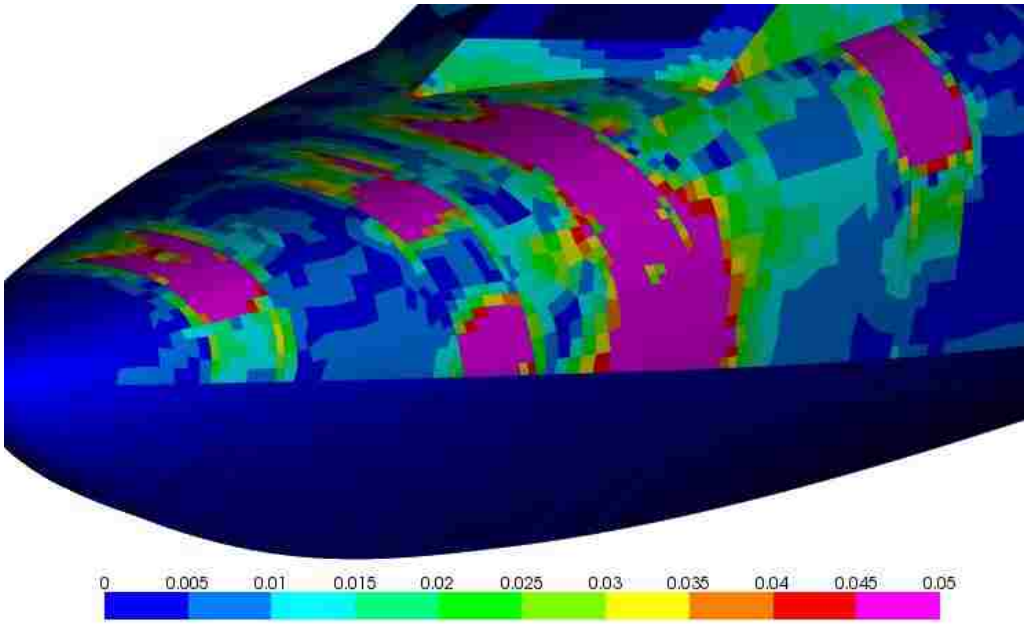

Figure 3.5-53: Front view of out-of-plane shear strains of cores, external composite structure

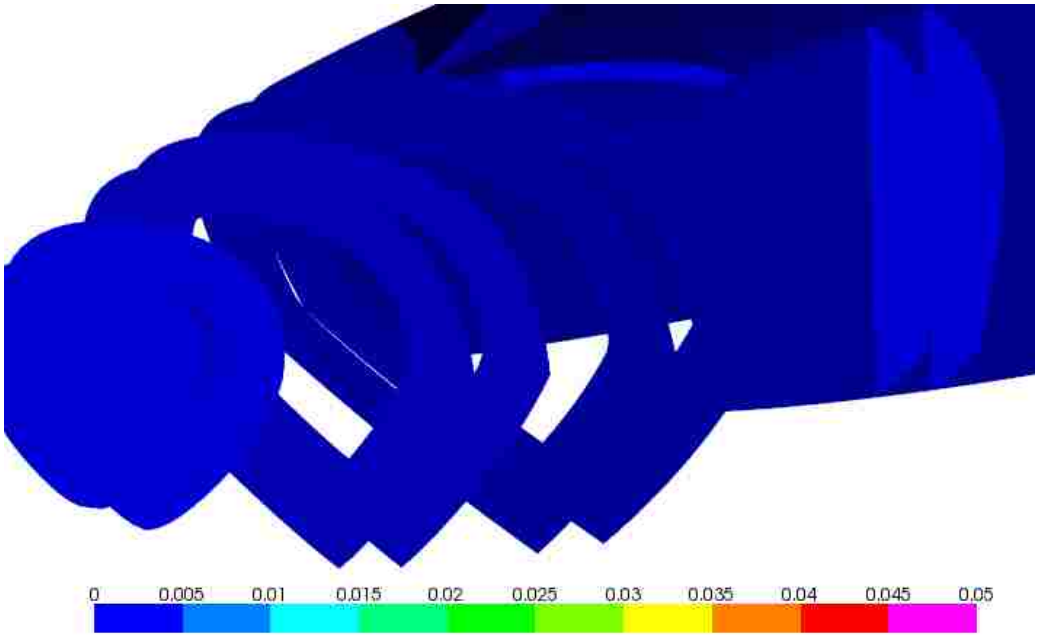

Figure 3.5-54: Front view of out-of-plane shear strains of cores, internal composite structure

VII. Contour plots for Load Case 7: left rear sponson taking horizontal loads

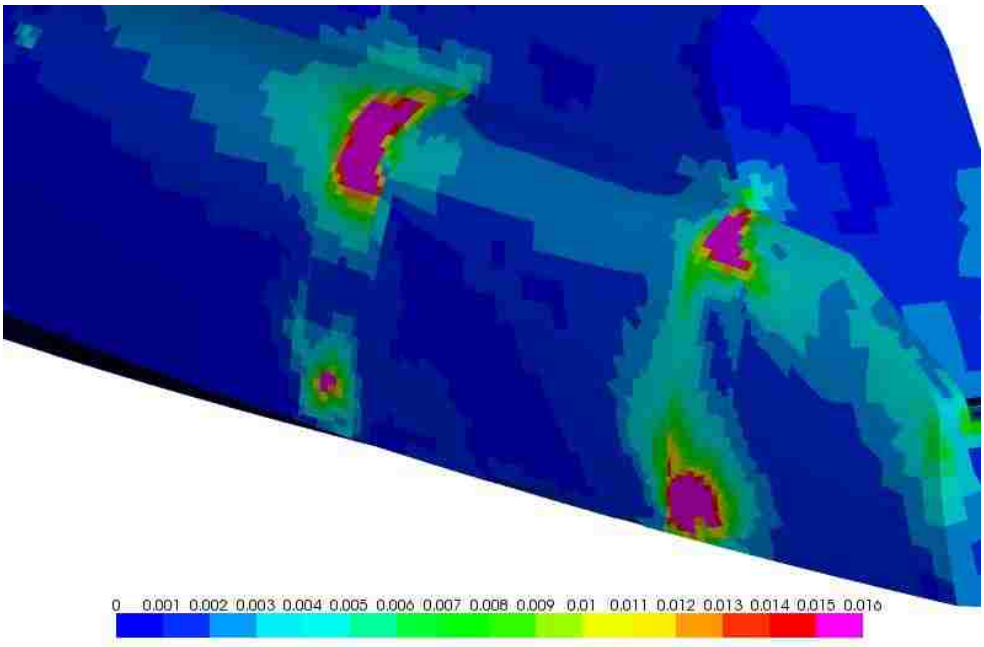

Figure 3.5-55: Rear view of maximum principal strains of CFRP, external composite structure

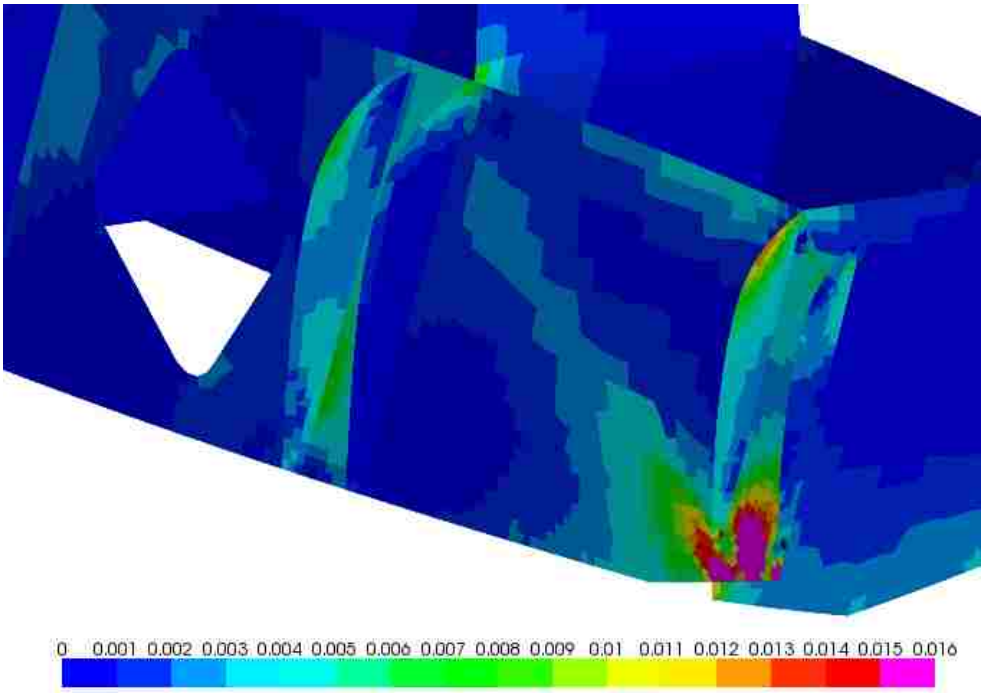

Figure 3.5-56: Rear view of maximum principal strains of CFRP, internal composite structure

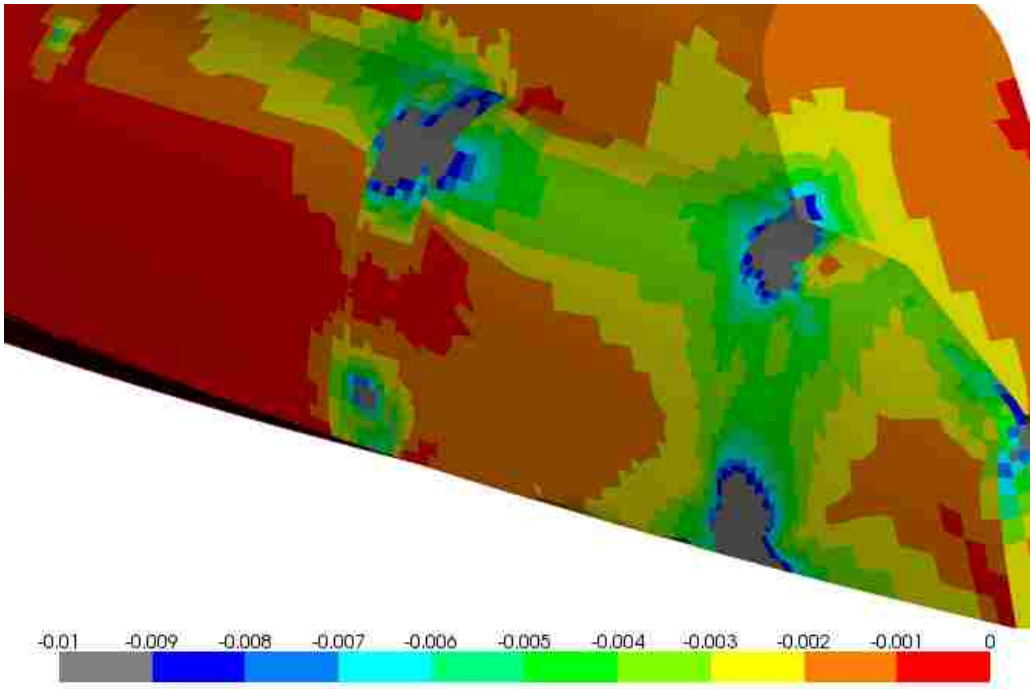

Figure 3.5-57: Rear view of minimum principal strains of CFRP, external composite structure

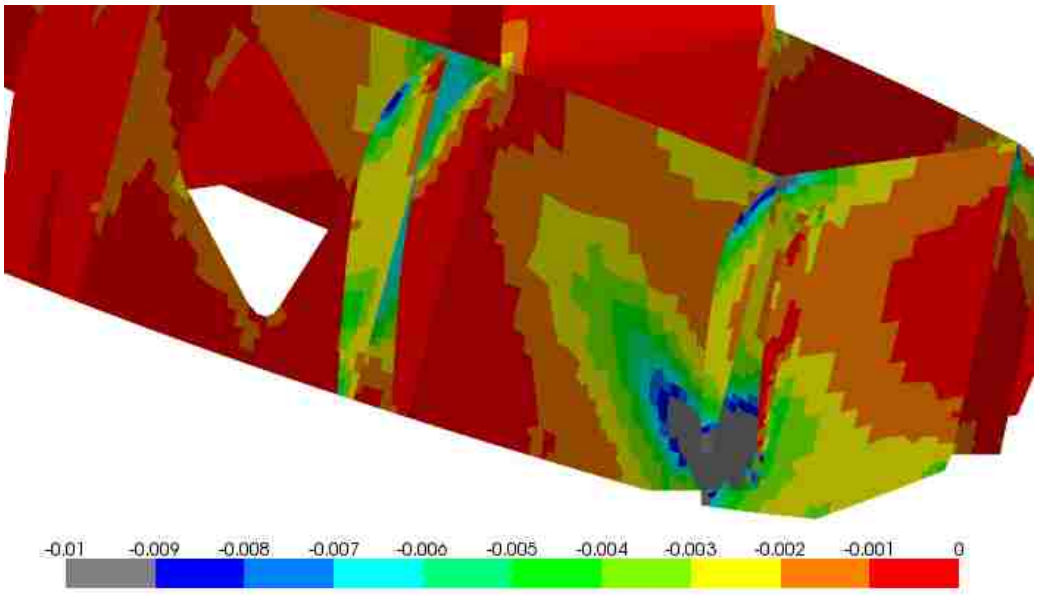

Figure 3.5-58: Rear view of minimum principal strains of CFRP, internal composite structure

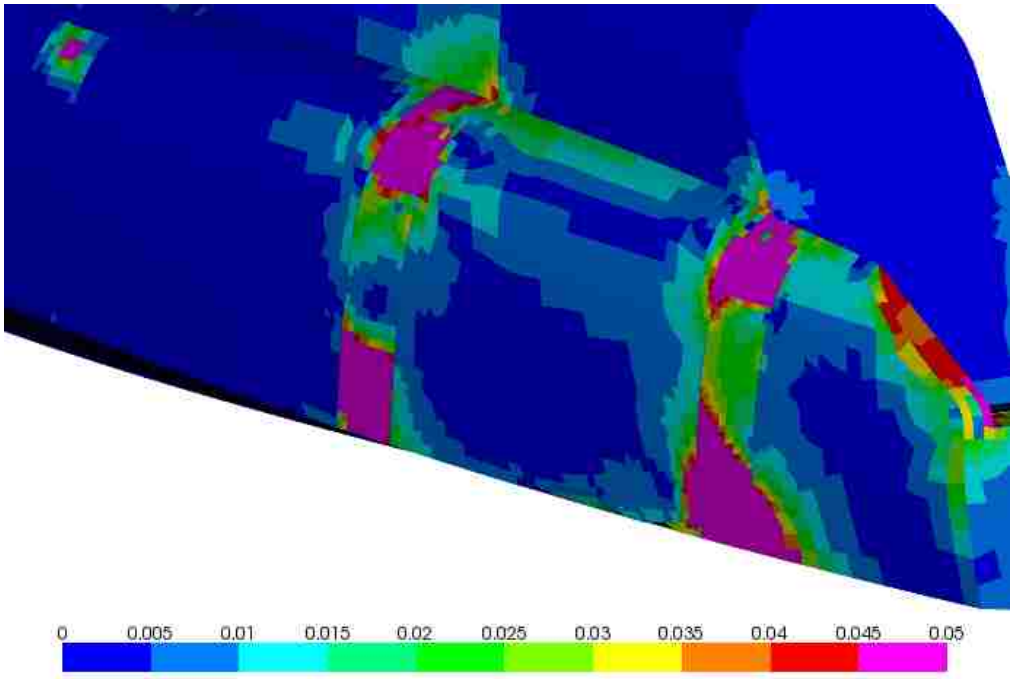

Figure 3.5-59: Rear view of out-of-plane shear strains of cores, external composite structure

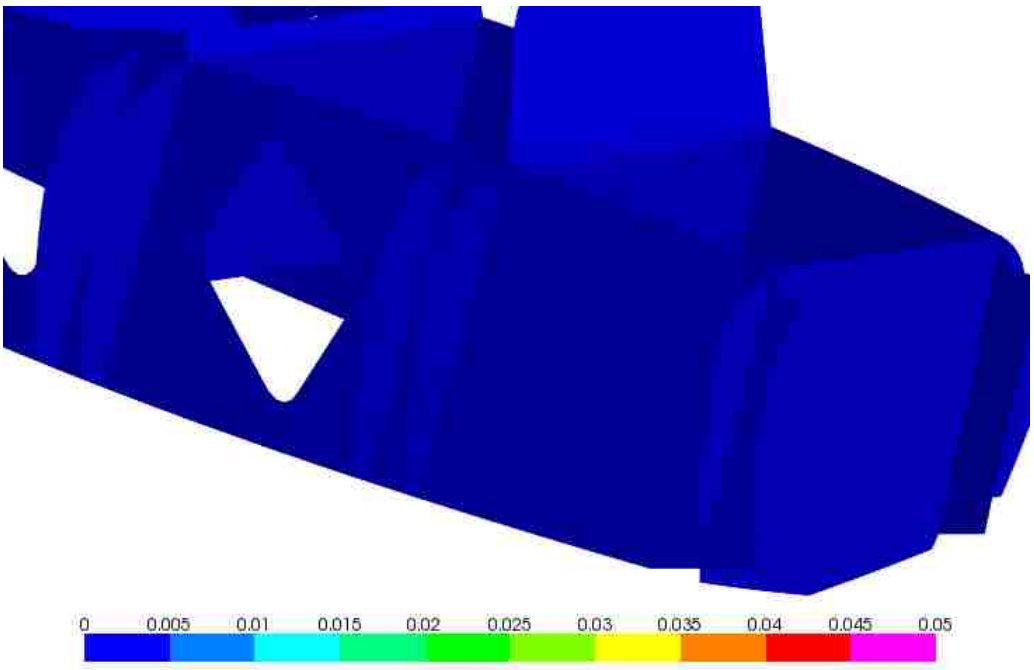

Figure 3.5-60: Rear view of out-of-plane shear strains of cores, internal composite structure

4. CONCLUSION AND FUTURE WORK

A finite element model of the center fuselage including internal structure of the suspension boat was made. Ten different load cases, representing both crashes and high speed normal operation were analyzed. The layup of all internal structure was determined iteratively, resulting in a relatively lightweight design that more or less fulfilled all strength requirements. There were some high stress areas, which will be locally reinforced during the manufacturing of the boat.

Regarding future work, it would be beneficial to perform buckling analyses of the complete structure. Local stress concentrations etc are not worth analyzing numerically as strength predictions of finite element analyses of complex geometry composites in general are not very good, and very computationally expensive. Sound judgement of experienced engineers during the manufacturing is far superior at this time.

REFERENCES

[1] Wang, Z., "Manufacturing and Testing of a Small Scale Suspension Boat," M.Sc. Thesis, Lehigh University, 2017, http://preserve.lehigh.edu/etd/2868

[2] Li, C., "Manufacturing and Preliminary Testing of a Subscale Suspension Boat," M.Sc. Thesis, Lehigh University, 2017, http://preserve.lehigh.edu/etd/2684

[3] Grenestedt, J.L., Boat suspension, US Patent 8220404 B2, 2012.

[4] Grenestedt, J.L., "Suspension Boat Dynamics," Transactions of the Royal Institution of Naval Architects (RINA), Vol. 155, Part B1, 2013, pp. 43-49.

[5] ANSYS® Mechanical, 17.2, help system, Mechanical Applications > Mechanical User's Guide > Configuring Analysis Settings > Analysis Settings for Most Analysis Type > Solver Controls > Inertia Relief - Linear Static Structural Analyses Only, ANSYS, Inc., 2017.

[6] ANSYS® Mechanical APDL, 17.2, help system, Mechanical APDL > Theory Reference > 14. Analysis Tools > 14.2. Inertia Relief, ANSYS, Inc., 2017.

[7] MIL-HDBK-17-3F, “Composite Materials Handbook”, Volume 3, Chapter 10, 2002.

[8] Diab Data Sheets, 2017, https://www.diabgroup.com/en-GB/Knowledge/Downloads?f=datasheet

[9] Dwivedi A., Bradley J., Casem D., " Mechanical Response of Polycarbonate with Strength Model Fits," ARL-TR-5899, 2012.

[10] UIM Offshore Cockpit Test Standard, 2017, https://www.uimpowerboating.com/Documents/Document/Questionnaire%20for%20Offshore%20Cockpits%20December%202016.pdf

[11] Thodal, R.S., "On Full Scale Slamming Testing of High-Speed Boats," Ph.D. Thesis, Lehigh University, 2016, http://preserve.lehigh.edu/etd/2841

[12] Lv, J., "Analytical Study of the Responses of Bottom Panels under Slamming Loads and Steel/Composite Hybrid Slamming Test Boat," Ph.D. Thesis, Lehigh University, 2014, http://preserve.lehigh.edu/etd/1549

VITA

Lean Fang was born to Junhan Fang and Qiong Luo in China. He went to the University of Science and Technology of China (USTC) and selected into the Hua Lo-Keng Honors Class of Mathematics in 2009. During his undergraduate years he developed a fondness of mechanical engineering with a special interest in computational methods such as CAD, CFD, FEA, and their applications in designing high performance vehicles. In 2012, he took one year off and worked at Falco Bike as a CFD practitioner and a core member of the company at its startup stage. He returned to USTC and finished his college education with a Bachelor of Science degree in Computational Mathematics in 2015. After that he went to Lehigh University to pursue a Master of Science degree in Mechanical Engineering. He worked on FEA of a high-speed suspension boat led by Professor Joachim L. Grenestedt.

He can be reached at:
lean_fang@alum.lehigh.edu